A SPATIAL AND TEMPORAL ANALYSIS OF NEIGHBORHOOD AIR QUALITY IN DOWNTOWN VANCOUVER

by

Annie Yi Wang

B.Sc., The University of British Columbia, 2012

A THESIS SUBMITTED IN PARTIAL FULFILLMENT OF

THE REQUIREMENTS FOR THE DEGREE OF

MASTER OF SCIENCE

in

THE FACULTY OF GRADUATE AND POSTDOCTORAL STUDIES

(Occupational and Environmental Hygiene)

THE UNIVERSITY OF BRITISH COLUMBIA

(Vancouver)

August 2017

Abstract

Rapid urban densification and an enhanced understanding of the health consequences of intra-urban air pollution exposure variability has led to a need for accurate estimation of traffic-related air pollution (TRAP) exposures, including temporal and spatial variability. To address this goal, a wireless real-time air pollution monitor was evaluated and the effect of street canyon geometry on TRAP levels was assessed. The AQMesh wireless monitor (with sensors for CO, NO, NO_2, O_3 and SO_2)—was evaluated in a co-location study with regulatory air quality monitoring stations in London, England and Vancouver, Canada. The amount of variability (R^2) explained by AQMesh sensors (algorithm version 3.0) ranged from 0.02% to 34.5% in Vancouver and 1.5% to 82.3% in London. Sensors for NO_2 and O_3 displayed the highest accuracy while the CO sensor accuracy was much weaker. AQMesh, as examined in this co-location, was not sufficiently robust for use in regulatory applications.

A simple GIS-based model for the identification of potential street canyons where TRAP levels may be elevated was created using 3D building information, aspect ratio and the prevailing wind direction. The model was evaluated in a mobile monitoring campaign in which particulate matter smaller than 2.5 micrometers ($PM_{2.5}$) and particle number concentration (PNC) were measured along 4 road segments: canyon high traffic (C HT), canyon low traffic (C LT), non-canyon high-traffic (NC HT) and non-canyon low traffic (NC LT). A linear mixed effects model found the effect estimates for C LT (i.e. the effect of canyon) to be 8% higher for $PM_{2.5}$ and 17% higher for PNC when compared to the reference road segment category, NC LT. In comparison, the effect estimates for NC HT (i.e. the effect of traffic) was 16% higher for $PM_{2.5}$ and 34% higher for PNC when compared to NC LT. This research suggests that the impact of

traffic may be greater than the impact of street canyons in determining TRAP exposures.

Lay Summary

Traffic-related air pollution (TRAP) exposure is associated with numerous cardiopulmonary health outcomes. With rising urbanization, greater populations residing in city centers may be exposed to spatially and temporally varying TRAP; one factor that may increase pollution concentrations is urban street canyons—regions with narrower roads bound by taller buildings. Newly marketed air pollution instruments capable of deployment in higher density networks may better capture nuances in spatiotemporal trends than existing measurement and monitoring approaches.

This research evaluated the performance of one wireless sensor technology against gold-standard instrumentation in Vancouver and London and determined it was not sufficiently developed at the time of study to enhance understanding of spatiotemporal air quality patterns.

To further examine TRAP in urban settings, a simple model was generated to identify potential street canyons in downtown Vancouver. Measurements along canyon segments suggest traffic density may be a more important determinant of TRAP levels than street canyons.

Preface

This thesis was designed to evaluate the near-roadway sensor performance of AQMesh in co-location studies next to reference stations in Vancouver and London. This project also investigated the impact of urban street canyons on the intra-urban variability of TRAP exposures. A simple model for street canyon identification was developed as this may be integrated into land use regression models for exposure quantification. The model was appraised using mobile monitoring techniques to determine if canyons were indeed important predictors of within-city TRAP levels. A. Wang conducted all work from conception to completion under the supervision of Dr. Michael Brauer who offered input on study design, field work and written composition.

Chapter 1 of this thesis is derived in part from Wang, A., Brauer, M., 2014. Review of Next Generation Air Monitors for Air Pollution. Available from: https://open.library.ubc.ca/cIRcle/collections/facultyresearchandpublications/52383/items/1.0132725.

The installation, maintenance and removal of AQMesh units in Vancouver was completed by author, A. Wang, with assistance from Ben Weinstein, Robert Tsin, Aaron Birch and Jeff Yeo. Dr. Ben Barratt and the Environmental Research Group at King's College London devised and implemented the London AQMesh co-location. This data was provided to A. Wang for analysis.

The street canyon model was conceptualized by A. Wang and Dr. Brauer. The model was built by A.Wang in consultation with Dr. Brian Klinkenberg and Joseph Lee from UBC's Department of Geography. The spatial analysis as described in Chapter 3 is in part a reappraisal of a student project submitted by A.Wang and Bonny Ho for a UBC course - Advanced Issues in

Geographic Information Science. All data collection necessary for the mobile monitoring campaign was performed by A. Wang, with the support of volunteers from the UBC School of Population and Public Health (Robert Tsin, Martha Lee) and M'hammed Bensahal.

Table of Contents

List of Tables

List of Figures

List of Abbreviations

AQHI – Air Quality Health Index

BC – Black carbon

CO – Carbon monoxide

EPA – Environmental Protection Agency

GIS – Geographic Information System

GPRS –General packet radio service

GPS – Global Positioning System

HAP – Hazardous air pollutants

IR – Infrared

LUR – Land Use Regression

MOS – Metal oxide semiconductor

NAPS – National Air Pollution Surveillance

NO – Nitrogen monoxide

NO_2 – Nitrogen dioxide

O_3 – Ozone

PM – Particulate matter

$PM_{2.5}$ – Particles with an aerodynamic diameter <2.5 µm

PM_{10} – Particles with an aerodynamic diameter <10 µm

SO_2 – Sulfur dioxide

SOAs – Secondary organic aerosols

TRAP – Traffic-related air pollution

UFP – Ultrafine particles– Particles with an aerodynamic diameter <0.1 µm

VOCs – Volatile organic compounds

Acknowledgements

First, I wish to extend my sincerest thanks to my thesis supervisor and mentor, Dr. Michael Brauer. Thank you for your unending support, patience, guidance and expertise over the years. I offer my gratitude for helping me to see the "big picture" when I got too lost in details. To my wonderful and extremely knowledgeable committee members, Dr. Ben Barratt and Dr. Ian McKendry, thank you for enriching this thesis experience by contributing your precious time and advice into our discussions!

Special thanks are owed to the SPPH faculty, staff and fellow students for your care and support. I am especially grateful for Dr. Hind Sbihi, Dr. Ther Aung, Angela Yao, Robert Tsin, Ivan Cheung and Martha Lee—thank you for your ever-present smiles and words of encouragement! Big thanks to my dedicated volunteers, M'hammed Bensahal (who endured the long sampling campaign without a single complaint), Aaron Birch and Jeff Yeo! Thank you to my generous funders: NSERC CREATE-AAP and BC Clean Air Research Fund.

I wish to thank my family and friends near and far for their moral support. To my closest friends, Linda, Gabby and Lillian, thank you for your unfailing confidence in me to accomplish my goals and for sharing in all of my joys and fears! To Johnny, thank you for your loving presence! To my parents, thank you for your unwavering support and unconditional love! Without you, this thesis would not have been possible.

Chapter 1: Introduction

1.1 Air pollution background

Air pollution is an unavoidable exposure for all populations and has been considered both an environmental and health problem for centuries. (1) The Global Burden of Disease 2015 attributed 4.2 million (95% uncertainty interval 3.7 million to 4.8 million), 2.9 million (2.2 million to 3.6 million) and 0.3 million (0.1 million to 0.4 million) deaths to the exposure of ambient particulate matter, household air pollution and ambient ozone pollution, respectively. (2) These three air pollutant categories accounted for 103.1 million (90.8 million to 115.1 million), 85.6 million (66.7 million to 106.1 million) and 4.1 million (1.6 million to 6.8 million) global disability-adjusted life years. (2)

Air pollution is comprised of a complex mixture of pollutants that are classified as: 1) primary (directly emitted) or secondary (produced in the atmosphere by chemical and physical reactions) by their formation; 2) gaseous or particulate by their state; and 3) biogenic, geologic, or anthropogenic by their emission mode. (1,3) An important source of air pollution in many urban areas and a key factor in spatial variability of pollutant levels within cities is traffic-related air pollution (TRAP).

Primary pollutants emitted in TRAP include nitrogen monoxide (NO), carbon monoxide (CO), heavy metals (e.g. cadmium, mercury), volatile organic compounds (VOCs), and particulate matter (PM). Anthropogenic sources of environmental NO_x and CO include motor vehicle emissions and combustion processes for power and heat. (4,5) VOCs are a class of carbon-containing gases that can be precursors for fine particulate matter and ozone. (6)

Particulate matter is composed of liquid, solid and/or a mixture of the two suspended in

air where the size fraction dictates its penetration into the respiratory airways. (4) Primary PM can be derived from industrial sources (e.g. construction, agriculture), wind erosion, biogenic sources (e.g. forest fires) and vehicular exhaust and non-exhaust emissions. (7,8) Mechanical abrasion from brake and tire wear, road surface wear, road dust re-suspension and construction and quarrying activities act as sources of non-exhaust emissions of especially coarse PM (i.e. $PM_{2.5\text{-}10}$ or particles with aerodynamic diameters less than 2.5 µm to particles with aerodynamic diameters less than 10 µm). (9,10) Smaller aerodynamic diameters of primary PM can include $PM_{2.5}$ (fine PM i.e. less than 2.5µm) and ultrafine particles (UFP i.e. PM less than 0.1µm). Ultrafine particles can be emitted from petrol and diesel engines alike; they are produced at high temperatures in the engine, exhaust pipe or immediately after release into the ambient air. (11)

Examples of secondary TRAP pollutants include nitrogen dioxide (NO_2), ozone (O_3), VOCs, secondary PM, and secondary organic aerosols (SOAs). Tropospheric ground level ozone is produced by photochemical reactions with VOCs and NO. (12) Suburban concentrations of ozone tend to exceed levels in city centers as NO from traffic can react with O_3 to form NO_2. (4,13) Secondary PM is created from precursor gases (nitrogen oxides, sulfur oxides and ammonia) and produces nitrates, sulfates and ammonium salts. (7) SOAs are low-volatility compounds that evolve from the chemical transformation of organic species. (14)

The body of evidence suggests that TRAP is causally linked to asthma exacerbation, while childhood onset of asthma is classified as borderline “suggestive but not sufficient” and “sufficient” with respect to causality; the remaining health effects are suggestive, inadequate or insufficient to assume causation. (15,16) Epidemiological studies have revealed that TRAP may lead to adverse effects in the cardiovascular system such as elevated risk of stroke, (17–19) atherosclerosis, (20–23) and related mortality. (24,25) Respiratory effects from ambient air

pollution and TRAP include chronic obstructive pulmonary disease, (26–28) asthma, (85–92) rhinoconjunctivitis, (37) wheeze, (38–40) and bronchiolitis. (41–43) In addition, TRAP has been linked to unfavorable pregnancy and developmental outcomes (44–50) as well as cancers of the lung, (19,51–53) prostate, (54) and breast. (55) All cause mortality has also been associated with TRAP exposure. (24,56,57) Moreover, associations have been reported between TRAP and Parkinson's Disease, (58) cognition, (59,60) and diabetes. (61–63)

The significance of TRAP and its consequential health impacts are further exacerbated by the world's rapid urbanization. Implications of urbanization include deteriorating air quality and increased exposure as pollution sources (e.g. vehicular combustion, power generation, and human activity) aggregate in close proximity to populations and energy consumption rises to meet the demands of these growing cities. (64) Financially, the burden of urban air pollution is substantial for both developed and developing nations (an estimated 2% and 5% gross domestic product, respectively). (65) The United Nations predicts that sixty-seven percent of the world's population will be urbanized by 2050 (66); hence, motivating experts and policymakers to review transportation and urban planning to abate the impacts of poor outdoor air quality. (16)

1.2 Intra-urban air pollution variability

Capturing intra-urban spatiotemporal trends is critical to understanding TRAP exposures across time and space. Air pollution research in the urban setting has primarily relied on a number of point measurements (from traditional air quality monitoring in combination with passive monitoring) as a basis for deriving long-term average concentration models (e.g. land-use regression models) in order to depict spatial variability. Temporal variability is underrepresented in most TRAP models (despite inclusion in dispersion models) and is best

described by traditional networks. Logistically, traditional air quality monitoring at a high level of spatial resolution (~100-500 meters) is not feasible (discussed further in Section 1.3) and hence limits the ability to holistically represent outdoor air pollution spatial trends. This section identifies factors that contribute to within-city spatial and temporal patterns.

Many variables can affect the spatiotemporal extent of a pollutant such as meteorological conditions (i.e. temperature, precipitation, wind speed, wind direction and turbulence), (1,67–69) pollutant characteristics (e.g. particle size, reactivity), (13,70) source type (i.e. industrial, vehicular), (71) infrastructure (i.e. street canyons (72–76) or elevated highways (77,78)), temporal patterns in emissions and meteorology (i.e. daily, weekly, seasonal), (79–82) topography, (83) source strength (84), and emission rate. (13)

Temporal variations in urban air pollution are possible at a diurnal, hebdomadal, and seasonal level. (85) Daily variability in traffic emissions can be explained by rush hour traffic. Morning rush hours have shorter and sharper emission profiles than the broader afternoon rush hours. (86) One study showed that traveling outside rush hours decreases concentrations and thus exposures by 10-30% for primary pollutants and 5-20% for secondary pollutants, with more pronounced reductions during the morning. (86) Nitrogen oxides have a noticeable double wave diurnal trend with peaks linked to rush hours, though this is more prominent for reactive NO when juxtaposed with NO_2 (possessing a longer lifespan). (82,87) NO concentrations during the morning rush hour are higher because the atmosphere near-ground is unstable compared to the evening when mixing is greater. (87) As photochemical O_3 is produced, the daily concentrations rise with solar intensity formation until the afternoon maximum is reached. (87)

Some pollutants, like ozone and nitrogen oxides, exhibit predictable weekly patterns. For example, ozone increases during weekends and nitrogen oxides increases on mid-weekdays.

(82,88) The ozone weekend effect occurs when mobile source emissions (particularly, heavy-duty vehicles) diminish on weekends but create a condition that favors ozone formation since the ratio of VOCs to NO_x is greater. (89,90) Other geophysical determinants (e.g. sunlight intensity, clouds, temperature, wind speed, transport, and mixing), besides the formation and destruction of O_3, can alter the weekend maxima of O_3. (82,87,89) Additionally, ozone has a characteristic seasonal pattern with peak concentrations during the spring and summer months in southern British Columbia. (91,92) An example of a seasonal behavioral factor that would affect the spatial representativeness in urban areas is the practice of residential wood burning during winter months. (93–95)

Spatial factors pertinent to within-city TRAP include pollutant type and presence of roadway features. Pollutant type (inert or reactive) can substantially change spatial "zones of influence". A meta-analysis of daytime near roadway studies showed individual TRAP concentrations could require distances of 115 m to 570 m (edge of road normalized) to decay to background levels. (96) Inert pollutants (e.g. CO, PM mass) have longer atmospheric lifetimes, resulting in more homogeneous spatial patterns within urban areas. (13) In contrast, reactive components (e.g. NO, NO_2, UFP) depend not only on ambient air dilution, but also on their chemical reaction rates in the atmosphere. (13,97) Consider the interplay between NO and NO_2 with increasing distance from the emission source: NO concentrations diminish rapidly downwind as O_3 is scavenged by NO to form NO_2; on the other hand, NO_2 levels decrease gradually since formation slows down dilution by air. (13) By and large, primary pollutants possess a greater spatial variation than do secondary pollutants. (85)

Roadway features including vegetative and structural (noise) barriers between roads and nearby buildings may cause a trade-off between the benefits of blocking pollutants from

concentrating in the vicinity of inhabitants, and the undesirable restriction of airflow causing elevated on-road concentrations for commuters. (16) Other roadway features such as tunnels and street canyons can result in pollutants becoming enriched within these constructs. (16,98,99)

Spatial factors can be influenced by temporal changes. For example, meteorological conditions including temperature inversions, (100) solar radiation, (16) precipitation, (101) and wind can all impact the spatial trends of pollutants. (13) Temperature inversions describe the situation when temperatures increase with altitude. (100) Inversion conditions are present in the morning or in instances where air from higher altitudes descend and results in minimal pollutant dispersion. (100) Solar radiation (16) and precipitation (and the resulting wet roads) will impact air pollution levels. (101) Wind speed is inversely related to concentration, and can influence initial dilution rates, travel time to measurement sites, coagulation of UFP and vertical dispersion. (13) Wind direction—upwind or downwind, and whether it is parallel or perpendicular to roadways—will considerably alter spatial patterns of pollutant distribution. (13)

In TRAP studies, emission rates increase with higher traffic counts (i.e. rush hours) leading to greater spatial effects. (13,102,103) In a study on road vehicle emissions, it was discovered that low driving speeds and transient driving modes (i.e. acceleration, deceleration) were far more polluting than steady-speed modes (i.e. cruising, idling). (104) While trends discussed thus far contribute to intra-urban variability, time activity patterns in differing microenvironments and infiltration into indoor environments will also modify personal exposures; host factors like socioeconomic status, behavioral habits (e.g. smoking), pre-existing conditions, age, and susceptibility can all affect the onset of a health outcome. (85)

1.2.1 Street Canyons

One infrastructure variable that can largely impact personal exposures is the presence of street canyons. Street canyons are defined by their aspect ratio— a ratio of the building height to the road width. (105) Aspect ratios above 0.7 may be at risk of pollutant accumulation, as the relatively stagnant air at the base of the canyon cannot adequately exchange with airflow passing above building tops. (106–108) For example, assuming a typical 4-lane roadway is 15 m wide, if the buildings lining the street are taller than 4 stories (measuring over 10.5 m in height), the street canyon effect might be present. When the incident wind speed is 4 m/s or greater and perpendicular to the canyon, a vortex forms within the canyon; on the other hand, if the wind is parallel to the canyon, the airflow runs in the canyon along the canyon axis. (108,109)

Street canyons are sometimes classified by their aspect ratio. For instance, canyons can be referred to as "regular" if the aspect ratio measures approximately one and few openings are present. If the aspect ratio is 2, it can be called a "deep canyon". Canyons may also be sorted into 3 categories: short canyons (L/H ~3), medium canyons (L/H~5) and long canyons (L/H~7) where L is the road distance between the flanking major intersections and H is the height of the canyon. Finally, canyons can be symmetric or asymmetric depending on the differential between building heights. (74)

In describing canyons, it is important to highlight two different regions; these are the obstructed sub-layer, also referred to as the urban canopy sub-layer and the free surface layer, also referred to as the urban boundary layer. The former runs from the ground surface to the building height while the latter extends above the building rooftops. Wind flow within the obstructed sub-layer is normally much lower than the undisturbed wind flow. This layer is further subjected to the impacts of local topography, building geometry and dimensions,

roadways, traffic, green space and diurnal patterns. (108,110,111)

Personal exposure calculations are the cumulative effect of different exposures to pollutant levels and the duration spent in each microenvironment; thus, understanding the location of potential street canyons becomes critical in personal exposure estimates. Johansson et al. (112) found PNC and PM_{10} concentrations within canyons were more than 5 times greater and 2 times higher than background, respectively. A measurement study in Leipzig, Germany found that the number fraction of externally mixed soot particles (80 nm particles on working summer days) decreased from a street canyon (60%) to an urban background (22%) to a rural site (6%). (113) In another canyon study, Tsai and Chen (114) measured and modeled 64-107% higher concentrations of gaseous pollutants on the leeward side when compared with the windward side in an urban street canyon.

Research by Spadaro and Rabl (111) suggest adverse health impacts (e.g. increased respiratory hospital admissions) may be greater as a result of the canyon effect, more specifically, the reduced ventilation within the urban infrastructure causing a delay in pollutants mixing with the free surface layer. In characterizing personal exposures within a canyon, a vertical profile should also be considered as dilution and dispersion effects can be quite large; Väkevä et al. (115) reports that within a street canyon, pollutant concentrations decreased by 5 fold at height of 25 m when compared to street level.

Mathematical and physical dispersion modeling of street canyons can be separated into groups— 1) source-oriented models (generally Gaussian plume models or a modification of one), 2) receptor models, 3) computational fluid dynamics models and 4) reduced-scale (or physical) models (e.g. performed in a wind tunnel). (74) These models are typically produced to quantify air pollution within the microenvironment of a street canyon configuration. Dispersion

model predications rely largely on the input quality of variables including traffic data, vehicle emissions, meteorological data, street geometry and background concentrations. (74) These variables are not always readily available for the monitoring area; hence, a simplistic screening model may help focus the regulatory monitoring efforts on canyon environments. (74) More importantly, a model across a larger spatial scale that can discern potential street canyons versus non-canyons can progress the estimates of personal exposures to air pollution in urban models.

While street configurations are commonly included in dispersion modeling, they are seldom incorporated into land use regression (LUR) models. (116,117) However, some research has suggested the characterization of street canyons and urban morphology may be important and can boost the explanatory power of models for exposure assignment. (118) Su et al. (105) determined increases in the predictive power of LUR models from 56% to 67% for NO_2 and from 72% to 85% for NO once an aspect ratio surface was added to the analysis. Similarly, Eeftens et al. (116) found that enhancing LUR models with a street canyon indicator (i.e. SkyView Factor measuring the fraction of visible sky) led to a greater explained variability (82% for NO_2 and 78% for NO_x) when compared with basic LUR models (80% for NO_2 and 76% for NO_x).

1.3 Air quality measurement

Air quality measurements are an integral part of providing data to the public, researchers and policymakers. Historically, air pollution management initiatives have focused on urban and regional air quality by relying solely on fixed-site monitoring networks with a limited number of monitoring sites within a designated area. These networks lay the groundwork for the current understanding of pollution trends and their associated health effects; they inform compliance

with standards, provide the public with air quality health risks (e.g. Air Quality Health Index, AQHI), (119) and are the basis for evaluating impacts associated with regulatory changes and air quality management programs.

In Canada, two federal air pollution-monitoring networks gather air quality data—the National Air Pollution Surveillance (NAPS) network (with 289 sites across 216 communities) and the Canadian Air and Precipitation Monitoring Network with 30 rural stations. (120) The NAPS monitors long-term ambient air quality indicators (CO, NO_2, SO_2, O_3 and $PM_{2.5}$) using nation-wide standards assuring measurement accuracy, precision, comparability and representativeness. (119,120) These networks contain a limited number of monitoring sites (e.g. 1-30 sites within an urban area), which operate continuously to provide pollutant concentrations at high temporal resolutions.

On a regional scale, the Lower Fraser Valley network is composed of monitoring stations focused on visual air quality (i.e. visibility, haze) and airborne contaminants—both gaseous (O_3, CO, NO_2, SO_2) and particles ($PM_{2.5}$, PM_{10}). (121) Despite having 28 stations (22 in Metro Vancouver and 6 in Fraser Valley Regional District) in the network stretching between Horseshoe Bay and Hope, spatial gaps are still present. (121)

A shortcoming of these fixed-site monitoring networks is the limited capture of significant spatial patterns in common air pollutants; this is a threefold problem. Firstly, these monitoring sites are stationary and their arrangement is governed by restrictive siting criteria that consequently limit the number of suitable locations. (122) Siting considerations include the availability of electrical power, accessibility, local emissions sources, pollution transport, security, installation and shelter specifications, and land use characteristics. (123,124) Secondly, because these stations have high costs and maintenance requirements (i.e. electrically powered

temperature-controlled facilities requiring security), (125) the networks cannot be setup with adequate density or distribution to capture fine spatial variability. For instance, Vancouver has a monitor density of approximately one station per 160,000 individuals, or 5 monitoring sites per 1000 square kilometers. (126) Rather, these parsimonious fixed-sites are operated to generate data on urban background concentrations, regional air quality or intercity differences, with a strong focus on larger urban centers. Thirdly, NAPS locations have traditionally been chosen to avoid local pollution sources. (16) For example, Hystad et al., (122) applied the NAPS data to derive national air pollution models for $PM_{2.5}$, NO_2, benzene, ethylbenzene and 1,3-butadiene, but revealed in the process, the scarce availability of NAPS monitors near major roads (35 monitors within 500 m) and industrial emission sources (7 monitors within 500 m).

Traditional networks are fundamental and irreplaceable; nevertheless, provisions are being made to expand these networks to include additional near-road sites for TRAP and to improve spatial resolution. (16) Although this network expansion will provide valuable new information, these networks are still available to few organizations (e.g. government) and industries. (118,127) Due to the limited accessibility of these monitoring devices, the current state of air quality exposure monitoring cannot feasibly solve all the new and complex research questions that have arisen.

With an increased awareness of spatial variability in air pollution within cities and a better understanding of pollution gradients from traffic and neighborhood sources, such as residential wood combustion, (15,16) there is recognition of the need to also evaluate air pollution variability at local or neighborhood scales. TRAP can be surveyed in numerous ways though the most critical exposure data may be missing and/or unattainable due to an absence of air monitoring at certain positions.

Improved knowledge of spatial gradients in air pollution has informed the understanding of air pollution health impacts. For example, numerous studies have reported relationships between TRAP with a wide array of health effects including birth outcomes, (46,128) childhood and adult respiratory disease, (30,35,37,41,44,129–132) and cardiovascular effects. (24,133–135) In Canada, approximately 10 million individuals, an estimated 32% of the population, are prone to elevated TRAP exposure because they reside within 100 m of a major roadway or 500 m of a highway. (16) Of these 10 million people, 2 million live within 50 m of a major road. (16) Furthermore, an estimated 16% to 36% of Canadian elementary schools within the 10 largest cities are located in high traffic zones (within 75 m or 200 m of major roads, respectively). (136) Taken together, the magnitude of TRAP exposure and the evidence of health impacts in Canada, suggests TRAP is one of the most important air quality issues facing the country.

A meta-analysis by Zhou and Levy (13) estimated the spatial extent of various air pollutants from their source based on four categories: 1) reactive pollutants formed in the atmosphere (350 m); 2) reactive pollutants removed from the atmosphere (175 m), 3) inert pollutants with low background (140 m) and 4) inert pollutants with high background (1000 m or more). (13) Another systematic review by Karner et al. (96) confirmed similar results showing edge-normalized TRAP pollutants require distances between 115 m to 570 m to decay to background levels. Pollutants displayed either no trend with distance (e.g. particle mass concentrations), a consistent decay with distance (e.g. NO_2, benzene) or a rapid initial decay of at least 50% by 150 m, followed by gradual decay (e.g. CO and some particle number concentrations). (96) Besides proximity to pollutant sources, other variables such as meteorological conditions, topography and landscape, and infrastructure can all shape spatial air pollution patterns.

As spatial monitoring improves, pollution sources, hotspots, dispersion patterns and health effects can all be better addressed while reducing the reliance on predictive models (i.e. proximity, interpolation, land use regression (LUR), and dispersion models). Thus, there is a need to supplement conventional spatially dispersed air quality monitoring networks with alternative approaches that capture this fine level of variability. Passive sampling arrays, mobile monitoring, and emerging sensor technologies are all approaches that have been used to address spatial coverage. Overall, additional spatial monitoring can help advance model building and augment existing government monitoring networks to provide more reliable evaluations of TRAP.

1.3.1 Passive samplers

Passive or diffusive sampling has been employed in urban and rural ambient monitoring since the 1970s to measure gaseous pollutants. (137) Diffusive samplers can be distributed at numerous locations (including remote regions) because they are unobtrusive, relatively inexpensive (excluding lab charges), lightweight, small, practical, and not burdened by power requirements. (137,138) The versatility of these monitors is demonstrated in their ability to provide information on both coarse-resolution temporal changes (typically 0.5 or more days) if used in succession, and spatial patterns (if deployed simultaneously). (139) Passive samplers are able to quantify cumulative air pollutant exposures (i.e. total or average levels) with low detection limits given a sufficiently long sampling period. (131) With their low cost, large numbers of samplers can be deployed within an area of interest to give a snapshot of the air quality over a particular time.

Despite these strengths, passive samplers are inherently limited in providing information on short-term pollutant concentrations (less than a few hours) and are inadequate for accurately addressing regulatory compliance.

Krupa and Legge (138) contended that co-locating passive samplers may enable their use as calibration points for continuous monitors at discrete locations to assist air quality distribution mapping on variable spatiotemporal scales. Besides serving as calibration points for spatial mapping, the use of passive samplers has been influential in LUR model development for many Canadian cities. For example, in the LUR model created for Windsor, Ontario, a deployment of passive samplers (for 2 week durations in all seasons) was used to model and map concentrations of NO_2, SO_2 and VOCs. (140)

While diffusive samplers are, by definition, only applicable to gaseous or semi-volatile pollutants, there are some examples in which particle sampling has been conducted passively. Guéguen et al. (141) used a network of passive coarse PM samplers to determine chemical and isotopic signatures from ambient traffic and industrial pollution over a long collection period. In another study, Wagner et al. (142) monitored the distance, and downwind and upwind effects of agricultural burns with passive PM monitors.

Passive samplers are a good option for networks because they are portable, low in cost and simple to operate. Therefore, even operators with limited experience (including citizen scientists and mailed survey participants) can employ these monitors to conduct spatial sampling campaigns for gaseous pollutants with few to no restrictions on location. Important caveats, however, are that these samplers will generally exhibit low precision compared to active monitoring approaches and their requirements for increased sampling durations of hours to days. (138)

1.3.2 Mobile monitoring

Mobile monitoring relies on a mobile platform (typically a vehicle) equipped with continuous air pollution monitors and a global positioning system (GPS) to relate high-density measurements to precise locations within an area of interest. (143) Mobile sampling capitalizes on the ability to be in motion while gauging pollution concentrations at proximal or distal distances from sources. (144) Mobile sampling is efficient due to the capacity to traverse large distances in a confined timeframe with limited real-time instrumentation collecting at high frequencies. (57,59) As long as there is a continuous monitor for the specific pollutant(s) of interest, sampling is not constrained by what can be measured. In order to account for temporal changes due to meteorology or emission patterns, repeated samples can be collected and a mobile campaign can include a fixed-location reference site. (143) For example, Larson et al. (93) applied temporal adjustments from fixed-site data to their mobile measurements to develop a highly resolved composite map of wintertime woodsmoke in Vancouver.

This measurement approach is highly malleable and based on the objective of a study, it can be adapted to characterize spatial patterns in road dust, (146) woodsmoke, (147) conditions associated with temperature inversions, (83) and within street canyons. Mobile monitoring can more accurately communicate the exposures of traveling inhabitants by participating in urban traffic flow in vehicles, (148–150) on bicycles (150,151) or attached to pedestrians. (148,149,152) Hankey et al. (153) modeled non-motorized traffic (pedestrian and cycling) with negative binomial and ordinary least squares regression to estimate 12-hour non-motorized traffic counts in Minneapolis. As mobile units instantaneously integrate data, finer temporal variations like those noticed during vehicular acceleration, deceleration, cruising and idling might be acquired. (154) In Boston, a community-based approach involving high school students

carrying mobile monitors in backpacks showed that urban neighborhood spatiotemporal variability was more prominent for UFP compared to $PM_{2.5}$. (155) Mobile monitoring campaigns using bus and truck chasing tactics were at the heart of investigations of on-road transportation emissions (CO, BC, UFP) in Beijing leading up to the 2008 Olympic games. (156,157)

Alternatively, mobile monitors can be stationed at designated locations (e.g. a high traffic intersection) for a predetermined time period on the scale of hours to days to act as a pseudo monitoring station. (143) An example of the latter function of mobile monitoring is the use of a mobile air monitoring station to collect data on NO, NO_2, SO_2, $PM_{2.5}$ and PM_{10} at a site near the cruise ship terminal. (158) In another application, mobile monitoring data revealed patterns in pollution resulting from beach fires and regional wildfires. (159)

By employing mobile air quality monitors to enhance the information obtained from isolated fixed monitors, spatial resolution is enriched (160,161) and hotspot detection becomes possible for pollutants varying across small spatial scales. In the course of monitoring, mobile platforms may perhaps provide data for model development or evaluation. (143) Isakov et al. (162) demonstrated a method to depict spatiotemporal varying air toxic levels. In Los Angeles, mobile monitoring equipment for BC, UFP, $PM_{2.5}$, particulate matter-phase polycyclic aromatic hydrocarbons, NO_X, CO and CO_2 established concentration differences among freeways, arterial roads, and residential streets. (163) Bowker et al. (164) verified a Quick Urban and Industrial Complex model for studying the effects of roadside barriers on pollution patterns from a highway through mobile monitoring of UFP spatial distributions.

Despite all the benefits of mobile monitoring, drawbacks do exist. Firstly, this technique is not appropriate for routine use as it is very resource intensive. Secondly, confirmation of temporal trends can be difficult, since temporal coverage is incomplete. This results from the

discontinuity of the sampling campaigns. Thirdly, if monitoring is performed in vehicles, the measurements are restricted to roadways which overestimates human exposures as populations spend the majority of their time further from the on-road environment (e.g. in homes with setback distances and on sidewalks). Fourthly, inconsistent GPS signals may negatively impact uncertainty. (165) Finally, if the goal of sampling is to evaluate a specific pollutant source (e.g. wood smoke), then the sampling strategy must either be carefully tailored to meet those needs (e.g. cold, winter nights when ambient traffic is less of a confounder), or a more source-specific measurement approach should be used. (143)

1.3.3 Intra-urban air pollution modeling

In addition to the use of mobile monitoring and passive samplers to provide information on fine-scale spatial variability, modeling approaches have also proved to be useful.

LUR models have gained popularity since their initial development by Briggs et al. in the 1990's. (166) LUR models assimilate traffic and geographic covariates in the context of a geographic information system (GIS) to predict ambient air concentrations that are measured as part of a spatial monitoring campaign. (167) With stochastic modeling, the ambient concentration serves as the dependent variable in a multivariate regression with numerous independent variables (e.g. road type, elevation, traffic count, population density and land cover) to explain the spatial distribution. (143,167,168) Once the model is developed, pollutant concentrations can be predicted for unmeasured locations falling within the study domain since values of predictive variables are available at all locations. (167–169)

These empirical models are cost-effective, (169,170) and support efforts to identify hotspots or regions where robust monitoring is necessary. (171) Monitoring data can be gathered

routinely (i.e. by traditional fixed networks); however, unless these characterize the full distribution of pollutant concentrations and predictor variables, the model applicability will be limited. Models developed with purpose-designed monitoring (normally passive samplers for gases, active samplers for PM, or mobile monitoring campaigns) are preferred, as monitoring locations can be selected to ensure they are representative of the full spatial extent of ambient pollution and the predictive variables. (143,169) Purpose-designed monitoring tends to integrate data from one to four campaigns lasting one to two weeks each while continuous routine monitoring provides annual averages; consequently, the costs associated with LUR model creation are higher than routine monitoring alone. (169) The major shortcoming of LUR modeling is the inability to resolve meaningful short-term temporal trends though small-area spatial patterns can be determined. (171,172) To preserve the predictive power of LUR models, calibrations and/or adjustments may be necessary, especially if the model is applied retrospectively in temporally unstable environments. (173)

At present, published LUR models for TRAP have been developed and applied in nine Canadian cities for use in epidemiological studies. (16) In Vancouver, LUR models have been generated for pollutants including BC, (174) $PM_{2.5}$, (172) UFP, (175) and NO_x. (172,173) A recent review describes 25 LUR models from North America and Europe for pollutants such as NO_x, $PM_{2.5}$, and VOCs. (169) National LUR models have been generated for 5 pollutants (NO_2, $PM_{2.5}$, benzene, ethylbenzene and 1,3-butadiene) in Canada to capture both between-city and within-city variability. (122) In the United States, a national LUR model for NO_2 has also been developed. (176) Within Canada, researchers have assessed the intercity transferability of LUR models and concluded that it is feasible; however, the predictions will largely depend on consistencies between the urban designs of these cities. (177,178) A study in the Greater

Vancouver Regional District compared 3 methods (LUR modeling, spatial interpolation and a chemical transport model: the Community Multi-scale Air Quality (CMAQ) model) for assessing spatiotemporal variability. (126) The results implicated LUR models as having the finest spatial resolution (neighborhood-scale) compared to the other approaches (representing urban-scales). (126)

Dispersion models calculate receptor level concentrations based on idealistic Gaussian pollutant dispersion from their source. (179) The parameters incorporated into the model include emissions inventory databases (e.g. traffic volume, street configurations, vehicle makeup), atmospheric conditions, topography, source-receptor distances and time. (143,170,179) Emission inventories are fashioned by totaling the contributions of primary pollutants by source type: point source (e.g. power stations, industrial sites), line source (e.g. road links) or area sources (e.g. domestic space heating boilers in a grid square). (3) These models have been applied to both urban (e.g. episodic pollution events) and regional scales (e.g. pollution migration events). (170) Although regulatory uses are possible, dispersion models are constrained by a demand for high-quality input data and in some applications the need for high-power computing. (180) Comparisons between LUR and dispersion models indicate similar success in explaining variability in measured concentrations of air pollutants. (181) New approaches of hybrid models have been developed to combine the desirable features of both LUR and dispersion models to complement one another. (182–184)

Although their spatial resolution is defined by the availability of monitoring data, spatial interpolation methods (e.g. kriging), can be applied to construct continuous surfaces for pollution across large areas (180) when monitor placement is sufficiently dense. (170,185) In many instances, a high temporal resolution is achieved with accompanying measures of standard error

to estimate uncertainty. (170) A concern is that artifacts may result from interpolation, especially edge effects and poor characterization of pollutant sources and sinks. (170) One study in Los Angeles showed that universal kriging and an ad-hoc 2-step approach consistently outperformed LUR modeling in summer, autumn and winter months. (186)

Proximity models are straightforward and simple (typically depicting the proximal distance between a pollution source and a subject); nonetheless, the weaknesses in exposure classification have resulted in this approach being phased out in favor of more sophisticated methods mentioned earlier. These limitations might include: an incomplete characterization of exposures by disregarding secondary locations; ignoring time-activity patterns; neglecting vehicular fleet composition; and violating the principle assumption of isotropic dispersion by overlooking wind and topographic effects. (170)

As conventional monitoring sites only provide a partial representation of air pollution with limited spatial coverage, modeling supported by additional monitoring, can assist in extrapolations to un-sampled locations.

1.4 New sensor designs and applications

Until now, the discussion has centered on air pollution monitoring and modeling methodologies. New sensor technologies, largely driven by the enhancement of modern communication (e.g. cellular, Wi-Fi), have the potential to improve air pollution monitoring by filling some of the spatiotemporal gaps.

The sensor market has flourished in recent years resulting in economical (reduced purchase and maintenance costs), low powered, miniaturized, autonomous (and typically wireless) air quality monitoring units. Although these units may be less precise when first

marketed, later generations will likely demonstrate improved reliability and rigor. The merits of these instruments include the collection of real-time, location-specific, open-access data. Outputs may be utilized by the public as an educational tool in promoting air quality awareness while assisting individuals in time-activity pattern modifications to reduce harmful exposures to air contaminants. Included among the new technologies are smartphone applications, real-time data from solar-powered systems—such as the Village Green Project, remote and passive fence-line monitors, wearable sensors and wireless sensors. This revolution in sensors and related applications may afford sustainable solutions for applications in personal monitoring, education, hotspot screening, community-based monitoring, air monitoring network supplementation, ambient air monitoring networks or even compliance assessments. (187)

New sensor designs offer potential solutions to the inability of traditional air monitoring networks to fully characterize spatial variability. Moreover, these innovations, which act as dispersed continuous monitors, should experience no problems in capturing time-varying components of air pollution. In fact, it is this feature that is absent in LUR models and oversimplified in dispersion models. Unlike passive sampling, mobile monitoring, and ambient pollution modeling, these new sensors can communicate in real-time (much like routine monitoring networks) to a central data-processing server. This is advantageous since these sensor arrays can in theory instantaneously deliver high-resolution spatiotemporal data.

As new sensor technologies appear, major organizations are actively contributing to and paying close attention to the development and maturation of this growing research field. A European Union partnership project called CITI-SENSE is focused on evaluating the use of sensors in community directed environmental monitoring. (188) Likewise, the United States Environmental Protection Agency's (EPA) (187) "Draft Roadmap for Next Generation Air

Monitoring" presented several strategies to assist technology advancement and testing while articulating some goals to overcome gaps in these rapidly emergent sensing systems. A publication by the US EPA, Air Sensor Guidebook, offers considerations and assistance to developers and users of lower cost consumer-based (typically ranging from $100 to $2500) air quality sensor technologies. (189)

New measurement technologies can be envisioned for use in four main avenues including fixed network augmentation, source or industrial site monitoring, personal exposure monitoring and participatory sensing. (125,165) The first strategy is to supplement static air quality monitoring networks by increasing sensor density to enhance spatiotemporal assessment in areas where fixed measures are unavailable. In this way, micro-sensors can be fixed at specified locations (e.g. schools, intersections) or be secured onto mobile platforms (to systematically resolve spatial patterns). (165) An example of this hybrid network was deployed in the Lower Fraser Valley to study neighborhood-scale ozone. (190,191) This network of low-cost devices and traditional monitors demonstrated a capacity to produce reliable data; the traditional monitors were able to complement unstable low-cost sensors embedded in the network. (190,191)

A second approach surveys source emissions or industrial pollutants (within the facility or around the perimeter). (125) Sensor response is likely better at or near sources due to the higher concentrations. (165) Condensed monitoring networks (e.g. AQMesh (Environmental Instruments Ltd., UK) and Cairpol CairNet (Environnement S.A, France)) can thus be used to detect contributions from automotive exhaust, (192) industrial accidents, or fugitive emissions. (125) Fujita and Campbell (193) suggest that sensor networks may prove useful for early warnings of high releases at refineries. Wan et al. (194) have proposed the use of sensor

networks in natural gas pipeline monitoring. Recently, Bennett et al. (195) applied an electrochemical gaseous sensor array to assess the effect of baffles on aircraft exhaust plumes at an airport perimeter. Mobile mounted platforms have also been used to test for the impact of ship emissions. (196,197) These examples illustrate the broad scope of applications that are conceivable with new sensor arrays.

In view of the fact that people are constantly on the go, moving between environments and changing their time-activity patterns, fast-response sensors can be used to improve estimates of individual-level exposures and the parameters that predict them. For instance, information from smartphone embedded sensors can be gathered to make better estimates of travel patterns (e.g. Personal Environmental Impact Report), locations visited, and hence, exposures. (198) Body-worn sensors (e.g. Sensorcon Sensordrone (Sensorcon, USA), universal serial bus pluggable sensors (e.g. Cairpol CairClip (Environnement S.A, France)), and Bluetooth transmissible sensors for cellular devices (e.g. CITI-SENSE) all facilitate personal exposure monitoring. (163) These sensors may be beneficial to sensitive populations, such as asthmatics. (165)

Finally, citizen science (also called crowdsourcing, citizen observation or participatory monitoring) is the notion that data accumulated by individuals (scientists and non-scientists alike) can be pooled to produce distributed datasets on personal, regional or global scales. This shift from restricting monitoring to professional organizations (e.g. researchers or government) to everyday people is made possible by cheaper and easy-to-operate instruments. Participant sensing initiatives have even begun projects to build and operate do-it-yourself sensors and sensor networks (e.g. Air Quality Egg (Kickstarter, USA) and AirCasting (HabitatMap, USA). However, citizen science can also be a source of concern as it is prone to issues in data quality,

data consistency, data interpretation and user privacy. To avoid such uncertainties, efforts should be made early on to educate users on the use and potential limitations of crowd-sourced data. (165,187)

Before new technologies are introduced in the following sections, it is important to emphasize the difference between sensors, and the devices and networks that contain them. Air pollution units, nodes, monitors, devices and systems may include one of two (or both) categories of sensors in their designs. Individual sensors can be created in-house by the vendor of the device (to match the needs of the monitor, i.e. purpose-driven designs) or they can be purchased from other manufacturers as ready to install, off-the-shelf sensors. Few sensing systems seem to integrate new purpose-designed sensors (e.g. Cairpol CairNet (Environnement S.A, France) and Sensorcon Sensordrone (Sensorcon, USA)); instead, monitors tend to depend on commercially available sensors.

1.4.1 Sensor operation

The abundant sensor technologies available today have exciting implications for personalized air quality monitoring, community-led sensing initiatives, network supplementation, and source and facility management as the devices are shrinking in size and becoming more affordable. Regardless of how they are applied, these new sensors and their use in distributed networks have the potential to improve spatial resolution of air pollution research, and boost public awareness. (187)

Most sensor development has focused on measurement of gaseous criteria pollutants; however, sensors for hazardous air pollutants (HAPs) and particles to aid enforcement and compliance regulations are also in need. (187) There is also a deficiency in devices to measure

the chemical speciation of PM, with the exception of the micro-Aethalometer (AethLabs, USA) for BC measurements. (125,199) Finally, HAPs detectors are few and far between; yet, the available ones tend to not be actively tested when exposed to complex mixtures of HAPs. (125)

As most of the sensors discussed are gas sensors, a brief overview of the qualities and limitations of electrochemical, metal oxide semiconductor (MOS) and infrared (IR) sensors are provided. Appendix A provides more details on their principles of operation.

Electrochemical sensors measure analyte concentrations related to changes in redox potential after the gas undergoes an electrochemical reaction with the sensing electrode. (200) Electrochemical sensors tend to be used to measure common air pollutants such as NO, NO_2, CO and O_3. (165,201) New miniaturized sensors (roughly 20 mm) are low in cost and power (i.e. in the hundreds of milliwatts range) consumption. (165) Mead et al. (201) demonstrated the ability of new electrochemical sensors to achieve low detection limits to the parts per billion level, while providing low noise and high linearity. Fairly consistent deviations in linearity of 2-5% (sometimes up to 10%) can occur in electrochemical gas sensors. (165) To maintain long-term stability of 2-15% per year, oxygen exposure is continually needed. (165) Interference cannot be eliminated (165); however, optimizing the sensing electrode's selectivity, integrating electrolytes efficient in carrying charge, and installing chemical scrubber filters (e.g. activated charcoal) above the sensing electrode can all reduce cross sensitivity. (200)

On the other hand, if an electrochemical sensor is highly sensitive, the capillary (the opening through which the gas enters) is generally less restricted and the membrane is typically more porous, thereby compromising sensor signal and operating life as it deteriorates with faster electrolyte evaporation. Life expectancy is generally 1-3 years but differs with gas exposure and environmental conditions. Temperature sensitivities are managed with internal temperature

compensation mechanisms. Humidity fluctuations change the ability of water vapor to pass the hydrophobic barrier; if a sensor is compatible for measuring low gas concentrations, the barriers are more porous and can pose a greater problem. (200)

MOS sensors measure gas concentrations by monitoring resistance or conductivity changes in the metal oxide sensing layer when gases undergo electrochemical reactions at this boundary. (165) These sensors weigh a few grams and are roughly a dozen millimeters in size. (165) MOS sensors are used frequently as a result of their low cost, short response time, and long lifetime. (202,203) In addition to this, they respond to a wide range of gas concentrations (few ppb to thousands of ppm). (165)

MOS sensors suffer from poor selectivity and high cross-sensitivity. (203) A limitation of this sensing method occurs when temperatures digress too far from the optimal sensing temperature, thus allowing non-target gas components to be more reactive than the desired gas. (203) On the other hand, if two gases had a large enough gap separating their optimal sensing temperatures, then one sensor could be adapted with a thermostatic cycle (for the sensing element) to relay between the temperatures in order to detect both constituents. (203) To compensate for drift in MOS sensors, recalibration efforts are necessary. (165)

Because some resistive sensors need elevated temperatures for measurement, power consumption moderation is important. One solution incorporates micro-heaters (with mixed tin dioxide particles and multi-walled carbon-nanotubes) and uses temperature pulsed methods with brief heating intervals. (204,205) Finally, prolonged recovery times may render MOS sensors impractical for certain devices when gas concentrations vary suddenly. (203)

In an IR sensor, when an IR light source is incident on a gas, the radiated energy is absorbed and the detector converts the electromagnetic energy or temperature changes into

measurable electrical signals. (206) Increases in availability of IR sensors have occurred in parallel with the advances in powerful amplifiers and electronic components. (206) IR gas detectors are small (often a few millimeters in size) and consume only a few hundred milliwatts of power. (165)

As gases are frequently reactive and/or corrosive, they may shorten sensor lifetime and induce drift. (206) This is prevented in IR instruments, since the target gas does not interact directly with the detector; instead, it only contacts the light beam and the chamber's entrance (which can be made anticorrosive or replaceable). (206) Therefore, sensor life expectancy is more than 10 years. (206) IR sensors do not experience loss of sensitivity since they are created to recognize gas molecules by their unique absorption peaks. (206) Cross sensitivities can occur in hydrocarbon detection with IR sensors because they share similar absorption characteristics (for the carbon-hydrogen bond). (165) Conversely, CO_2 detection is highly sensitive as these molecules have distinctive absorption bands. (165) By performing zero calibration checks, accuracy is preserved. (206)

Concerns with IR gas sensors include time dependent light intensity changes from contamination leading to a zero drift. One way to guard against this is to use a two-detector arrangement where one acts as an active detector and the other as a reference. Because IR detectors sense temperature, they are susceptible to ambient temperature fluctuations and perform even worse with sudden changes. Ambient temperatures are slow to alter, so performance outdoors is not severely hindered. If water vapor condenses on the optics or detector, the units may become faulty. For this reason, the sensors are run at temperatures marginally above surrounding temperatures. IR analyzers can die if humidity is especially high, as contamination and corrosion become serious issues. (206)

1.4.2 Wireless Sensor Networks

Wireless sensor networks (WSNs) can provide real-time communication while gathering and processing massive amounts of data. WSNs have been applied to environmental monitoring as well as agriculture (e.g. monitoring temperature, humidity, animal behavior and movement patterns), indoor living (e.g. home security systems and fire detection), industry (e.g. power grid and oil and gas pipeline sensing), medicine (e.g. body area sensor networks for monitoring vital signs in patients), and the military (e.g. ad-hoc deployment to detect and track enemy intrusion). (207–212) Their environmental applications include monitoring and management of traffic conditions, weather, and air quality. Sensors integrated in these networks are typically small, inexpensive, and power efficient. Battery-powered sensor nodes have four components: 1) sensors and microcontrollers that accomplish the task of pollutant measurement and data processing; 2) memory which stores data; 3) transceivers that transmit and receive data; and 4) a power unit. Because sensor nodes are densely deployed, they can rely on cooperative multi-hop communication to selectively transmit partially processed, pertinent data. This multi-hop communication to the sink node for data fusion expends less power than single hop communications. Remote control of these nodes is possible by users via the Internet once all sensor nodes communicate with one another and the sink node. (207,213)

Wireless sensor arrays have the potential to form the foundation of dynamic, real-time, dense monitoring networks for use in a wide variety of applications. Because these devices are inexpensive compared to traditional fixed-site regulatory stations, it is feasible to complement existing networks by placing wireless sensors at new locations. Additionally, a wireless dispersed sensor array can augment the power of public communications tools such as the AQHI to support the public in conscientious decision-making (e.g. route planning) based off of fine-

scale spatially resolved air pollution levels; this aligns well with the goals of air quality management agencies such as Metro Vancouver's Integrated Air Quality and Greenhouse Gas Management Plan which includes an aim to increase public understanding and engagement on the topic of air quality. (214) The portability and ease of use of these sensors can also allow researchers the opportunity to study horizontal and vertical spatial patterns in pollutant dispersion, which may in turn provide insight to exposure mitigation.

The primary concerns for WSNs are sensor performance (i.e. data validity and data quality). (215,216) While much of the available and emerging WSNs are accessible to consumers, only a limited number have undergone evaluations. (217) In addition, signal connectivity, reliable maintenance, hardware failure, and flexibility in adding, removing or changing the number of stations may also limit their performance. (207) Other limitations may surface such as the sensor's energy efficiency (that could compromise network lifetime), usability, standardization, security, and area coverage (dependent upon the number of deployed sensors). (215,216) A summary of other next generation air monitors is available on UBC cIRcle. (218)

1.4.3 Sensor performance and characterization

Presently, there is a lack of testing to ensure adequate sensor performance prior to marketing such instruments. While manufacturers and sales representatives are able to provide detailed specification sheets, there is little guarantee that the specifications can actually be met in a real-world setting. (202) In comparison, existing reference stations housed in proper enclosures can be fairly exact when it comes to meeting monitor descriptions. (226) Data quality is a pertinent concern as poor or unknown quality may be worse than a lack of data and can lead to

incorrect or inappropriate decisions. (125) The US EPA (187) recognizes that data from new monitors may not be on par with data generated by reference instruments; however, they expect that reliability will grow with time.

In 2013, the US EPA proposed that next generation air monitoring could be classified into 5 tiers by cost of instrument and anticipated user group. (187) Since 2014, the classification scheme has evolved to include suggested performance goals for i) precision and bias error and ii) data completeness. (189) The five tiers now target applications in: I) Education and Information (for all pollutants: requiring precision and bias error <50%, data completeness ≥50%), II) Hotspot Identification and Characterization (all pollutants: <30%, ≥75%), III) Supplemental Monitoring (criteria pollutants, air toxics (including VOCs): <20%, ≥80%), IV) Personal Exposure (all pollutants: <30%, ≥80%) and Regulatory Monitoring (requiring precision and bias error <7% for O3, <10% for CO and SO2, <15% for NO2, and <10% for PM2.5 and PM10 while requiring data completeness ≥75%). (189)

Snyder et al. (125) argue that monitoring objectives may not demand that sensors meet robust monitoring benchmarks; rather, users need to acknowledge the uncertainty and performance specifications. By using sensors in larger arrangements, confidence in measurements may be improved; this is the concept of "do more – less well". (125,187) Because of this, it is critical to match data quality requirements to sensor performance and network scope. The discussion below focuses on two phases of data quality assessment (laboratory and field evaluations). Afterwards, there is an examination of calibration, data integration and processing.

1.4.3.1 Laboratory evaluations

Controlled laboratory testing of sensors is a necessary step; so, standardized protocols should be developed to evaluate next generation air monitors. According to the EPA, most sensors have not undergone validation and few developers have air quality expertise; therefore, they advocate the creation of tables to help developers and users understand pollutants (e.g. sources, health effects, ambient ranges, acceptable detection limits), performance objectives (e.g. accuracy, precision, detection limit), the frequency of monitoring specific pollutants, and how appropriate mobile or stationary monitoring may be with the application on hand. (187)

Currently, no lower cost sensors evaluated by (or formally submitted to) the US EPA was able to meet the strict requirements for regulatory monitoring using the 2014 Tier V criteria. (189) Other field and lab assessments are available from the Air Quality Sensor Performance Evaluation Center. (219)

Parameters that should be evaluated include accuracy, which measures how exact values are (in comparison to reference instruments or known concentrations) and precision (assessing inter-sensor correlations in high density networks). The closeness of agreement between successive measurements at same conditions (repeatability) and at different conditions (reproducibility) should also be determined. (200) Selectivity, sensitivity and interference all describe the ability of a sensor to discriminate a constituent within a mixture.

Certainly, for a sensor to be valuable, the detection limit and range needs to encompass the concentrations found in ambient air. (202) Response and recovery times are particularly important during mobile campaigns because the measurements need to keep pace with the travelling monitor. Drift (the change in a zero or span calibration with time) and operating temperature and humidity conditions are also important for proper sensor function. (200)

Controlled exposure facilities may provide an environment for sensor designers to test parameters like the ones listed above. (187)

Examples of some in-house, bench experiments that can be performed include bump tests, step tests and stability tests. In a bump test, the sensors are dosed with a gas concentration for a nominal time interval, followed by a no exposure period. This is then repeated. From this iterative testing protocol, sensor response, response rate and hysteresis (or the dependence of system on recent history) can be checked. Step tests are performed by successively increasing gas concentrations in phases (with or without intermediate zero air exposures). By this test, response time, and saturation can be determined. Alternating gases between step tests without air exposures verifies cross-sensitivities that may exist. Stability or drift tests are accomplished by letting the system respond to a stable gas concentration over a prolonged time. (202)

Other criteria to assess prior to enrolling sensors into the real-world testing phase should filter based on size, power, communications and data storage, cost, and availability. Systems should be of portable size for deployment on persons and ought to be suitable for setup in areas that are not enclosed with heating or cooling requirements. Having a battery powered option lasting several hours is preferable. These sensors need to provide real-time data communication or store data locally for subsequent export. Regarding cost, for feasible application in spatial arrays (i.e. near-road), a cost of a few hundred dollars per unit is preferred. Finally, sensing systems need to be commercially available or be adaptable for monitoring purposes. (202)

The US EPA's Sensor Evaluation Report describes an initiative to compare nine institutions (O_3 and NO_2 sensors) using extensive laboratory-based sensor performance trials against reference analyzers at the National Exposure Research Laboratory. Overall, sensors exhibited excellent linearity (typically $R^2 > 0.9$) across a large challenge range (upper testing

conditions of > 200 ppb) and displayed low ppb range sensitivity with good to excellent precision. In addition, the trailed sensors often displayed short rise and lag times (~ 1 min) with little evidence of hysteresis indicating usability in non-static environments (i.e. continuous or near-continuous monitoring). However, exposure to relative humidity and temperature extremes showed a wide range of performance including sensors failing to report the challenge concentration. Similarly, susceptibility to interference from mixtures of O_3, NO_2 or SO_2 varied largely (from <3 ppb interfering responses to a failure to report an output). (220)

In another US EPA lab study, five next generation air monitors for VOCs were subjected to known concentrations of benzene that are environmentally relevant (<25 ppb). If the response was adequate for the first test, a secondary exposure to a tri-mix (including benzene, 1,3-butadiene, and tetrachloroethylene) was conducted. Coefficients of determination for the benzene test were found to be 0.90 for UniTec SENS-IT and 0.78 for APPCD-PID while the three-component coefficients of determination were 0.93 and 0.79, respectively. The 3 other sensors (ToxiRAE- PRO, CanAirIT and CairClip) failed to properly detect benzene concentrations below 25 ppb. (221)

The South Coast Air Quality Management District performed a number of laboratory chamber co-locations compared to Federal Reference Methods, Federal Equivalent Methods, or the Best Available Technology instrument on sensors with successful field evaluations. At conditions of 20℃ and 40% relative humidity, PM sensors (R^2 of 0.87-0.99) and gas sensors (R^2 of 0.82-0.99) both yielded comparable results (R^2) to their reference counterparts. (219)

1.4.3.2 Field evaluations

Once performance is deemed appropriate in controlled environments, a second stage of assessment should involve real world testing, as laboratory tests and performance cannot emulate field conditions entirely. (165) With small, focused field studies, operational issues that may arise during deployments may be evaluated beforehand. (202) Hence, it is advised that sensors be appraised next to reference monitors in a range of unknown environments to safeguard its performance.

Apart from the usual set of sensor parameters mentioned (to be tested in the lab), key elements for field investigations include linearity, environmental sensitivity and short-term responsiveness. Linearity between sensor pairs is typically appraised using ordinary least-squares regression models and coefficients of determination (for precision) and root mean squared error (for accuracy). (222) Real-world studies are scarcer than laboratory tests and sensors often show less convincing results in ambient conditions because of extraneous factors (e.g. meteorological conditions, real emission sources) that can influence performance. (165) In a paper by Holstius et al. (222), instrument sensitivity to three external factors—temperature, humidity and ambient light— were explored in their field testing strategy. The examiners also mentioned the logistic challenges of setting up observational calibration since it requires access to a monitoring site for an extended time period in close proximity to the co-located sensor. Short-term responsiveness of sensors should be measured in the real-world as sensor deviations from expected readings are possible (Figure 1.1). This parameter may be expressed as a number of deviations greater than or less than a percentage range (around the real concentration, as measured by the standard method).

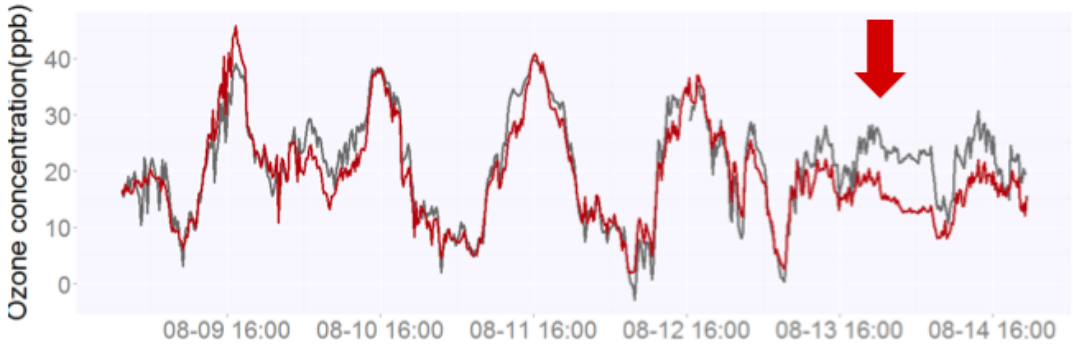

Figure 1.1 Co-location results from a field test for an ozone sensor (grey) against an ozone monitor (red). The red arrow indicates one instance of sensor deviation from the reference. Reprinted with permission from Mykhaylova et al. (223)

Other considerations that call for attention are data analysis and interpretation given the sensor platforms' variable responses to environmental conditions (e.g. temperature and relative humidity). Data privacy should also be an area of concern since confidential data must be secured (e.g. password protected access). With respect to user privacy, citizen science initiatives should be addressed since reverse engineering of data has the potential to expose private information (e.g. location). (224) To deploy sensors, usability is also a major concern. Here, issues such as the ease of installation, operation, data management, having a user-friendly interface and sufficient quality wireless communication need to be factored into the examination of sensors.

The US EPA's Air Climate & Energy research program has engaged in efforts to evaluate an array of low cost sensor technologies; summarized below are some of the key findings from this program. A month-long co-location of eight PM devices on a PM monitor test platform found that most sensors displayed short duration responses (on the order of 1 sec); however, results weighted over 1 to 5 minutes better depicted general ambient conditions (rather than instrument noise). These studied sensors showed linearity less than 0.8 (R^2) with some sensors

having little to no statistical significance (R^2<0.1). Both particle counters and algorithm-based particles mass concentration sensors had comparable results. A wide variability was noticed in the response of sensors to temperature and relative humidity extremes. Six of the eight devices had a relative humidity limit of 90% or 95% meaning the instruments no longer produce reliable measurements beyond that relative humidity level. (225)

More recently, the US EPA evaluated two PM sensor technologies, Carnegie Mellon Speck and the PerkinElmer Elm (formerly, Airbase CanarIT) in a 45-day winter co-location next to a field reference instrument. Sensor agreement was poor for Speck (R^2 = 0.04) and no relationship was discerned for Elm (R^2 = 0.0001). Once again, relative humidity greater than 95% had a poor impact on sensor output. (226)

The South Coast Air Quality Management District tested sensors in side by side field deployments with Federal Reference Methods, Federal Equivalent Methods, or the Best Available Technology instruments. The sensors were housed in custom-made aluminum enclosures to protect against elemental conditions (e.g. windblown rain, sunlight, animals). Results of the 30 to 60 day co-locations show PM (R^2 of 0.0-0.98) and gas (R^2 of 0.0 -1.00) sensor performance varied dramatically depending on the technology tested. (219)

1.4.3.3 Calibration, data integration and processing

Quality control and quality assurance of data integration and processing begins with calibration. Calibrations are important to alleviate sensor aging effects, humidity effects and interference effects. Low-cost sensors are often purchased as uncalibrated or factory calibrated units not intended for low concentration (or ambient) measurements. Normally, manufacturer

calibrations rely on 2-3 gas concentration measurements at one temperature and humidity; thus, users should re-calibrate devices to suit their needs. (227)

To tackle the problem of sensor calibration, one remedy is to use two nearby sensors. If two sensors are exposed in similar environments at similar times and experience similar gas concentrations, the sensors can improve one another's calibration quality. To do this, temporal and spatial filtering preserves relevant calibration sequences for input into calibration algorithms to compute calibration parameters. Hasenfratz et al. (227) proposed two novel on-the-fly calibration algorithms besides the traditional forward calibration based on measurements of a perfect sensor (a single-hop calibration). "Forward calibration" is completed with recent sensor readings to estimate new calibration parameters, "backward calibration" re-evaluates the latest calibrated sensor readings offline (causing a delay) to estimate calibration parameters, and "instant calibration" gains similar accuracies to backward calibration without delay by continually adjusting calibration parameters based on new calibration sequences and earlier calibration sequences stored in calibration memory. Instant calibration can reduce measurement error by a factor of 2 compared to forward calibrations. (227)

Multi-hop calibrations are used to calibrate sensors that are rarely or never near perfect; instead, they depend on unreliable sensor readings. Essentially, a concentration is computed by weighting measurements of unreliable sensors by the calibration age (i.e. time elapsed since most recent calibration and the quality of the reference used in that calibration). In short, accuracy can be maintained so long as the total number of calibration hops is limited. (227)

Three potential methods for data integration and processing are possible and will be outlined here. The first method is data fusion; it is implemented by sensor node cross-communication when tuning sensors within networks. (228) By aggregating sensed data from

multiple nodes, the decision quality at the base station is improved. (228) Data fusion can be parallel, where all nodes send raw data to the base station directly, or serial, where routing is used, or hybrid. (228) Sensor fusion is complementary (sensors are independent but data is pooled to give a holistic perspective), cooperative (using independent sensors to get data that would not be acquired by a single node) or competitive (redundant measurements made with independent sensors). (228) Tan et al. (229) have suggested a two-tiered architectural framework where the first tier is a local calibration and the second tier is a system-level calibration.

The second method uses a "sensor array detection" whereby sensor replicates are incorporated into a single monitor. The underlying premise is that using redundant and multidimensional sensors for each pollutant of interest can increase sensitivity (by correcting for drift) all while detecting multiple pollutants and mixtures. From calibrations and near-road inter-comparison of instruments, Mykhaylova et al. (223) noted increasing correlation in ozone measurements (at ambient conditions) with increasing numbers of ozone sensor replicates (especially when 2 types of ozone sensors were used). When temperature and humidity sensors were added to further correct ozone measurements, the associations strengthened still. (223)

A third method relies heavily on server-based post-processing (e.g. AQMesh (Environmental Instruments Ltd., UK)). This means there is a black box of algorithms that is run on the inputs prior to presenting the outputs to the user. When a cloud network processes data, two advantages are seen. First, the system may conserve power, as the processor requires less power. Secondly, sensor specific parameters are assimilated in the calculations during cloud computing to correct for gas responses. In the case of AQMesh, field measurements from each individual sensor undergoes correction factors specific to that sensor as documented at the time of production. These inherent corrections maintain accuracy and include temperature sensitivities

and calibration coefficients. Another integral correction factor depends on the cross-sensitivities of gas sensors; this means the algorithm may be using the response of one gas to smooth the response of another gas. (230)

1.4.4 AQMesh

The AQMesh technology is discussed in more detail as this instrument was selected for use in this thesis.

AQMesh battery-powered wireless units were designed in partnership with the University of Cambridge to monitor five gaseous pollutants with Alphasense sensors. Table 1.1 outlines the technical specifications of the AQMesh units that were used. Newer generations of AQMesh have additional sensors for particulate matter ($PM_{1,}$ $PM_{2.5,}$ PM_{10} and particle count), noise and NO_x. (231)

Table 1.1 AQMesh specifications. Reprinted with permission from Geotech. (232)

Electrochemical Gas Sensors	**Range (ppb)**	**Accuracy (ppb)[2]**	**Limit of Detection (ppb)**
NO	0-20000	±5	<3
NO_2	0-200	±5	<5
O_3[1]	0-200	±5	<5
CO[3]	0-50000	±10	<5
SO_2[3]	0-100000	±10	<5
Other Sensors	**Range**	**Accuracy[2]**	**Limit of Detection**
Pod Temperature (℃)	-20 to 100	±2	0.1
Pressure (mb)	500-1500	±5	1
Humidity (%RH)	0-100	±5	1

[1]Reading given using digital signal processing, thus needs a number of data points to give comparable readings to reference instruments; last readings will be projected in a straight line. Data is retrospectively corrected with new input data.
[2]Under stable temperature and humidity, without interference at 20 ℃ and 80% RH.
[3]Optional sensors

The small size (150 x 180 x 200 mm), light weight (< 2 kg) and battery operation of AQMesh devices makes them adaptable to urban hotspot and traffic monitoring, fence-line monitoring, or industrial plant fugitive emissions monitoring. AQMesh units are well suited for installations on lampposts, signposts, fences or walls and can function in network arrays with hundreds of units. This technology incorporates electrochemical gas sensors with a fourth electrode to increase stability and combat drift. Precision is maintained by reducing noise levels in the circuit to a few parts per billion. According to the manufacturer, it also uses proprietary catalyst loading and stack structure to certify steady operation at low concentrations. Relying on mobile general packet radio service (GPRS) technology limits signal access, but roaming with modern telecom networks can overcome this problem. Battery trickle charging gives short power bursts to connect the wireless GPRS link for data transmission. The data is uploaded to a multi-user, password controlled web browser-based server where data is processed, accessed, and downloaded. Algorithms correct for temperature sensitivities, calibration coefficients and factors for each sensor pod. (230,232–234)

The AQMesh system had undergone some field-testing against reference air quality monitors. Figure 1.2 shows the results from a Version 3.0 comparison conducted by Geotech in November 2012. (230,233)

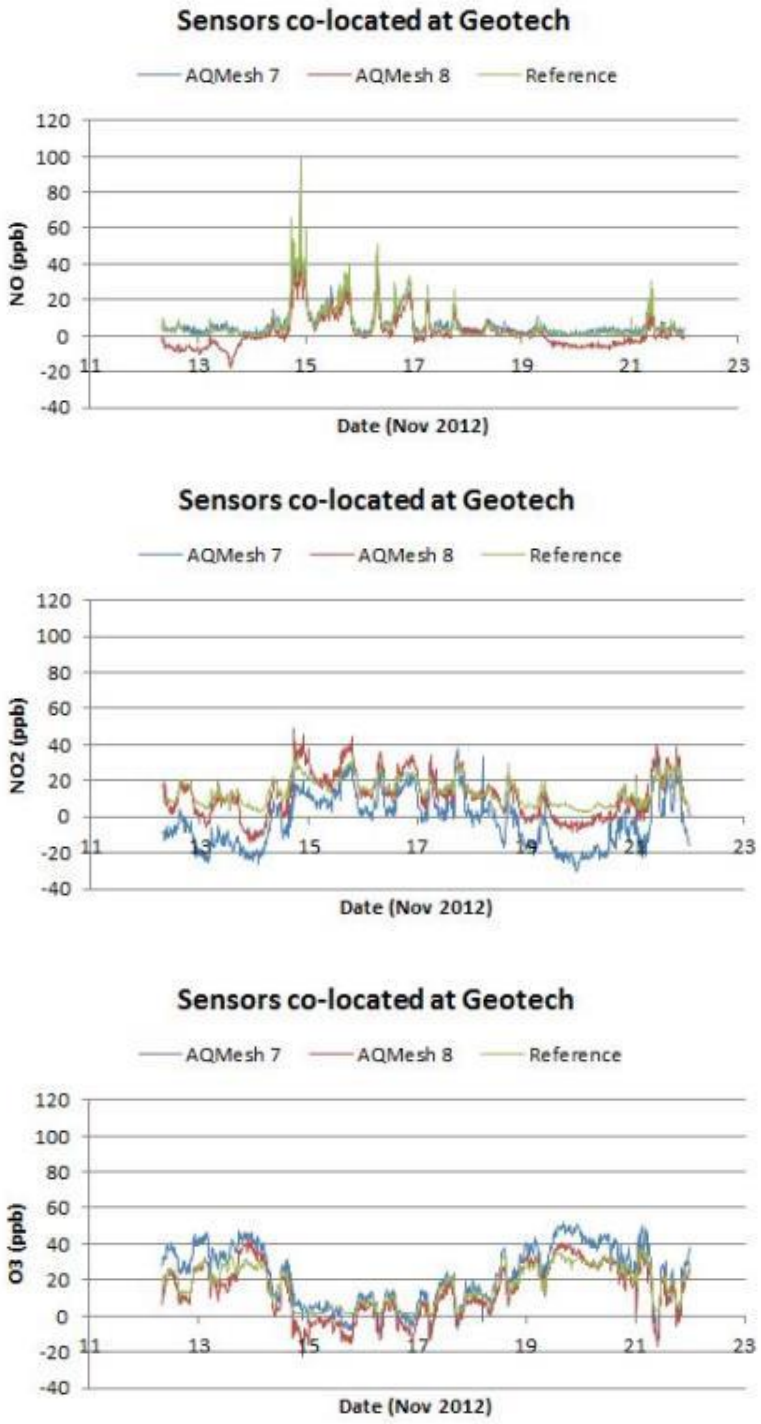

Figure 1.2 AQMesh (Version 3.0) co-location test results for nitrogen monoxide, nitrogen dioxide and ozone. Reprinted with permission from Geotech. (230)

1.5 Rationale

Rapid urban densification and an enhanced understanding of the health consequences of air pollution exposure has placed an urgency on the need to understand intra-urban TRAP as populations gather and pollution sources aggregate. Currently, characterization of TRAP relies heavily on the use of traditional air quality monitoring, passive badge monitoring, mobile monitoring and spatial modeling. However, gaps in outdoor pollution monitoring persist due to weaknesses in the ability to discern pollution trends across time and space. Manufacturers of air pollution equipment and citizen scientists alike are introducing new instruments and methods (e.g. crowd-sourcing) to meet the challenge of gathering spatiotemporal air pollution data in cities.

This research focuses on evaluating the near-roadway sensor performance of a new technology—AQMesh. AQMesh was selected for two reasons. Firstly, a side-by-side comparison was already underway in London, so it was decided that concurrent monitoring in another location would better capture its usability elsewhere. Dr. Ben Barratt of the Environmental Research Group at King's College London led this effort in London. Secondly, the AQMesh air monitors aligned well with the criteria for 2013 Tier IV instruments as outlined by the United States EPA in the "Draft Roadmap for Next Generation Air Monitoring". Tier IV instruments should be: 1) between $5,000 and $10,000 in cost and 2) designed for regulators (the anticipated user group) to enable supplementation of existing ambient and source monitoring. (187) Thus, AQMesh may be used to supplement present regional (Metro Vancouver) and national (Environment Canada NAPS) air quality monitoring networks.

Intra-urban air pollution varies depending on pollutant sources, meteorology, and

infrastructure; one important cause of this variability is the street canyon effect. Presently, it is understood that street canyons can elevate TRAP; however, this avenue of research is still emerging and the bulk of street canyon studies focus on the microenvironment within a canyon. This study designed a model to identify potential urban street canyons. The model can be applied to various metropolitan areas using relatively accessible data sources.

1.6 Objectives

Specifically, this thesis aims to address these two objectives:

1. To evaluate a wireless sensor technology, AQMesh, (with CO, NO, NO_2, O_3 and SO_2 sensors) in a field study by co-locating these units in Vancouver and London with traditional reference monitors.
2. To create a simple model for identifying potential urban street canyons and to appraise this model using mobile monitoring techniques to determine if canyons are an important predictor of intra-urban TRAP concentration variability.

Chapter 2: Comparing AQMesh air quality monitors to traditional air quality monitoring stations

2.1 Methods

2.1.1 Instrument setup and data collection

This study tested the comparability of gaseous air quality measurements made by an autonomous system, AQMesh (Figure 2.1), when co-located with two regulatory air quality monitoring stations situated in London, England and Vancouver, Canada.

Figure 2.1 AQMesh unit (left) equipped with the solar shield and the pipe clamps (right)

In Vancouver, three instruments (pods 45150, 239150, 240150) were deployed near the Robson Square Metro Vancouver fixed air quality monitoring station. Instruments were setup after gaining approval from Al Luongo, the Manager of the Utilities Management Branch at the

City of Vancouver. Instruments were fixed to the lamp post using circular pipe clamps and fabricated cross beams.

In London, the four instruments (pods 157150, 160150, 163150, 165150) were secured to pipes with smaller diameters with cable ties as pictured in Figure 2.2.

Figure 2.2 Six AQMesh pods attached to the pipe railing using cable ties. Reprinted with permission from Barratt, B. (235)

2.1.2 Site details

In Vancouver, the AQMesh instruments (measuring CO, NO, NO_2, O_3 and SO_2) were co-located near the Vancouver-Downtown Station (Station ID: T1) of the Lower Fraser Valley Air Quality Monitoring Network. The Vancouver-Downtown Station (49.2823° N, 123.1219° W) in

Robson Square Complex is situated below ground in a concrete walled room with an air intake that extends upwards to 3.8 m above ground (Figure 2.3). This station is located in a heavily trafficked area with varied multiple-story and high-rise residential and commercial buildings. The air intake is 15-20 m from the one-way road, Hornby Street, which has two lanes, a parking lane and a divided bike lane. Due to the station's underground construction, no AQMesh units could be located immediately beside the air intakes. Instead, the three AQMesh units were installed approximately 25 m from the air intake on the nearest lamppost (post reference number: 4/8). The units were mounted on the post at 120-degree angle offsets from one another (i.e. 0°, 120° and 240° if viewed from above). These instruments were fixed at heights between 3 m and 4 m aboveground. For clarity of the AQMesh positioning, refer to Figure 2.3. (236)

Figure 2.3 Curved air intake of the Vancouver-Downtown Station (in silver) and the lamppost (in black) on which the AQMesh were attached (left). Left image reprinted with permission from Doerksen et al. (236). Two of the three units installed on the lamppost (right).

Unlike the below ground configuration of the Vancouver-Downtown Station, the London co-location site (UK-AIR ID: UKA00315) is housed in a ground level air-conditioned cabin a meter from Marylebone Road, which has six lanes of urban traffic (Figure 2.4). This Marylebone Road Station (51.522530° N, 0.154611° W) is part of the King's College London Automatic Urban and Rural Network (AURN) and will be referred to by its abbreviation, MY1 from this point onward. The four AQMesh units (measuring CO, NO, NO_2 and O_3) were positioned on top of the reference site so each unit was within 100 cm of the gas inlet (Figure 2.2 and Figure 2.4). (237)

Figure 2.4 Marylebone Road AURN Station (left) and the view from the North (right). Reprinted with permission from the Department for Environment Food & Rural Affairs. (237)

2.1.3 Study duration

The instrument co-location was conducted between May 16, 2014 and April 21, 2015 in Vancouver and between January 1, 2014 and December 31, 2014 in London. The shorter co-location time period in Vancouver was a result of unforeseen delays in instrument acquisition.

In Vancouver, two units (pods 239150 and 240150) were setup on May 16, 2014 and the third unit (pod 45150) was deployed to the same location at a later date, June 13, 2014, as a result of a delay in shipping the mounting bracket for the demo unit. Solar shields were fixed on the units on August 16, 2014; this date also marks the end of the co-location for pods 45150 and 240150.

In London, two units (pods 157150 and 163150) were deployed on January 1, 2014 and two more instruments (pods 160150 and 165150) were deployed at a later date, May 1, 2014.

2.1.4 Data downloads, quality and conversions

Co-location analyses were conducted using the 15-minute (or hourly) averaged AQMesh "final readings" which were exported from the online user platform, Envirologger (http://www.envirologger.net/login.aspx?ReturnUrl=http%3a%2f%2fwww.envirologger.net%3a80%2fdefault.aspx). The comparisons were performed on these final readings rather than another data form (i.e. raw, pre-scaled or scaled readings) as the proprietary AQMesh Version 3.0 algorithms (used until December 2014) were applied to the pre-processed data to arrive at the final estimates of outdoor pollutant levels. Moreover, the final outputs were assessed since the raw outputs may not be readily available to all AQMesh users. Downloaded data had no applied user offsets. An exception to this was the deleted data recovered from the backend server for a demo unit in Vancouver, AQMesh 45150, which had variable user offsets indicated.

Three operating statuses were automatically flagged in the data export: below LOD (limit of detection <5 ppb), rebasing (period when pods are calculating a baseline and determining the cross-gas correction algorithms) and stabilizing (period lasting up to 5 days post pod re-location to a different climate). Occurrences of these statuses were recorded but omitted in subsequent

analyses, as measurements taken under these conditions were deemed sub-optimal for co-location comparisons.

Reference data for Vancouver and London were obtained from Envistaweb (https://envistaweb.env.gov.bc.ca/) and London Air (https://www.londonair.org.uk/london/asp/datadownload.asp), respectively. For ease of analysis in R, the Vancouver reference data was converted to Greenwich Mean Time from Pacific Standard Time. Hourly averaged reporting of Metro Vancouver data was used because this was the smallest time base available. All of the data was reported as being preliminary; that is, quality assurance had not been completed at the time of analysis. Ken Reid at Metro Vancouver was able to provide validated gas data for 2014 for the Vancouver-Downtown Station (T1). As T1 lacks meteorological monitoring, data from Richmond-Airport (Station ID: T31) was used to address this gap. Ideally, meteorological parameters from Vancouver-Kitsilano (Station ID: T2) would be applied to downtown Vancouver because of the proximity, but this site was out of commission throughout the study duration.

The 15-minute averaged AURN gas sensor data for London Marylebone Road Station (MY1) had already undergone a rigorous ratification procedure while the local temperature data was indicated to be provisional. Other London-scale meteorological conditions were obtained from the hourly-based import KCL command in the openair R Package (Version 1.1-0): Tools for the Analysis of Air Pollution Data. The MY1 concentration data (expressed in $\mu g/m^3$) was converted to ppb for comparison with AQMesh data using standardized factors at a temperature of 293K and a pressure of 101.3 kPa. (238,239) The applied conversion factors were 1 ppb = 1.1642 $\mu g/m^3$ for CO, 1 ppb = 1.2473 $\mu g/m^3$ for NO, 1 ppb = 1.9125 $\mu g/m^3$ for NO_2 and 1 ppb = 1.9957 $\mu g/m^3$ for O_3. (238,239)

2.1.5 Statistical analysis

Hourly or 15-minute averaged AQMesh concentrations were compared with the corresponding concentrations measured by reference stations (T1 for Vancouver and MY1 for London) using descriptive and evaluation statistics. The descriptive statistics included count, mean, standard deviation, minimum, median and maximum. Evaluation statistics were calculated to explain the correlation between AQMesh and standardized instruments. The statistics for assessing accuracy and precision/repeatability were root mean square error (RMSE) and the coefficient of determination (R^2), respectively. Percent bias was also computed to characterize the tendency for the various AQMesh gas sensors to bias measurements in a predictable direction (e.g. overestimate or underestimate true concentrations). Formulas for these statistical parameters are presented in Table 2.1. No spatial or temporal adjustments were required since the instruments were co-located.

Table 2.1 Formulas for evaluation statistics

Statistic	Abbreviation	Formula	Optimal Value [Range]
Coefficient of determination	R^2	$R^2 = 1 - \frac{\sum_{i=1}^{n}\left(x_i^{Ref.} - x_i^{AQMesh}\right)^2}{\sum_{i=1}^{n}\left(x_i^{Ref.} - \bar{x}^{Ref.}\right)^2}$ $where\ \bar{x}^{Ref.} = \frac{1}{n}\sum_{i=1}^{n} x_i^{Ref.}$	1 [0, 1]
Root mean squared error	RMSE	$RMSE = \sqrt{\frac{1}{n}\sum_{i=1}^{n}(x_i^{AQMesh} - x_i^{Ref.})^2}$	0 [0, +∞]
Percent bias	% Bias	$\%Bias = \frac{\sum_{i=1}^{n}(x_i^{AQMesh} - x_i^{Ref.})}{\sum_{i=1}^{n}(x_i^{Ref.})} \times 100\%$	0 [-∞, +∞]

Visual representation of data quality for co-located AQMesh instruments, such as accuracy and precision in tracking fluctuating pollutant concentrations, were illustrated using time series and scatter plots. As certain meteorological states are expected to impact ambient pollutant levels (e.g. temperature, relative humidity, wind speed, seasonality), further investigations were completed through the generation of correlation matrices.

Computer software used in the analyses included: R, Version 3.2.1 (© R Foundation for Statistical Computing, 2015), RStudio, Version 0.99.903 (RStudio, Inc., 2016) and Microsoft Excel 2011 (Microsoft® , Redmond, WA, 2011).

2.2 Results

2.2.1 Descriptive statistics

Instrument modes of operation that were flagged and omitted across the 15-minute time averaged concentrations are summarized in Table 2.2 and Table 2.3. Server errors led to AQMesh 45150 reportedly having no flagged statuses after data retrieval; however, this anomaly is likely not representative of the real dataset judging by the number of flagged statuses on co-located pods.

Table 2.2 Summary statistics for flagged modes of operation in Vancouver AQMesh pods. n is the total number of flagged statuses while N is the total number of records.

AQMesh ID	Gas Sensor	Operation Status			Omitted Data	
		Below LOD	Rebasing	Stabilizing	n	n/N (%)
45150 (N=6096)	CO	–	–	–	0	0.0
	NO	–	–	–	0	0.0
	NO_2	–	–	–	0	0.0
	O_3	–	–	–	0	0.0
	SO_2	–	–	–	0	0.0
239150 (N=32608)	CO	3051	388	484	3923	12.0
	NO	24997	388	484	25869	79.3
	NO_2	4475	–	–	4475	13.7
	O_3	13829	–	484	14313	43.9
	SO_2	15	–	–	15	0.1
240150 (N=8800)	CO	679	196	–	875	9.9
	NO	6506	196	–	6702	76.2
	NO_2	1282	–	–	1282	14.6
	O_3	146	–	–	146	1.7
	SO_2	–	–	–	0	0.0

Table 2.3 Summary statistics for flagged modes of operation in London AQMesh pods. n is the total number of flagged statuses while N is the total number of records.

AQMesh ID	Gas Sensor	Operation Status			Omitted Data	
		Below LOD	Rebasing	Stabilizing	n	n/N (%)
157150 (N=35040)	CO	2622	202	–	2824	8.1
	NO	9586	196	6	9788	27.9
	NO_2	6535	–	–	6535	18.7
	O_3	4212	–	–	4212	12.0
160150 (N=23483)	CO	1861	186	–	2047	8.7
	NO	5344	186	–	5530	23.5
	NO_2	841	–	–	841	3.6
	O_3	1404	–	–	1404	6.0
163150 (N=35040)	CO	2634	192	–	2826	8.1
	NO	11654	186	6	11846	33.8
	NO_2	4968	–	–	4968	14.2
	O_3	10485	–	–	10485	29.9
165150 (N=23482)	CO	1778	192	–	1970	8.4
	NO	3971	186	6	4163	17.7
	NO_2	8385	–	–	8385	35.7
	O_3	54	–	–	54	0.2

Table 2.4 and Table 2.5 outline the descriptive statistics for all the co-located AQMesh and the air quality reference instruments. From these tables, it is clear that the AQMesh instruments in Vancouver were inadequately flagging the limits of detection as 6 of the 15 AQMesh sensors reported minima below the recorded limit of detection (5 ppb). This trend was not apparent in the London dataset and hence can explain some of the difference in performance between London and Vancouver. A possible explanation for the high frequency of flagging limits of detection in Vancouver is negative sensor drift. Both London and Vancouver AQMesh relied on the same processing algorithm (Version 3.0). In general, the results from London showed a higher degree of consistency when compared with the results from Vancouver. This is

true for both situations: between pairs of AQMesh sensors and between AQMesh sensors and the nearby reference sensors.

Table 2.4 Descriptive statistics of CO, NO, NO_2, O_3, and SO_2 concentrations for co-located AQMesh pods and the T1 Vancouver reference station. N is the total number of hourly averaged records. Mean, standard deviation (SD), minimum (Min), median and maximum (Max) are in ppb.

Gas	Instrument	N	Mean ± SD	Min	Median	Max
CO	T1 Ref.	7833	348.3 ± 175.3	90.0	300.0	1560.0
	45150	1524	269.8 ± 130.9	5.4	265.8	1514.2
	239150	7641	544.1 ± 1945.0	5.1	116.0	18392.9
	240150	2110	111.3 ± 231.0	5.1	88.7	9794.6
NO	T1 Ref.	7918	24.4 ± 24.9	0.2	16.8	196.2
	45150	1524	10.2 ± 15.3	0.0	1.5	114.9
	239150	2114	196.0 ± 1552.4	-723.9	30.5	25958.3
	240150	681	23.2 ± 18.9	5.0	17.6	179.3
NO_2	T1 Ref.	7918	17.2 ± 6.1	2.0	16.9	44.2
	45150	1524	15.6 ± 11.0	0.0	15.3	50.9
	239150	7245	39.5 ± 15.4	5.0	40.4	102.2
	240150	2006	18.1 ± 8.6	5.0	17.0	51.0
O_3	T1 Ref.	7896	6.9 ± 7.4	-0.6	4.1	39.9
	45150	1524	15.3 ± 9.2	0.0	15.2	46.3
	239150	4759	18.9 ± 10.5	-60.6	18.1	52.0
	240150	2171	26.3 ± 9.2	5.3	25.7	59.2
SO_2	T1 Ref.	7892	1.5 ± 1.3	0.0	1.2	18.8
	45150	1524	4.4 ± 5.1	0.0	3.1	68.3
	239150	8152	45.6 ± 36.4	5.5	42.7	1781.4
	240150	2200	42.3 ± 27.1	16.4	38.2	1057.5

Table 2.5 Descriptive statistics of CO, NO, NO_2 and O_3 concentrations for co-located AQMesh pods and the MY1 London reference station. N is the total number of 15-minute averaged records. Mean, standard deviation (SD), minimum (Min), median and maximum (Max) are in ppb.

Gas	Instrument	N	Mean ± SD	Min	Median	Max
CO	MY1 Ref.	33323	450.1 ± 241.7	0.0	429.5	3951.2
	157150	32216	200.7 ± 169.0	5.0	155.2	2004.0
	160150	21436	166.2 ± 136.2	5.0	132.1	1463.5
	163150	32214	171.2 ± 144.9	5.0	138.3	3959.4
	165150	21512	174.2 ± 141.1	5.0	137.6	1424.2
NO	MY1 Ref.	33908	124.7 ± 94.6	1.1	99.0	705.7
	157150	25258	105.7 ± 89.9	5.0	78.2	721.6
	160150	17953	106.7 ± 93.8	5.0	75.2	625.1
	163150	23200	108.7 ± 95.8	5.0	78.9	651.6
	165150	19325	103.7 ± 90.3	5.0	73.6	649.6
NO_2	MY1 Ref.	33907	49.3 ± 22.3	4.0	45.8	201.7
	157150	28505	32.8 ± 20.2	5.0	29.1	151.1
	160150	22642	39.8 ± 23.5	5.0	34.5	146.0
	163150	30072	41.6 ± 23.8	5.0	37.7	177.3
	165150	15097	28.5 ± 18.6	5.0	23.8	114.7
O_3	MY1 Ref.	32771	7.0 ± 6.3	-0.4	4.8	38.5
	157150	30828	31.0 ± 12.4	5.0	31.1	97.0
	160150	22079	37.6 ± 14.2	5.0	37.3	107.2
	163150	24555	23.1 ± 11.7	5.0	21.7	79.2
	165150	23428	1157.4 ± 2777.3	5.0	47.5	10053.9

2.2.2 Evaluation statistics

Figure 2.5 and Figure 2.6 show the hourly averaged concentrations from AQMesh pods and reference stations for Vancouver and London, respectively. One pollutant is displayed per panel for viewing considerations. The portion of the plots where no data is presented relates primarily to periods when the AQMesh pods were not co-located. Some of the data gaps could also be due to data exclusion from suboptimal operating statuses. These graphs visually describe the trends seen in the descriptive tables earlier on.

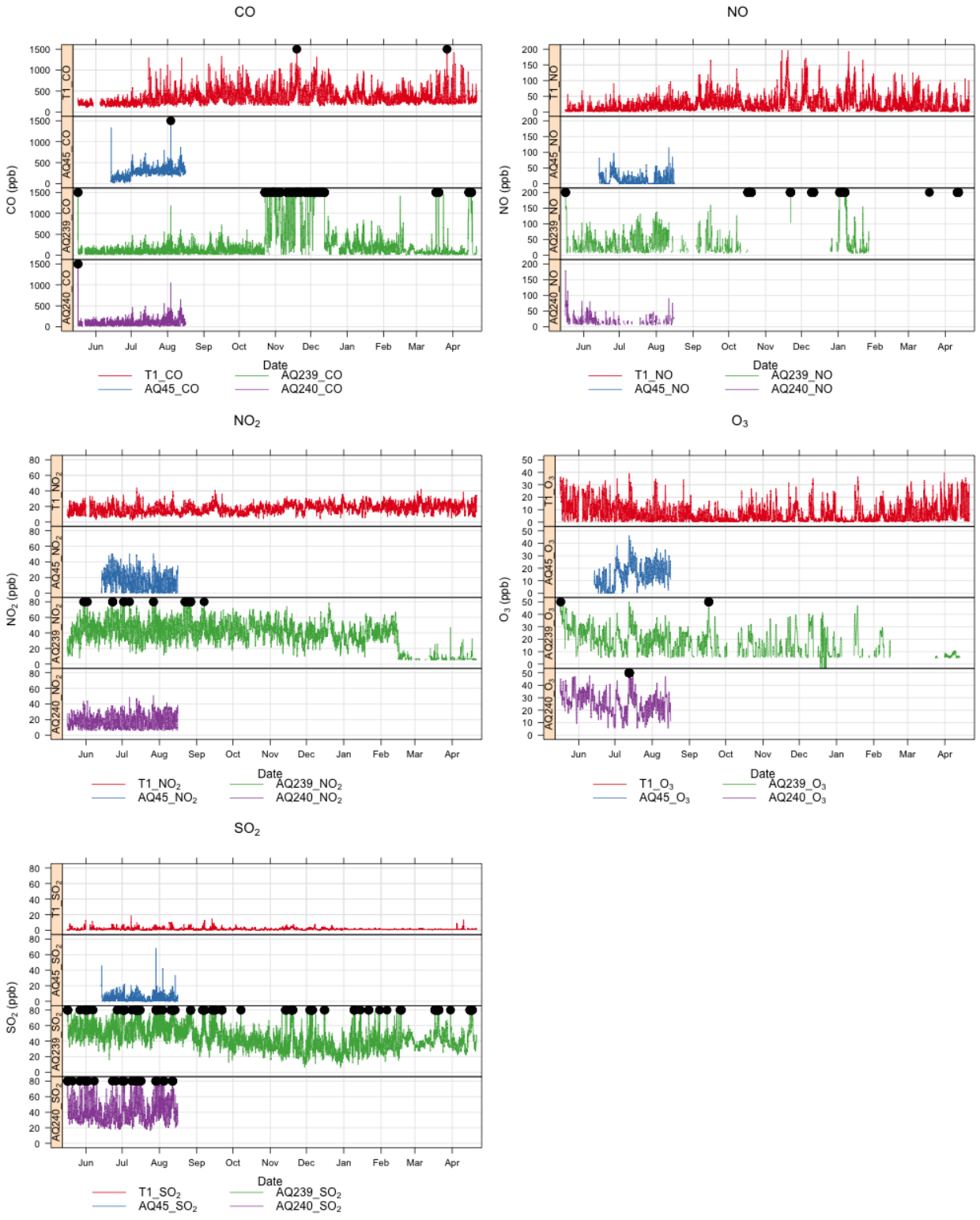

Figure 2.5 Hourly averaged time series plots for the concentration of pollutants as measured by AQMesh and the T1 Vancouver reference station. The black dots indicate concentrations that exceeded the y-axis cutoff.

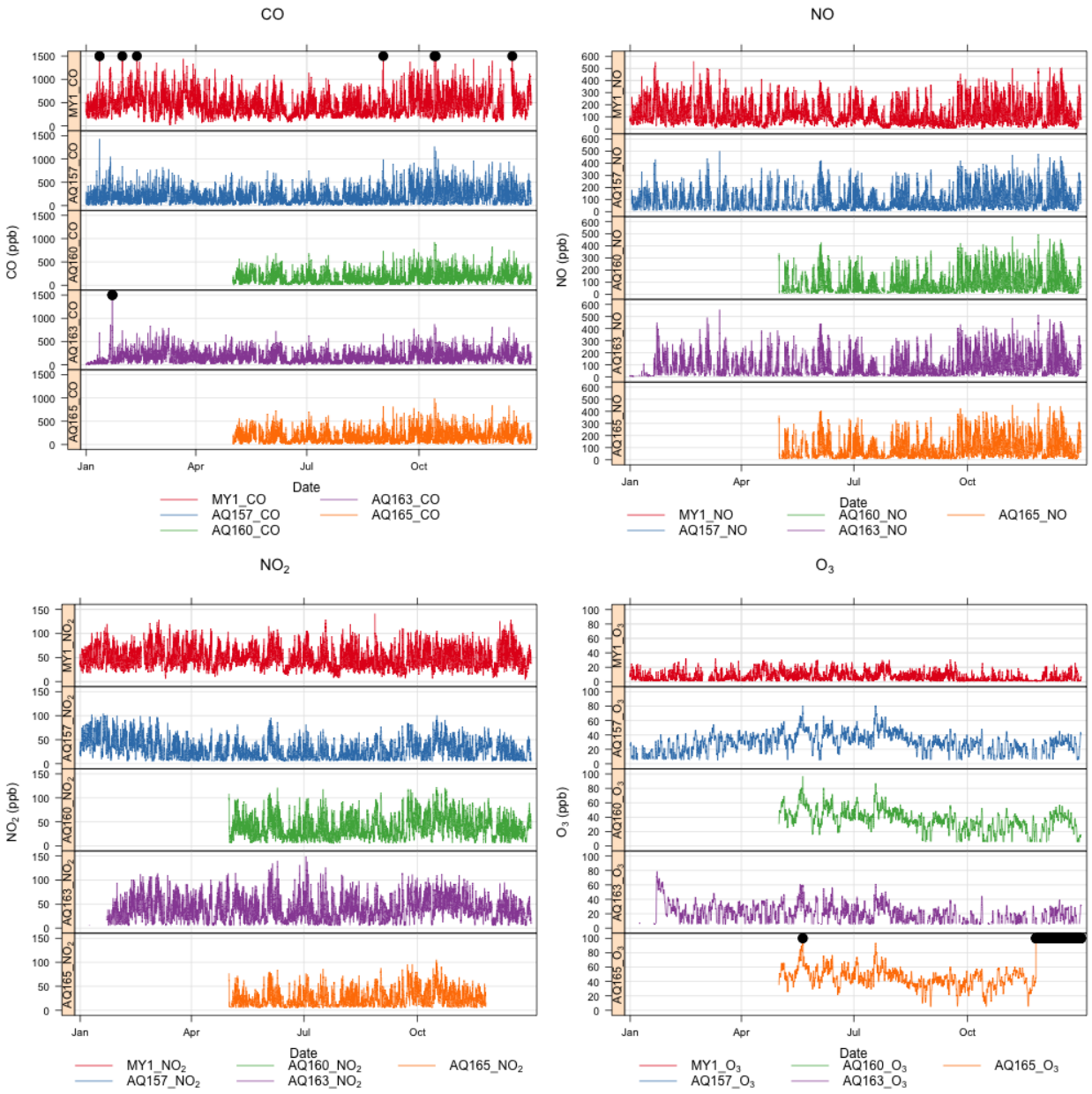

Figure 2.6 Hourly averaged time series plots for the concentration of pollutants as measured by AQMesh and the MY1 London reference station. The black dots indicate concentrations that exceeded the y-axis cutoff.

In Table 2.6 and Table 2.7, the evaluation statistics and the simple linear regression equations are summarized for Vancouver and London, respectively. In each entry, the statistics are calculated for the AQMesh sensor using the appropriate reference sensor. The coefficients of determination (R^2) highlight the stronger correlation of London AQMesh sensors to their reference (MY1) when compared with the R^2 results from Vancouver AQMesh sensors to their reference (T1). This is illustrated in Figure 2.7 and Figure 2.8.

Table 2.6 Evaluation statistics for co-located AQMesh pods as compared to T1 Vancouver reference station.

Gas	Instrument	R^2	RMSE (ppb)	% Bias	Regression Equation
CO	45150	0.186	141.4	-2.5	T1[CO] = (AQ45[CO] x 0.438) + 159
	239150	0.021	1964.2	57.5	T1[CO] = (AQ239[CO] x 0.013) + 347
	240150	0.016	295.0	-56.0	T1[CO] = (AQ240[CO] x 0.0648) + 252
NO	45150	0.091	18.4	-37.5	T1[NO] = (AQ45[NO] x 0.273) + 13.6
	239150	0.001	1589.6	639.5	T1[NO] = (AQ239[NO] x -0.000484) + 27.4
	240150	0.001	25.0	27.7	T1[NO] = (AQ240[NO] x 0.0311) + 17.3
NO_2	45150	0.021	11.7	8.2	T1[NO2] = (AQ45[NO2] x 0.0789) + 13.3
	239150	0.006	27.8	133.6	T1[NO2] = (AQ239[NO2] x 0.0311) + 15.7
	240150	0.058	9.9	23.6	T1[NO2] = (AQ240[NO2] x 0.169) + 11.6
O_3	45150	0.099	12.0	85.7	T1[O3] = (AQ45[O3] x 0.249) + 4.42
	239150	0.219	14.1	117.3	T1[O3] = (AQ239[O3] x 0.341) + 2.26
	240150	0.345	18.0	158.9	T1[O3] = (AQ240[O3] x 0.529) + -3.74
SO_2	45150	0.004	5.9	157.1	T1[SO2] = (AQ45[SO2] x 0.0205) + 1.62
	239150	0.010	57.5	2856.0	T1[SO2] = (AQ239[SO2] x 0.00339) + 1.39
	240150	0.000	49.2	2377.4	T1[SO2] = (AQ240[SO2] x 0.000953) + 1.67

Table 2.7 Evaluation statistics for co-located AQMesh pods as compared to MY1 London reference station.

Gas	Instrument	R^2	RMSE (ppb)	Bias (%)	Regression Equation
CO	157150	0.517	312.0	-56.7	MY1[CO] = (AQ157[CO] x 1.03) + 258
	160150	0.481	314.7	-61.7	MY1[CO] = (AQ160[CO] x 1.17) + 238
	163150	0.293	349.6	-62.4	MY1[CO] = (AQ163[CO] x 0.906) + 300
	165150	0.479	307.3	-59.7	MY1[CO] = (AQ165[CO] x 1.13) + 235
NO	157150	0.711	66.7	-27.1	MY1[NO] = (AQ157[NO] x 0.929) + 47.1
	160150	0.805	52.9	-22.3	MY1[NO] = (AQ160[NO] x 0.911) + 40.3
	163150	0.671	72.5	-28.1	MY1[NO] = (AQ163[NO] x 0.841) + 60.2
	165150	0.823	49.0	-21.0	MY1[NO] = (AQ165[NO] x 0.953) + 32.8
NO_2	157150	0.336	28.3	-38.5	MY1[NO2] = (AQ157[NO2] x 0.631) + 32.6
	160150	0.516	19.1	-17.3	MY1[NO2] = (AQ160[NO2] x 0.668) + 21.6
	163150	0.504	19.9	-18.1	MY1[NO2] = (AQ163[NO2] x 0.659) + 23.5
	165150	0.436	28.9	-45.0	MY1[NO2] = (AQ165[NO2] x 0.764) + 30.2
O_3	157150	0.139	26.5	322.0	MY1[O3] = (AQ157[O3] x 0.191) + 1.44
	160150	0.166	33.1	416.1	MY1[O3] = (AQ160[O3] x 0.178) + 0.602
	163150	0.072	19.1	184.1	MY1[O3] = (AQ163[O3] x 0.15) + 4.7
	165150	0.015	3028.9	16501.0	MY1[O3] = (AQ165[O3] x -0.000268) + 7.35

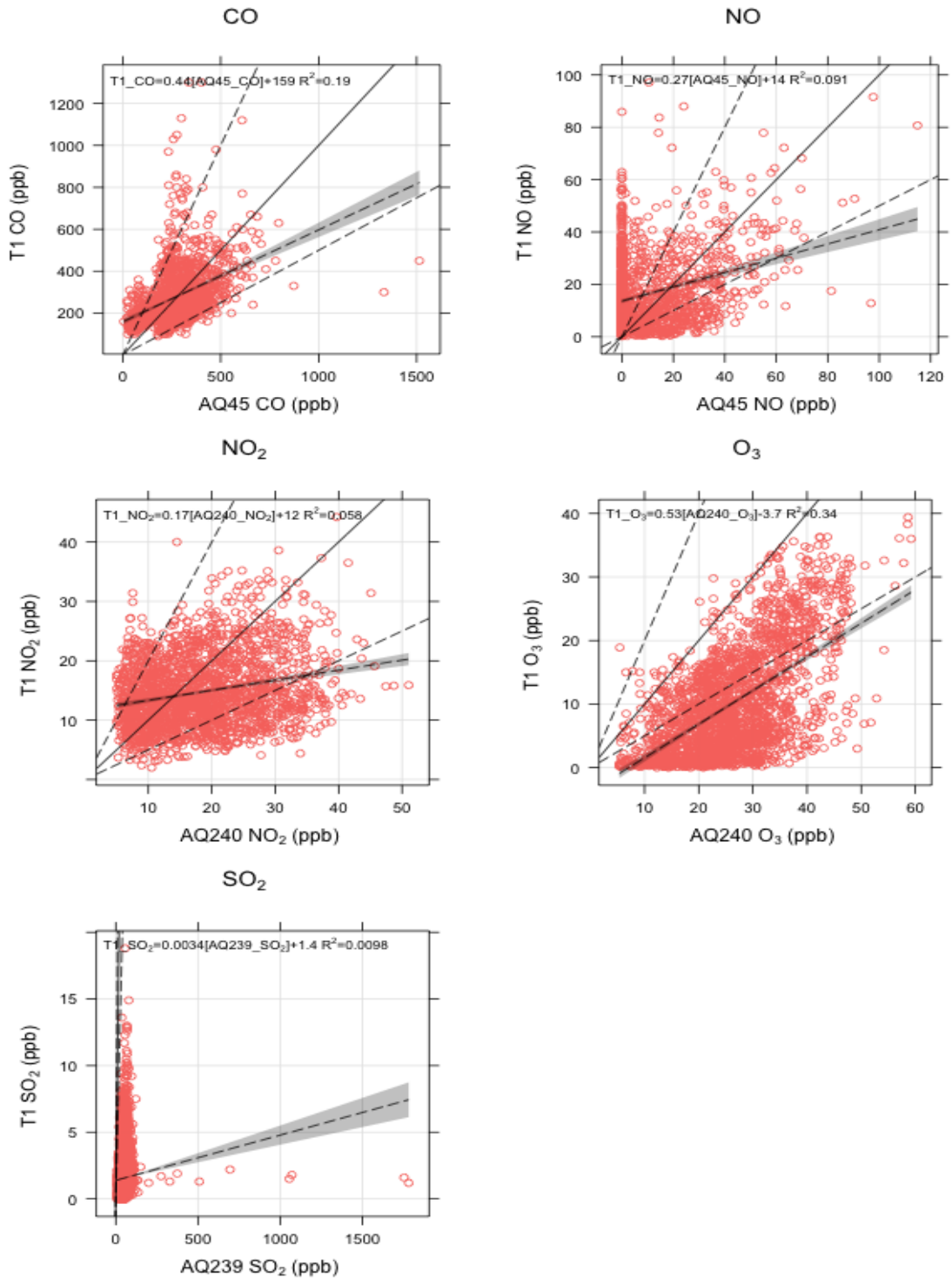

Figure 2.7 Scatter plots for the highest coefficients of determination (R^2) per pollutant in Vancouver. Three reference lines are included: the 1:1 solid line and the 1:0.5 and 1:2 dashed lines. The line of best fit is drawn as a dashed line with the 95% confidence interval shaded in grey.

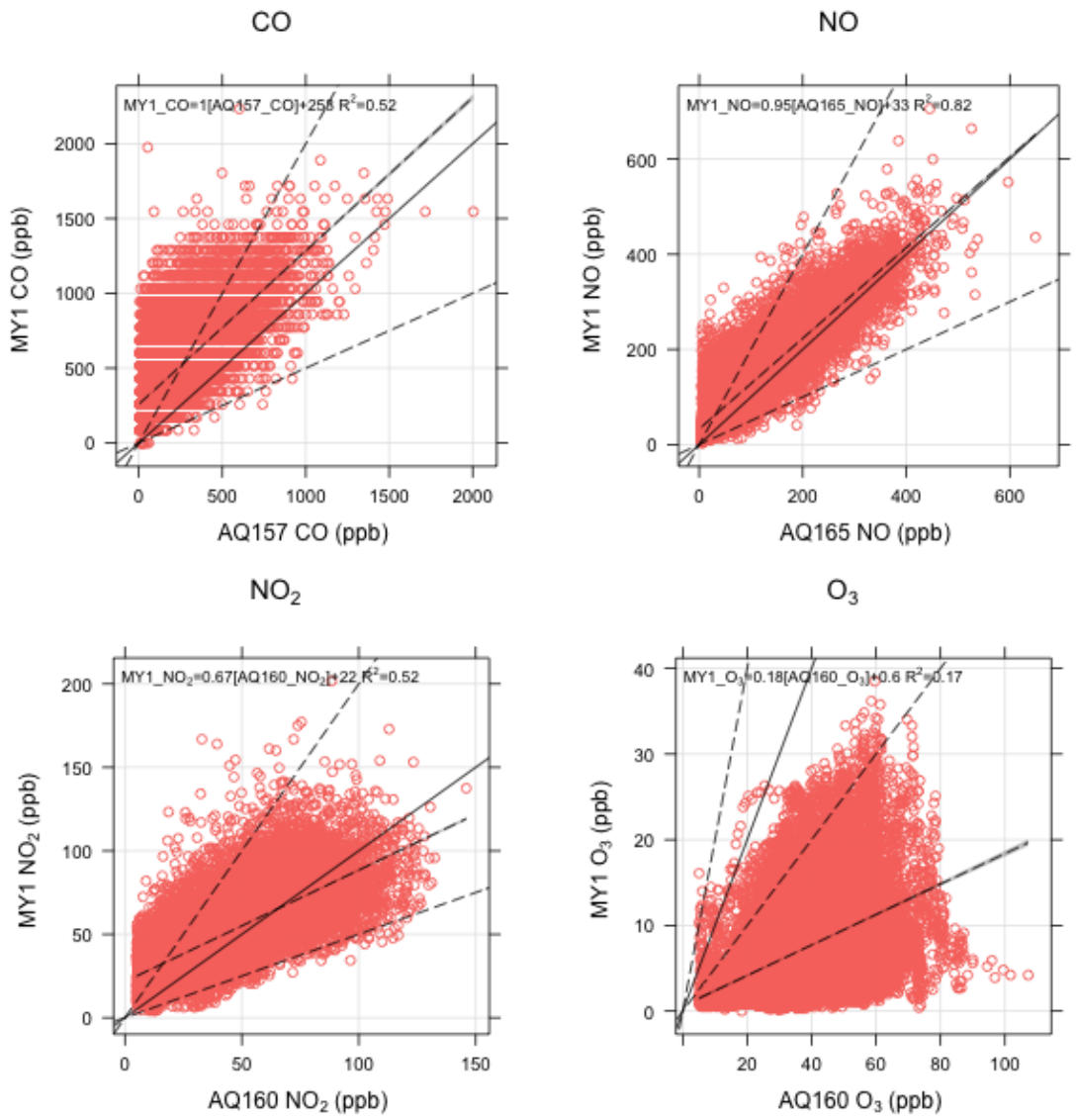

Figure 2.8 Scatter plots for the highest coefficients of determination (R^2) per pollutant in London. Three reference lines are included: the 1:1 solid line and the 1:0.5 and 1:2 dashed lines. The line of best fit is drawn as a dashed line with the 95% confidence interval shaded in grey. Please note the confidence interval is narrow.

Four meteorological factors including temperature, relative humidity, wind speed and seasonality were investigated to determine the impacts on correlation for co-located sensors. These variables were selected as changes in them may cause significant differences in sensor performance and hence the measured pollutant levels (Appendix B). All but the last meteorological variable was numeric, so the correlation between air pollutant concentrations measured by reference and AQMesh sensors were analyzed by quantiles of each meteorological condition. Pre-stratified correlation matrices for concentrations for Vancouver and London are plotted below (Figure 2.9 and Figure 2.10). These plots show better alignment of measurements between AQMesh sensors (referred to as AQMesh-AQMesh correlation) than between AQMesh sensors and the reference sensors (referred to as AQMesh-reference correlation). Table 2.8 outlines the descriptive statistics for the local meteorological conditions experienced throughout the period of co-location.

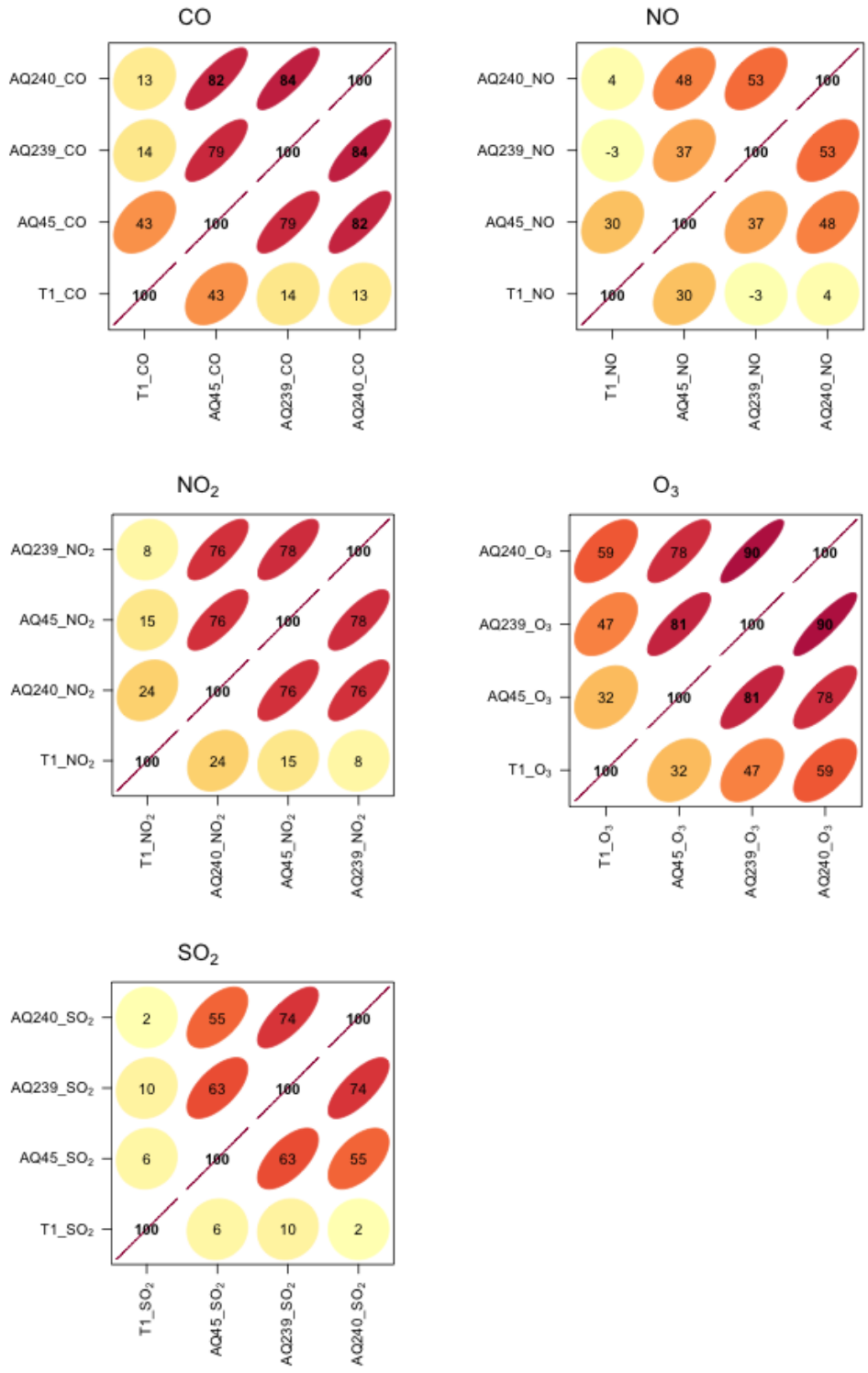

Figure 2.9 Correlation matrices for Vancouver. The shape, color and numeric value indicate the degree of correlation.

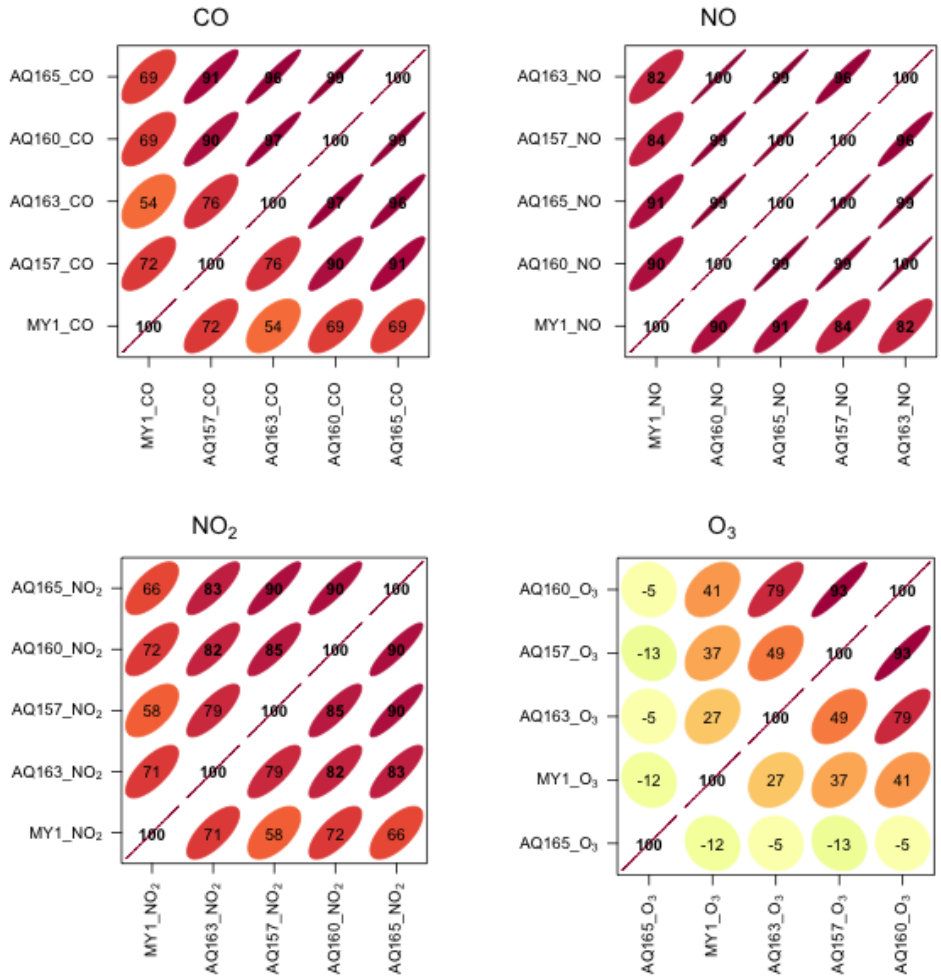

Figure 2.10 Correlation matrices for London. The shape, color and numeric value indicate the degree of correlation.

Table 2.8 Descriptive statistics of local meteorological conditions for Vancouver (data from Richmond-Airport station) and London during the study. N is the total number of hourly averaged records.

Location	Meteorological Variable	N	Mean ± SD	Min	Median	Max
Vancouver	Temperature (℃)	7957	12 ± 6	-6.5	11.8	28.7
	Relative Humidity (%RH)	7957	79.8 ± 14.1	21.8	82.4	99.9
	Wind Speed (km/hr)	7957	9.3 ±5.4	1.1	8.2	40.9
	Rain (mm)	7957	0.1 ± 0.5	0	0	8.0
London	Temperature (℃)	6141	14.3 ± 5.5	0.2	14.6	31.7
	Relative Humidity (%RH)	8222	76.2 ± 16.6	29.8	79.6	99.9
	Wind Speed (km/hr)	8760	5.8 ± 4.3	0	5.0	30.6
	Rain (mm)	8015	0.02 ± 0.1	0	0	2.0

2.3 Discussion

The descriptive statistics for data omission are highlighted in Table 2.2 and Table 2.3. In general, the NO_2, O_3 and SO_2 sensors were quite resilient and did not require extra periods of rebasing or stabilizing. On the contrary, the NO and CO sensors experienced the greatest flags of these types irrespective of the geographical locale. As anticipated, the flagged modes of operation for AQMesh 239150's NO sensor corresponded well with the sensor change out. On the other hand, AQMesh 239150's CO sensor replacement on the same day, December 2, 2014, did not seem to trigger any flagged statuses. In sum, the indicated statuses represented 0% to 79.3% of all the recorded concentrations data.

Taken together, the statistics for mean, standard deviation, median and range in Table 2.4 and Table 2.5 show a stronger degree of correlation between co-located instruments in London than in Vancouver. A few plausible explanations can be offered for this effect. A major factor would be the substantially shorter distance between the AQMesh instruments and the reference station sensors in London as compared to Vancouver. Furthermore, it appears the AQMesh units

failed to flag certain suboptimal statuses in Vancouver when compared to London (e.g. below LOD). Also noteworthy, is the fact that AQMesh was designed and tested by Geotech in London (230). As such, the instruments may be better conditioned or optimized to London's ambient environment and meteorological conditions. Table 2.8 summarized 4 local meteorological variables (temperature, relative humidity, wind speed and rain). The results indicate that Vancouver experienced more wind and rain than London during the co-location; this may partially explain the difference in instrument performance.

Visually, time-series plots for each co-located sensor type and location depict how agreeable or disagreeable the AQMesh sensors traced the outdoor air pollutant concentrations when compared to the traditional monitors. The Vancouver results (Figure 2.5) illustrate multiple instances where hourly-averaged pollution data was seen to spike on the AQMesh where the Vancouver T1 data showed little to no increase. The London data (Figure 2.6) displayed far fewer occurrences of this type.

The amount of variability (R^2) explained by co-located AQMesh in the two cities varied from 0.02% to 34.5% in Vancouver to 1.5% to 82.3% in London (Table 2.6 and Table 2.7). Overall, accuracy, as reflected in RMSE values, was found to be lowest for CO sensors and highest for NO_2 and O_3 sensors. Only ozone sensors showed a consistent direction of bias (i.e. positive bias) in both locations when compared to their reference sensor counterparts. In Vancouver, NO_2 and SO_2 sensors veered towards overestimating concentrations while CO and NO sensors showed no evident bias trends. With the exception of O_3, the remaining pollutant sensors in London (CO, NO and NO_2) had a tendency to underestimate concentrations.

Notable trends from meteorological analysis include improved sensor performance (both AQMesh-AQMesh and AQMesh-reference linearity) at higher temperatures (Appendix B.1) and

non-winter months (Appendix B.4). No clear trends could be discerned from Vancouver's seasonal dataset as most measurements were obtained in spring and summer months. It was discovered that some sensors (CO, NO, SO_2) performed best at higher relative humidity, while O_3 sensors preformed best at lower relative humidity. Nitrogen dioxide sensors exhibited consistent linearity across the relative humidity strata. For relative humidity stratified NO measurements in London, the AQMesh-AQMesh Pearson correlation coefficient was near perfect (ranging between 0.98 and 1.00, see Figure B.4).

Wind speed results were the most interesting. In Vancouver, at higher wind speed quantiles, the correlation coefficients decreased for CO, NO, NO_2 and SO_2, but increased for O_3. In London, at higher wind speed quantiles, the correlation coefficients decreased for CO and O_3 (for AQMesh-reference correlation) but remained relatively constant for NO and NO_2. The highest Vancouver wind quantile was 12.2 to 40.9 km/h while the highest London wind quantile was 2.33 to 8.5 m/s (equivalently, 8.388 to 30.6 km/h). Since wind speeds in London never reached the maximum wind speeds in Vancouver, the lighter winds in London may have resulted in stagnant conditions. The wind speed variable likely played a role in the difference in sensor performance between the two cities.

Weaknesses of this study include logistical co-location restrictions and data proxy decisions. An advantage of the London Marylebone Road co-location over the Vancouver Hornby Street one was the proximity of AQMesh to the gas inlets (within 1 m rather than 25 m). However, the distance between the AQMesh units and the reference stations can only partially explain the disparity in AQMesh-reference correlations between Vancouver and London; this distance does not explain the AQMesh-AQMesh correlation discrepancies. The co-location in Vancouver was guided by security considerations and the prospective use of AQMesh in the

mobile monitoring campaign should the co-location demonstrate high comparability. On a smaller magnitude, the AQMesh instruments in Vancouver were offset vertically and angled 120° from each other on the lamppost during sampling. Because the Vancouver-Downtown reference station did not measure meteorological conditions, the Richmond-Airport station was used as a proxy for standard climatic data.

The power of this AQMesh comparison is this is the first documented appraisal of the data quality against gold-standard instrumentation used for regulatory purposes. Furthermore, this study spanned a prolonged duration of approximately one year in two urban hubs that are prone to TRAP exposures.

A data authentication step permitted us to ensure the comparisons were grounded in the highest quality AQMesh data. Removal of data collected during substandard instrument function was possible owing to the status indicators (e.g. below LOD, rebasing, stabilizing) in AQMesh data exports. The aforementioned step also led us to use the post-processed output in all comparisons. Where available, ratified reference data was used (i.e. London MY1 gas data and 2014 Vancouver T1 data).

All in all, the co-located instruments showed a limited potential for use in Vancouver as the single best sensor explained 34.5% (O_3) of the variation in the reference method. Interpreting data from instruments with low R^2 values can be misleading, as they may not fully explain the air pollution variability. The London co-location showed a higher degree of precision (R^2 of 0.67 – 0.82) for its best gas sensor type (NO). Following the conclusion of this study, AQMesh published a series of co-location comparisons on their web platform. The coefficients of determination and accuracy measured were far improved compared to the values obtained in these co-locations. Because these co-locations were based on later versions of the algorithm

(v4.0, v4.1 and v4.2), where both the Vancouver and London co-locations depended on v3.0 outputs, further reassessments are required to confirm sensor performance. (240)

An AQMesh co-location study by Jones (241) for AQMesh at an AURN site with ratified data found a R^2 of 0.65 and 0.74 for NO and NO_2, respectively. Another field assessment by Borrego et al. (217) identified a comparable performance of AQMesh sensors when compared to a standard reference: O_3 (R^2: 0.70), NO_2 (R^2: 0.89), CO (R^2: 0.86) and NO (R^2: 0.80). (217) These results are consistent with the London co-location study for NO which had R^2 of 0.67 - 0.82. However, the other research reported a higher R^2 for NO_2, CO and O_3 than what this study concluded for London (NO_2: 0.34 - 0.52, CO: 0.29-0.52, O3: 0.02-0.17).

In October 2014, the 1st EuNetAir Air Quality Joint Intercomparison Exercise tested different microsensors against reference methods; the initiative observed R^2 values in the range of 0.12–0.77 for O_3, 0.53–0.87 for CO, 0.02–0.89 for NO_2, 0.09–0.20 for SO_2 and 0.07–0.36 for PM. The researchers propose this experimental campaign is essential for the research and development of air quality technologies and emphasize the need to further address sensitivity, selectivity, sensor stability, data validation, calibration and evaluation using field testing. (217)

To confidently justify AQMesh use in regulatory applications, accuracy improvements are needed so comparisons can be made with air quality benchmarks. To ensure sensors within network deployments are comparable to one another, precision levels must be developed further.

Chapter 3: Creation and evaluation of a prototype model to identify street canyons

3.1 Methods

3.1.1 Site details

The aim of this component was to develop a simple geospatial model to identify potential street canyons based on readily available inputs (building height, street widths, and prevailing wind direction) and to then assess whether such locations were associated with higher concentrations of traffic-related air pollutants. In this chapter, the term "potential street canyons" is applied. Although geometry and wind direction act as predictors of street canyons; without measurement, one cannot guarantee these structures behave as canyons. The downtown Vancouver core was selected as the desired study location because of its prevalence of high-rise residential and commercial buildings. Unique to downtown Vancouver is the presence of lower story buildings in addition to built-up complexes. The structural composition of streets is seen to vary drastically between narrow, single-lane roads in housing zones to multi-lane roads in busy corridors. Finally, located in the heart of downtown is a Lower Fraser Valley Air Quality Monitoring Network station: Vancouver-Downtown Station (Station ID: T1). This station was described in detail in Chapter 2, Section 2.1.2.

3.1.2 Model components and data acquisition

The goal of creating a model to detect potential street canyons was realized using two equally weighted components: 1) aspect ratios and 2) the predominant wind direction. Aspect

ratios were determined by the ratio of building heights to street width. Dr. Rory Tooke from The University of British Columbia's Faculty of Forestry provided primary building footprints with a height attribute for Vancouver in December 2013. Secondary buildings such as garages and sheds were excluded in this dataset. Public street data and local area boundaries were downloaded from the City of Vancouver Open Data Catalogue. (242)

These two components were selected for the following reasons. The likelihood of street canyon formation increases with aspect ratio; with 0.7 being the level beyond which one can assume there is a risk of pollutant accumulation - as relatively stagnant air is present near the base of the canyon. (106)

Prevailing wind direction also plays a critical role in street canyon formation. If wind direction runs perpendicular to the length of the street, the likelihood of there being a canyon increases as the airflow above building tops is unable to adequately exchange with air trapped within the canyons. Therefore, aspect ratio and wind direction are cumulatively accounted for in the model (using multi-criteria analysis). Historical Vancouver wind data for 2013 was obtained from an Environment Canada webpage. (243).

3.1.3 Prototype model formation

Prior to any analyses, all of the input data (except prevailing wind) was geo-referenced to the Universal Transverse Mercator (UTM) projection system using zone 10N of the North American Datum of 1983 (NAD 1983). Computer software used in the analyses included: ArcMap, Version 10.1 (ESRI, Redlands, CA, 2012), R, Version 3.1.0 (© R Foundation for Statistical Computing, 2014), RStudio, Version 098.1056 (RStudio, Inc., 2013) and Microsoft Excel 2011 (Microsoft® , Redmond, WA, 2011). The basic three-step structure of this model

development is shown in Figure 3.1.

Figure 3.1 Flowchart showing the three steps of model development

3.1.3.1 Step 1: Determining aspect ratio

The first step in the analysis was to construct a polygon that covered the area of interest (downtown Vancouver) using the local area boundary layer. This polygon was used to truncate the public streets, right-of-way street widths, and building footprints layers to the area of interest. (Figure 3.2)

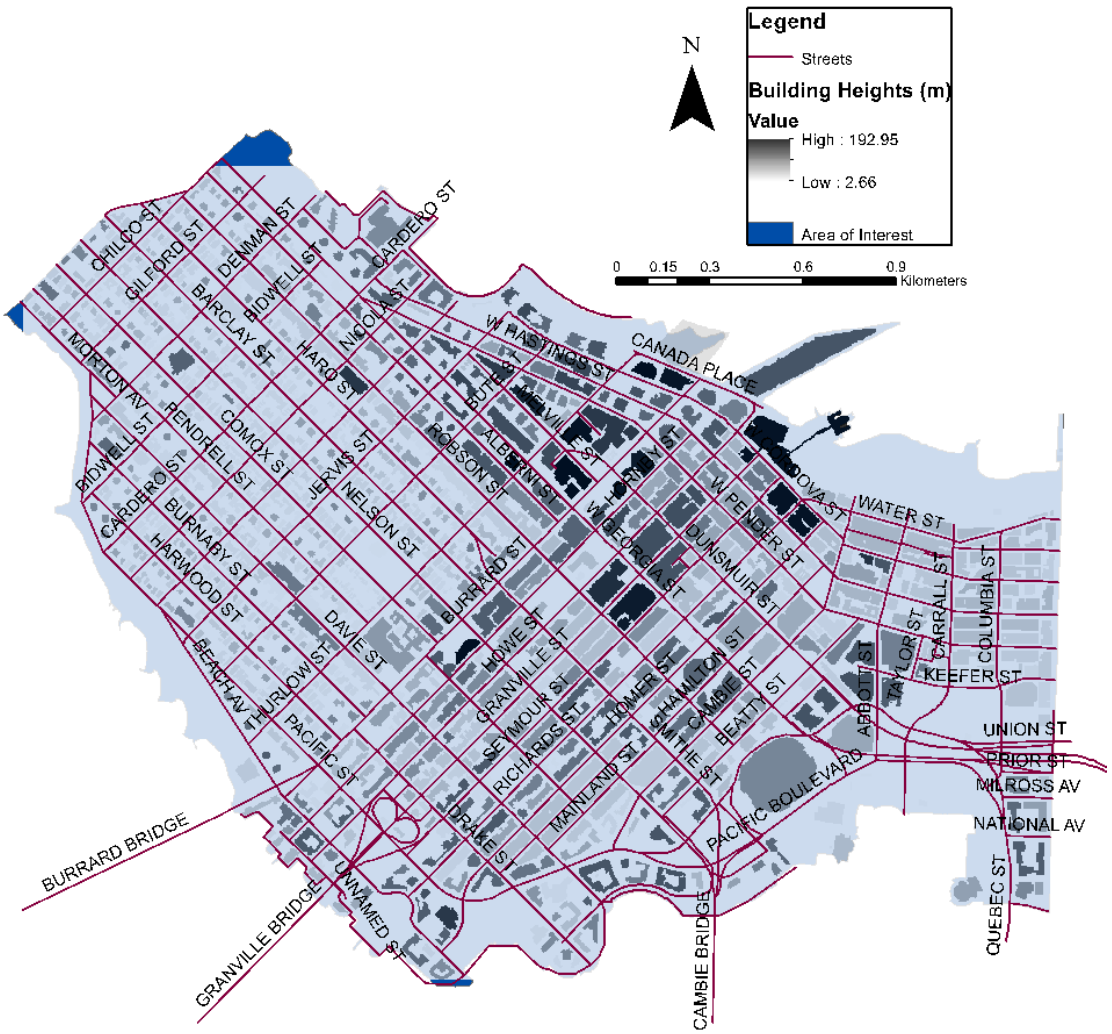

Figure 3.2 Streets and buildings in area of interest

Some data cleanup was performed on the street widths layer as metrics used in the raw file included both feet and meters. Individual road segments on the public streets layer were made continuous and buffers were applied. This ensured adequate spatial joining to the right-of-way widths layer. Further manipulations created a polyline street layer containing street width information as an attribute.

This layer served as the input for all further analysis. All fields in which the street width values were “0 m” were deleted since street width is the denominator in the aspect ratio calculation (Equation 3.1). The “0 m” streets corresponded to bike lanes along the Seawall and streets that no longer existed.

Before moving on to the next step, it was necessary to determine the street bearings in order to find buildings that were perpendicular to the street. This was accomplished using an Easy Calculate Add-In. (244)

The “generate near table” tool was applied to the new layer to search for the 5 nearest neighbors (i.e. close by buildings from the building footprint layer) falling within a suitable search radius (i.e. 35 m). The tabulated data was spatially joined to the street segments and exported for manipulations in Microsoft Excel and R. The street bearings coordinate system (0°=North, 90°=East, 180°=South, 270°=West) from the previous step was converted to the polar coordinate system to match the way in which nearest-distance angle data (0°=east, 90°=north, ±180°=west, -90°=south) was reported. Conditional nested “if”, “and” and “or” statements were used to select the 2 nearest perpendicular buildings (falling within 90°± 5° of the street bearing) from the 5 potential nearest neighbors. The output from this analysis (building identification numbers) was sorted into 2 columns using R. The “index”, “match”, “if” and “sum” functions in Microsoft Excel helped compile the street width data for each street segment centroid (by summing the shortest distance between the centroid and the 2 nearest perpendicular neighbors). In instances where a centroid only had 1 near neighbor, the right-of-way street width was used as a proxy for street width.

This information was saved and added to ArcMap. By spatially joining this layer based on building identification number, up to 2 corresponding building heights were extracted as 2

new attribute columns (one height for each near building). Aspect ratio was determined with the "Field Calculator" following Equation 3.1. Details of the ArcMap procedure are outlined in Table 3.1.

Equation 3.1 Aspect Ratio

$$Aspect\ Ratio = \frac{\frac{h_1+h_2}{2}}{w}$$

h_1, h_2 = heights of perpendicular buildings (m)

w = street width (m)

Table 3.1 Summary of steps to determine aspect ratio

Step	Input Layer	Tool Used	Output Layer
1	local_area_boundary (raw data file)	Dissolve, Edit and Merge "Downtown" and "West End"	DT_Crop
2	Van_FP_Primary (raw data file)	Select Layer by Location using DT_Crop	DT_FP_Primary has FIDs for each building (polygon) and a building height field.
3	public_streets (raw data file)	Select Layer by Location using DT_Crop	DT_public_streets
4	right-of-way_widths (raw data file)	Select Layer by Location using DT_Crop	DT_row_widths
5	DT_row_widths	Add Field, Select by Attributes and Field Calculator to convert widths to meters in a new field titled WIDTH_m	DT_row_widths
6	DT_public_streets	Add Field, Split Function and Field Calculator to transfer HBLOCK's street names to a new field titled STREET	DT_public_streets
7	DT_public_streets	Dissolve based on STREET field	DT_dissolved_streets
8	DT_dissolved_streets	Buffer (5 m, full sides, round ends)	DT_buffered_streets

Step	Input Layer	Tool Used	Output Layer
9	DT_buffered_streets	Spatial Join (average) with DT_row_widths	DT_buffered_widths
10	DT_buffered_widths	Feature to Point (inside)	DT_buffered_centroid
11	DT_buffered_centroid	Buffer (5 m)	DT_centroid_5m
12	DT_dissolved_streets	Spatial Join (average) with DT_centroid_5m	DT_street_widths
13	DT_street_widths	Densify (distance: 0.5 m)	DT_street_widths
14	DT_street_widths	Dice (vertex limit: 10)	DT_dice_stwdth
15	DT_dice_stwdth	Add Field and use "polyline_Get_Azimuth" from an Easy Calculate Add-in to determine street bearing.	DT_dice_stwdth has FIDs for each street (polyline). Other fields include street width and street bearing.
16	DT_dice_stwdth	Generate Near Table (search radius: 35 m, include angle, maximum number of closest matches: 5) with DT_FP_Primary	DT_near_analysis (table output) has OIDs for each street (polyline) - building (polygon) pair, IN_FIDs for streets and NEAR_FIDs for near buildings. Other fields include nearest distance and nearest angle.
17	DT_near_analysis (table output)	Select by Attributes 5 subsets of data using this query: SELECT*FROM DT_near_analysis WHERE: MOD ("OID",5)=0. Repeat with ("OID",5)=1, ("OID",5)=2, ("OID",5)=3, and ("OID",5)=4. Export tables.	DT_near_0 DT_near_1 DT_near_2 DT_near_3 DT_near_4 (table outputs)
18	DT_dice_stwdth	Join (keeping all records) with table outputs (DT_near_0, DT_near_1, DT_near_2, DT_near_3, and DT_near_4) using street (polyline) FIDs. Then export.	DT_near_poly (table output) shows streets (with width and bearing) and the FIDs of the 5 nearest buildings and the angle and distance to them.

Step	Input Layer	Tool Used	Output Layer
19	DT_near_poly (table output)	In Excel and R: determine up to 2 closest perpendicular neighbors using nested conditional "if", "and", "or" statements. Data cleanup (using "index", "match", "if" and "sum" statements) prior to export.	Near_Dist (table output) shows streets (with width) and the FIDs of the 2 perpendicular neighbors and the distance to each neighbor.
20	DT_dice_stwdth	Join (keeping all records) with table output (Near_Dist) using street (polyline) FIDs.	DT_dice_stwdth shows streets (with width) and the FIDs of the 2 perpendicular neighbors and the distance to each neighbor.
21	DT_FP_Primary	Export	DT_FP_Primary2
22	DT_dice_stwdth	Join (keeping all records) with DT_FP_Primary using building (polygon) FIDs to include height information for a nearest neighbor. Repeat with DT_FP_Primary2 to include height information for the second nearest building.	DT_dice_stwdth shows streets (with width) and the FIDs of the 2 perpendicular neighbors (with heights) and the distance to each neighbor.
23	DT_dice_stwdth	Add Field and Field Calculator to define aspect ratio.	DT_dice_stwdth

3.1.3.2 Step 2: Determining ideal street bearing with respect to wind direction

For the purposes of this study, the dominant wind direction from the previous year (i.e. 2013) was chosen. According to Environment Canada data, the dominant direction was easterly. (243) This model employs regional weather station data rather than data specific to the study area of interest. Extrapolating this weather monitoring data to the study area involves making an assumption that weather conditions remain stable and are applicable to the entire downtown area. Street bearings indicative of canyon conditions (i.e. 0^{o} and 180^{o}) should run perpendicular to the wind direction (i.e. East=90^{o}) and are dealt with in the normalization step (explained in the next

section).

3.1.3.3 Step 3: Multi-criteria analysis

The final step was to perform a multi-criteria analysis. First, the aspect ratio and street bearings were normalized so they can be compared with one another. The normalization tool used was “fuzzy membership”. Only aspect ratios exceeding 0.7 were exported for this stage of assessment. After converting the aspect ratio shapefile into a raster using the “point to raster” tool, this layer was assigned values from 0 to 1 based on a “linear” membership type. The highest aspect ratio was assigned a value of 1, and the lowest aspect ratio (0.7) was assigned a value of 0, because higher aspect ratios indicate greater likelihood of street canyon formation.

Normalizing street bearings required a more complicated method as there was more than one ideal bearing. In addition, 0° and 360° indicated the same bearing (North), so a “linear” membership type would not suffice. To overcome this problem, all street bearings that fell between 0° and 89° were selected, and 360° were added to each entry. Then the streets layer was separated into two distinct layers: one for street bearings between 90° and 269° and the other for street bearings between 270° and 449°. This way, an ideal value of 1 can be assigned to two bearings (i.e. 180° = South and 360° = North)–those streets that run perpendicular to wind direction. A non-ideal value of 0 was assigned to those streets that run parallel to wind direction (i.e. 90° = East and 270° = West). This is depicted in Figure 3.3.

The street bearing layers were converted into raster format. Then, the "fuzzy membership" tool was applied to both street bearing layers, this time using the "Gaussian" membership type with a spread of 0.0001. For the 90° to 269° and 270° to 449° layers, the assigned midpoints were 180° (South) and 360° (North), respectively. The “Gaussian”

membership type was chosen since two ideal bearings (180° and 360°) had to be assigned. Street bearings falling on either side of these ideals would gradually decrease in importance as a smaller spread (0.0001) was selected.

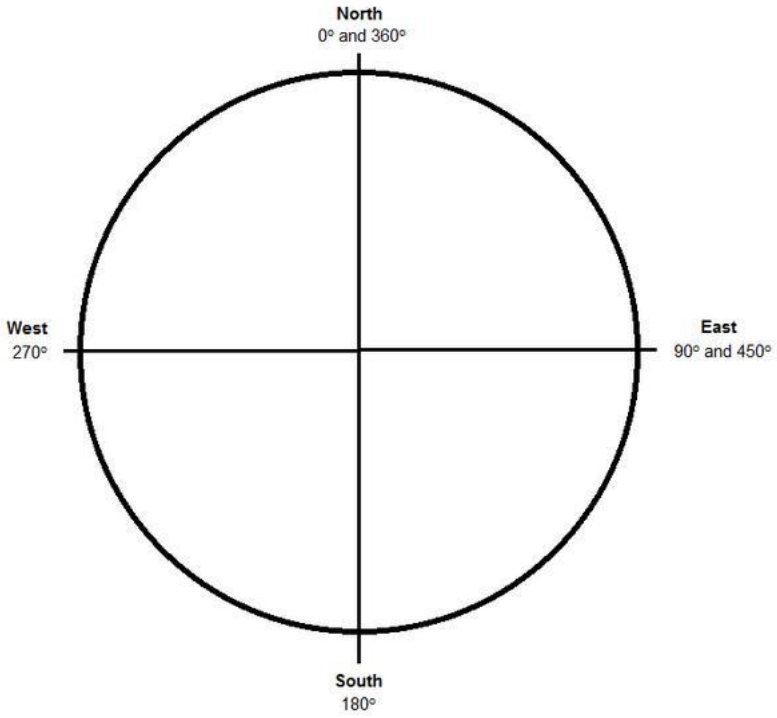

Figure 3.3 Wind direction

After normalizing the aspect ratios and street bearings, a multi-criteria analysis was performed by adding the normalized values together using the "raster calculator". Equal weighting of the aspect ratio and the wind direction was done. In theory, the best street canyons would hence have a total value of 2 while the worst canyons would have a value of 0.

3.1.4 Mobile monitoring evaluation

3.1.4.1 Route selection

Through the development of the multi-criteria analysis model, probable street canyon locations were mapped. To assess whether such locations are areas of higher pollutant concentrations, particulate matter ($PM_{2.5}$ and PM_{10}) and particle number concentrations (PNC) were measured in potential street canyon and non-canyons locations with both high and low levels of traffic. As a preliminary means of characterizing streets of variable traffic (high and low), the traffic count data from the City of Vancouver was visually inspected on the online platform. (245) To qualitatively confirm regions of higher and lower traffic, multiple walkthroughs were completed. In the end, a route measuring approximately 4 km in length was chosen as it contained four roughly equidistant complementary street segment classes. These are pictured in Figure 3.6 as non-canyon low traffic (NC LT), non-canyon high traffic (NC HT), canyon low traffic (C LT) and canyon high traffic (C HT).

3.1.4.1 Instrument setup and data collection

The selected 4 km route was walked a total of 46 times (lasting 1.5 to 2 hours per walk) between July 14, 2014 and August 11, 2014 according to the sampling schedule (Appendix C.1). The sampling campaign hoped to capture concentrations at variable times throughout the week. Regrettably, two of the sampling runs were omitted in subsequent data analyses as a flow error occurred in a mobile device. Overall, 23 runs were completed during rush hours (7:00 – 9:00 am or 4:00 – 6:00 pm) and 21 runs were completed in non-rush hour periods (ranging from 9:00 am – 4:00 pm and 6:00 pm – 11:00 pm).

Prior to starting each run, the walking direction (clockwise or counterclockwise) and the side of the street (left or right) was randomly determined. This information was recorded in the sampling form (Appendix C.1). The instruments, summarized in Table 3.2, were setup following manufacturer guidelines (i.e. daily zero calibrations for the CPC 3007 and DustTraks, flow calibrations to 3 L/min for the DustTraks) and synced with the same world clock. Once this was completed, the two DustTraks—the fixed background instrument (desktop DustTrak) and the mobile instrument (handheld DustTrak)—were placed side-by-side for a 10-minute co-location as a quality control measure. This was repeated again at the end of the run. The following methods sections outline how these co-locations were used, in part, to determine a between-instrument correction factor.

Table 3.2 Mobile sampling instruments

Function	Instrument	Monitors
Fixed	Desktop: DustTrak™ DRX Aerosol Monitor 8533EP (TSI® , Shoreview, MN)	PM (Mass and Size Fraction)
Mobile	Handheld: DustTrak™ DRX Aerosol Monitor 8534 (TSI® , Shoreview, MN)	PM (Mass and Size Fraction)
	Condensation Particle Counter (CPC) 3007 (TSI® , Shoreview, MN)	PNC
	Kestrel® 4500 Pocket Weather Tracker (Nielsen-Kellerman, Boothwyn, PA)	Meteorology (Wind Direction)
	DG-200 GPS Data Logger (GlobalSat Technology Corporation, Chung Ho City Taipei Hsien, Taiwan)	Latitude and Longitude

All 5 instruments were operated at a sampling frequency of 10 seconds; the Kestrel was only run for 3-minute intervals at 8 labeled stop points (refer to Figure 3.6). While the Kestrel was monitoring for the 3 minutes, a manual counter was used to record traffic counts.

Throughout the sampling campaign, one individual would remain with the desktop DustTrak stationed at the fixed site on Bute St. (labeled as a yellow square in Figure 3.6) while the other individual walked the route with the portable instruments. The handheld DustTrak and CPC 3007 were carried in a backpack while the GPS and traffic counter were worn around the neck. Additional equipment included an Optex DPT175 Digital Pro Compact Tripod (for Kestrel mounting) and a clipboard attached sampling form; both of these were carried in hand. Instrument and battery charges (Powerex MH-C899S Eight Cell Smart Charger/ Powerex Rechargeable NiHM AA and AAA Batteries) were completed overnight.

3.1.4.2 Data downloads, quality and conversions

Instrument data was downloaded daily using TrakPro™ Data Analysis Software, v. 4.6.1.1 (TSI® , Shoreview, MN), TSI Aerosol Instrument Manager® Software (TSI® , Shoreview, MN), DG-200 PC Utility (GlobalSat Technology Corporation, Chung Ho City Taipei Hsien, Taiwan) and the Kestrel® Communicator Interface Software, v 2.1.1 (Nielsen-Kellerman, Boothwyn, PA).

To better detect the true differences in PM and PNC for the 4 street segment classifications: C LT, C HT, NC LT and NC HT, corrections were applied. Correction factors (CFs) were incorporated as a means of removing the effect of variability between DustTraks (CF1), within runs (CF2) and between days (CF3). Since the study design had 2 co-located continuous monitors of the same type (DustTraks) at the start and end of each run, and no co-located standard reference instrument, Wallace et al.'s (246) approach to calculate instrument bias using instrument inter-comparison measurements as the "true" value was adopted. In this case, the mean measurement was used as the "true" value to determine relative between-

instrument bias; 258 sets of 10-minute averaged co-locations (from in-lab co-locations and pre- and post-run co-locations) were included in the calculation of CF1 (Equation 3.2). Equations for the latter two temporal corrections, CF2 and CF3, are displayed in Equation 3.3and Equation 3.4, respectively.

Equation 3.2 Between-instrument correction factor (CF1) uses desktop or handheld DustTrak bias (calculated from 258 sets of 10 min lab and field co-locations) to correct instrument variability.

$$Bias_A = \frac{1}{258} \times \sum_{m=1}^{258} \left(\frac{1}{60} \times \sum_{o=1}^{60} \left(\frac{A - \left(\frac{D+H}{2}\right)}{\left(\frac{D+H}{2}\right)} \right) \right)$$

$$CF1_A = \frac{1}{Bias_A + 1}$$

CF1 = Correction Factor 1

A = reading on DustTrak of interest (desktop or handheld)

D = desktop DustTrak reading

H = handheld DustTrak reading

o = observation number (1-60); 60 observations = 10 min since the sampling frequency is 10 sec

m = number of 10 min bias calculations (1-258)

Equation 3.3 Within-run correction factor (CF2) uses the 15-min desktop DustTrak's rolling average divided by the desktop DustTrak's overall run average to correct the Handheld DustTrak and CPC 3007 (corrected using the CF2 values for $PM_{2.5}$). The CF1 corrected desktop DustTrak readings are used in this calculation.

$$CF2_i = \frac{\frac{1}{90}\sum_{i=x-44}^{i=x+45} D_i}{\frac{1}{n}\sum_{i=1}^{n} D_i}$$

CF2 = Correction Factor 2

D = desktop DustTrak reading

i = i^{th} desktop DustTrak reading in the sampling run of interest

n = total number of Desktop DustTrak readings in the sampling run of interest

x = 45^{th} observation within the 90 observations; 90 observations = 15 min since sampling frequency is 10 sec

Equation 3.4 Between-day correction factor (CF3) uses the daily Burnaby South Station $PM_{2.5}$ concentration (or PM_{10} concentration where $PM_{2.5}$ is unavailable) divided by the average PM concentration across all sampling days to correct the Handheld DustTrak and CPC 3007.

$$\boldsymbol{CF3_d = \frac{B_d}{\frac{1}{23}\sum_{d=1}^{23} B_d}}$$

CF3 = Correction Factor 3

B = Burnaby South Station's daily average $PM_{2.5}$ (or PM_{10}) concentration

d = day of sampling (1-23)

3.1.4.3 Statistical analysis

Outdoor air pollution typically follows a lognormal distribution; as such, histograms of the untransformed and log-transformed $PM_{2.5}$, PM_{10}, and PNC were plotted. Descriptive statistics

including count, minimum, maximum, mean, standard deviation, median, geometric mean, geometric standard deviation, skewness and kurtosis were also evaluated to confirm the need to log-transform the dataset. Values below the DustTrak's limit of detection (LOD) of 0.001 mg/m^3 were substituted with LOD divided by the square root of 2 to minimize the effect of missing values. (247,248) After the substitution, the three correction factors were applied prior to the logarithmic transformation.

Descriptive statistics summarized the differences in traffic counts from the eight sampling locations. In every run, each set of 3-minute traffic counts within the street segment categories (C LT, C HT, NC LT, NC HT) were averaged and divided by three to calculate the mean vehicles per min. This was done to confirm the decision to classify road segments as low or high traffic.

To investigate the statistical relationship (significance level, $\alpha = 0.05$) between log-transformed concentration of $PM_{2.5}$ or log-transformed PNC and the four street segment classifications, a linear mixed effects model was used (Equation 3.5). An advantage of the linear mixed effects model is the ability to account for repeated air quality measures within runs. The i and j indices refer to i^{th} measurement in the j^{th} run. The β_1 intercept signifies the fixed effect of the street segment category on the log-transformed outcome variable while β_2 intercept signifies the fixed effect of rush hour on the outcome. A random intercept accounts for repeated measurement by runs while an overall random error term is denoted by e_{ij}.

Equation 3.5 Linear mixed effects model

$$logY_{ij} = \beta_0 + \beta_1 category_{ij} + \beta_2 rush\ hour_{ij} + e_{ij}$$

$logY_{ij}$ = log-transformed PM or PNC

β = intercepts

i = i^{th} measurement

j = j^{th} run (1-44)

$e_{ij} \sim N(0, \sigma_e^2)$ = overall random error term

3.2 Results

3.2.1 Multi-criteria evaluation model

The final multi-criteria evaluation model for potential street canyons in downtown Vancouver is presented in Figure 3.4. Building heights in the downtown area ranged from 3 m to 193 m in height. In considering only aspect ratios greater than 0.7 and the predominant wind direction, locations were designated a value between 0 and 2 for their ability to theoretically act as street canyons. From the multi-criteria analysis, the range of outputs were 0.45 - 1.82. The multi-criteria analysis is superimposed on the mobile monitoring route in Figure 3.5. In visualizing this, the choice to designate the canyon and non-canyon segments becomes quite clear. These are pictured in Figure 3.6 as NC LT, NC HT, C LT and C HT.

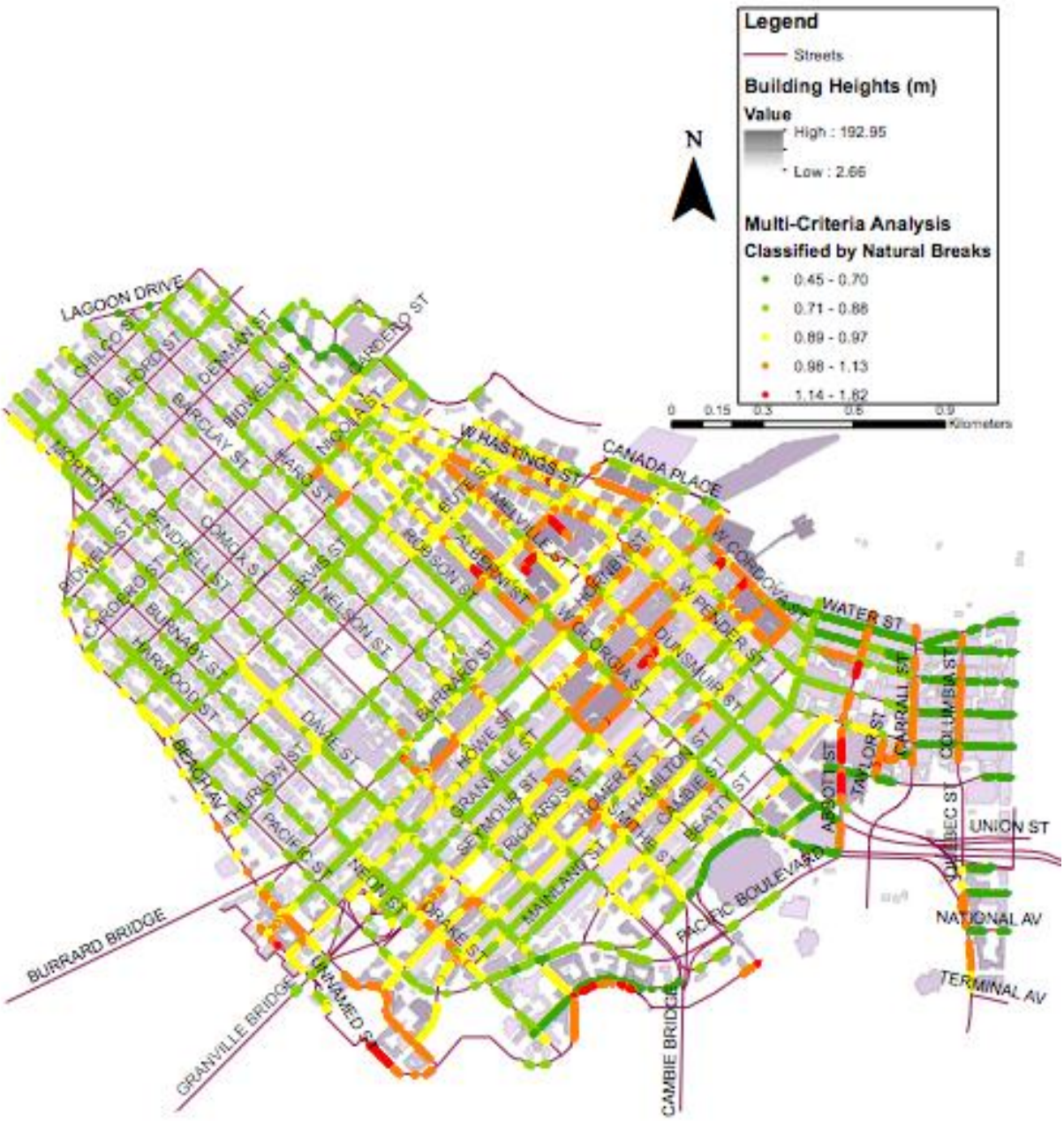

Figure 3.4 Multi-criteria analysis classified by natural breaks

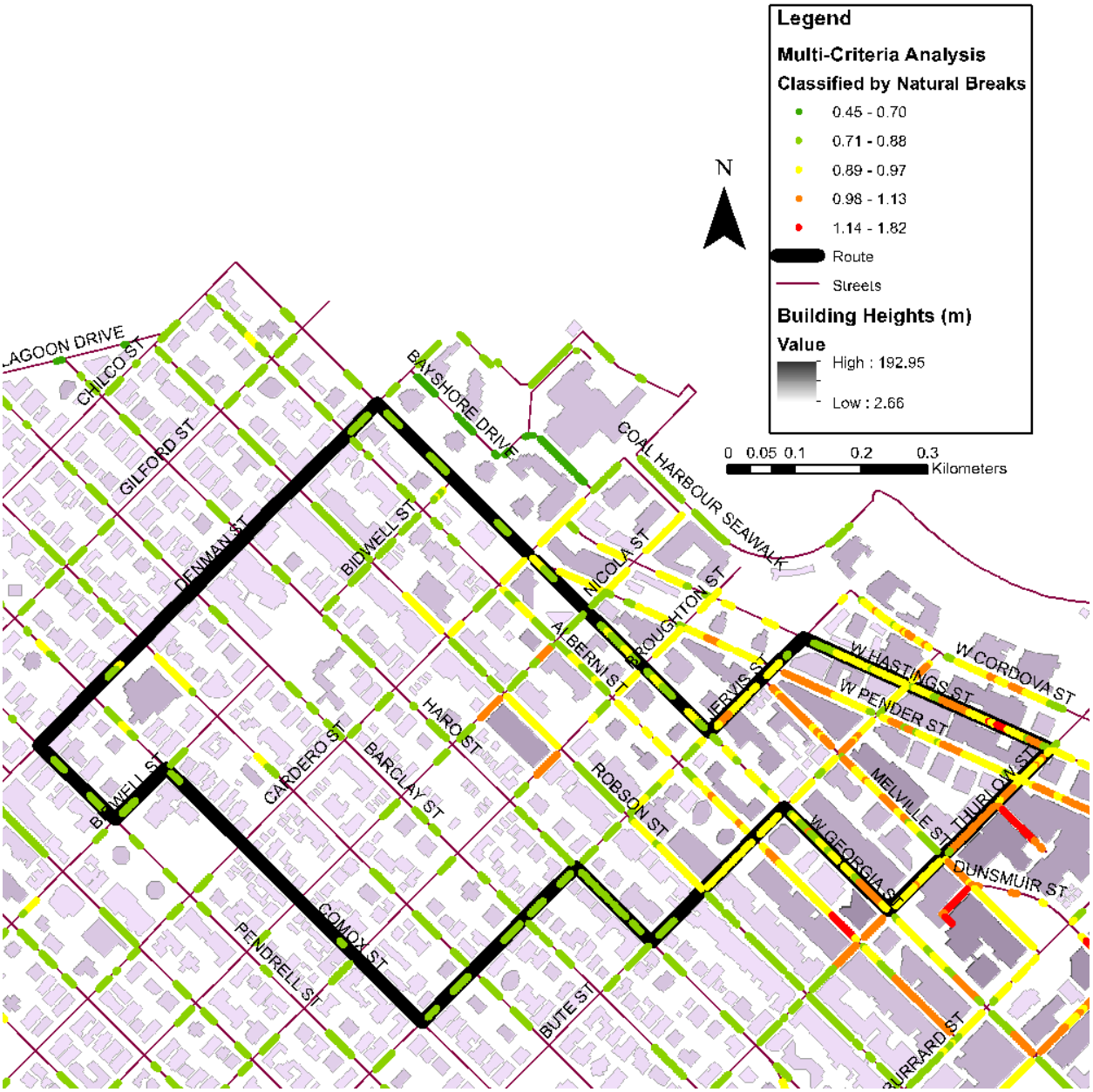

Figure 3.5 Mobile sampling route overlaid with the multi-criteria analysis outcome. The thick black line denotes the path for mobile model evaluation. Where any color is present on the black route, a canyon is expected. Warmer tones show stronger canyons while cooler tones show weaker canyons.

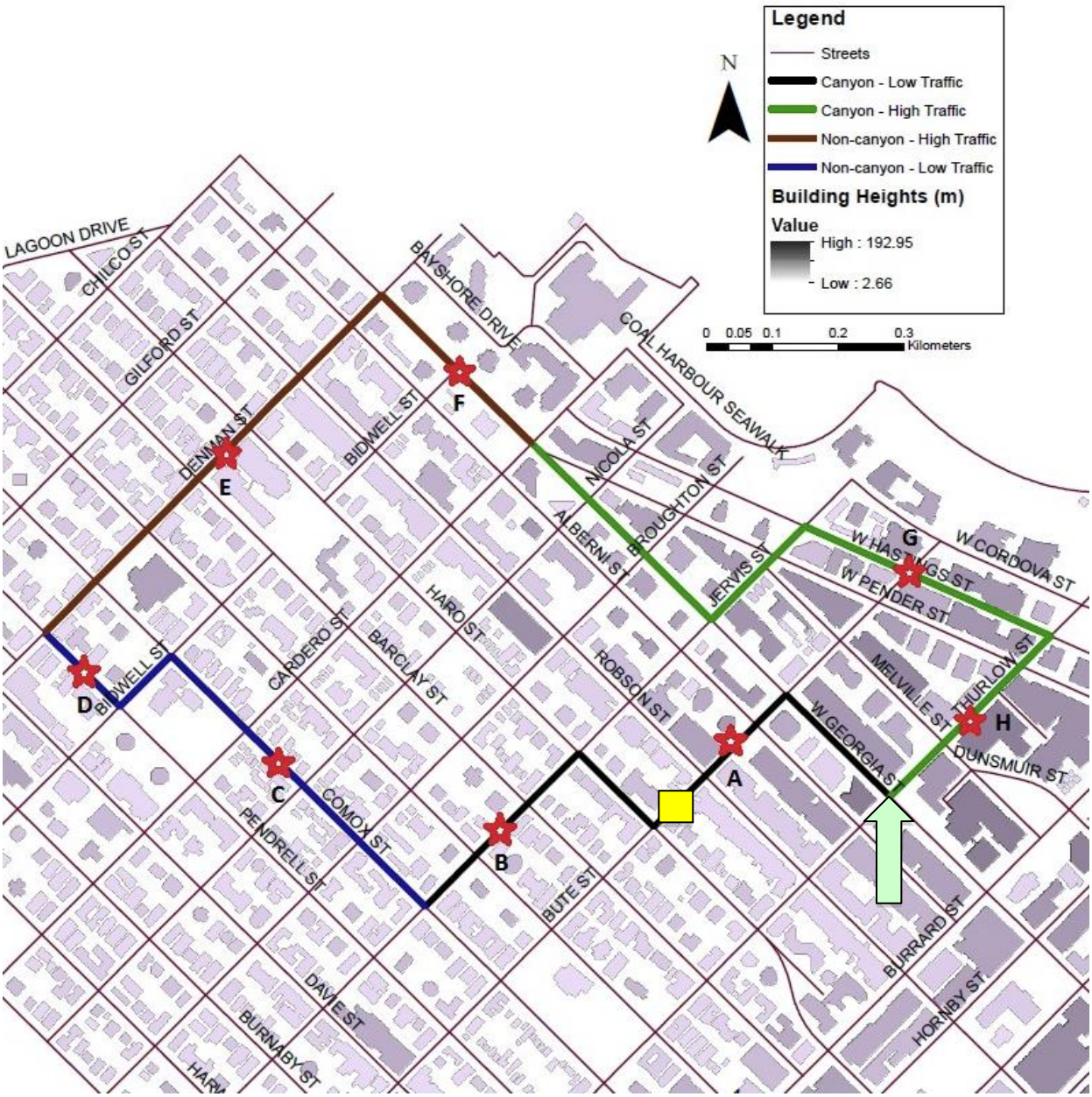

Figure 3.6 Mobile monitoring route classification scheme: C HT [MCE value = 1.9], C LT [MCE value = 1.0], NC HT [MCE value = 0.2] and NC LT [MCE value = 0.3]. Red stars labeled A through H denote measurement locations for traffic count and meteorological conditions. The fixed site is represented by the yellow square and the starting point is shown as a green arrow.

Table 3.3 summarizes the aspect ratios entered into the multi-criteria model (grouped by street segment classifications). Bearing this in mind, and taking into account traffic patterns, Figure 3.6 was constructed to illustrate the four road classifications. The four road segments were divided as:

1) NC HT: Denman St./Pendrell St. to W. Georgia St./ Cardero St.,

2) C HT: W. Georgia St./ Cardero St. to W. Georgia St./ Thurlow St.,

3) C LT: W. Georgia St./Thurlow St. to Jervis St./ Comox St., and

4) NC LT: Jervis St./ Comox St. to Denman St./ Pendrell St.

Table 3.3 Aspect ratio summary statistics for the four street segment classes. The total number of aspect ratio inputs is represented by n. Mean, standard deviation (SD), minimum (Min), and maximum (Max) are all dimensionless parameters.

Statistic	Classification			
	C HT	C LT	NC HT	NC LT
n	299	243	233	196
Min	0	0	0	0
Max	5.1	4.5	1.3	1.6
Mean	1.88	1.04	0.20	0.33
SD	1.64	1.22	0.26	0.35

Care was taken to verify the lognormal distribution of PM and PNC data. Histograms in Figure 3.7 suggest the data were lognormally distributed as the transformation caused the right-tailed distribution to better approximate a Gaussian spread. Notice how the positively skewed untransformed data (skewness of 76.11 for $PM_{2.5}$, 67.38 for PM_{10} and 6.45 for PNC) tends toward a zero for skewness once log-transformed (skewness of -0.56 for log-transformed $PM_{2.5}$, -0.59 for log-transformed PM_{10} and -0.25 for log-transformed PNC); this is a sign of an

asymmetric distribution balancing out. The large, critically non-normal kurtosis values in the pre-transformed dataset (7989.71 for $PM_{2.5}$, 6543.99 for PM_{10} and 81.46 for PNC) imply a taller and skinnier y-axis distribution than a normally distributed dataset (i.e. post-transformation values of 2.37, 2.21 and 2.00, respectively). Further justification is available in Table 3.4. Regardless of the pollutant measured, the mean was always greater than the median value. Additionally, the median and geometric mean were very close. These are all characteristics of lognormal distributions.

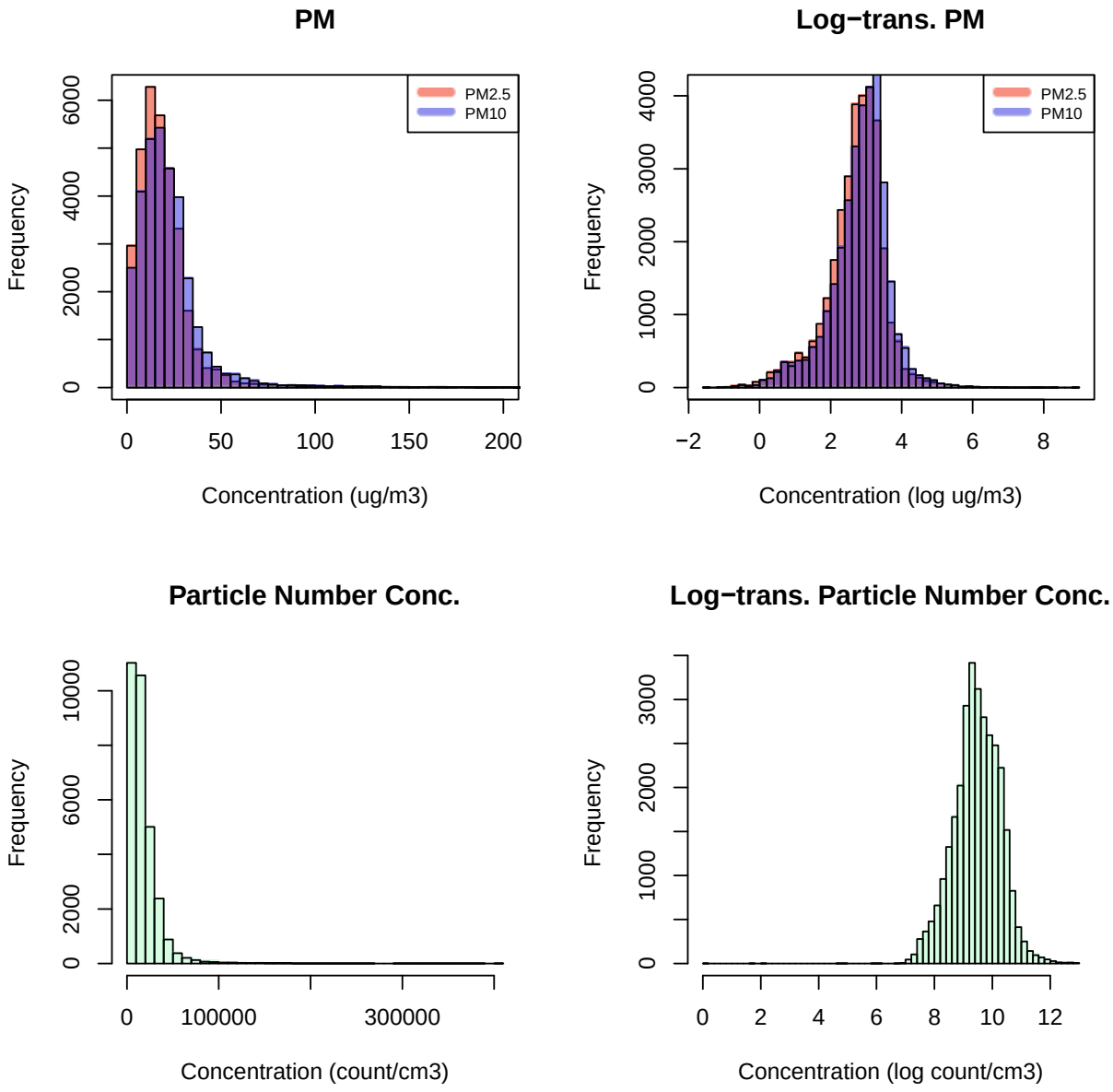

Figure 3.7 Untransformed (left) and log-transformed (right) histograms for corrected and LOD/√2 substituted $PM_{2.5}$ and PM_{10} [top panel] and PNC [bottom panel]. Note: the untransformed corrected $PM_{2.5}$ and PM_{10} [top left] is shown with a truncated x-axis.

Table 3.4 Summary statistics for untransformed, corrected, and LOD/√2 substituted $PM_{2.5}$, PM_{10} and PNC. The total number of measurements is represented by n. Mean, standard deviation (SD), 5^{th} percentile, 95^{th} percentile, median and geometric mean (Geo. Mean) are measured in $\mu g/m^3$ for PM results and particles/cm^3 for PNC results. Geometric standard deviation (Geo. SD), skewness and kurtosis are all dimensionless parameters. The averaging time was 10 seconds.

Statistic	$PM_{2.5}$	PM_{10}	PNC
n	32119	32119	30900
5^{th} percentile	2.92	3.44	3271
95^{th} percentile	43.84	50.56	42986
Mean	21.13	23.71	17798
SD	63.54	58.20	18475
Median	16.51	18.88	12998
Geo. Mean	14.80	16.90	12963
Geo. SD	2.27	2.27	2.23
Skewness	76.11	67.38	6.45
Kurtosis	7989.71	6543.99	81.46

In dealing with the left-censored lognormal data, the geometric standard deviations (GSDs) were analyzed for the raw (i.e. uncorrected and pre-substituted) DustTrak datasets. The GSDs of the handheld DustTrak for $PM_{2.5}$ and PM_{10} were 1.79 and 1.78, respectively; similarly, the GSDs of the desktop DustTrak for $PM_{2.5}$ and PM_{10} were 1.50 and 1.51, respectively. Hornung and Reed (248) recommend a substitution of LOD/√2 as the LOD/2 replacement should only be used when the data are highly skewed with a GSD of 3.0 or greater.

Three correction factors were applied to the instrument readings. These corrected for inter-instrument (DustTrak) variability (CF1), within-run variability (CF2), and between-day variability (CF3). CF1 was determined to be 1.104 and 1.117 for desktop DustTrak $PM_{2.5}$ and PM_{10}, respectively. For handheld DustTrak $PM_{2.5}$ and PM_{10}, CF1 was 0.914 and 0.905, respectively.

The within-run adjustment factors utilized the desktop DustTrak to correct the handheld DustTrak $PM_{2.5}$ or PM_{10} readings (with $PM_{2.5}$ or PM_{10} CF2s) and the CPC 3007 PNC readings (with $PM_{2.5}$ CF2s). CF2s ranged from 0.370 - 2.730 for $PM_{2.5}$ and from 0.333 - 2.571 for PM_{10}. The CF2 mean and standard deviation for $PM_{2.5}$ was 0.987 and 0.192, respectively. The CF2 mean and standard deviation for PM_{10} was 0.983 and 0.190, respectively.

Burnaby South Station's $PM_{2.5}$ and PM_{10} daily averages were used to calculate CF3 to adjust handheld DustTrak and CPC 3007 measurements. Since a high correlation ($r = 0.84$) existed between the $PM_{2.5}$ and PM_{10} estimated correction factors (Figure 3.8), the daily PM_{10} CF3s were used as a proxy for $PM_{2.5}$ CF3s for the last four sampling days (August 5th, 9th, 10th and 11th). During this period, the reference $PM_{2.5}$ monitor was removed for unexpected instrument servicing. The third correction factor (CF3) ranged from 0.39 to 1.64 with a mean of 1.01 and a standard deviation of 0.33 (Appendix C.2).

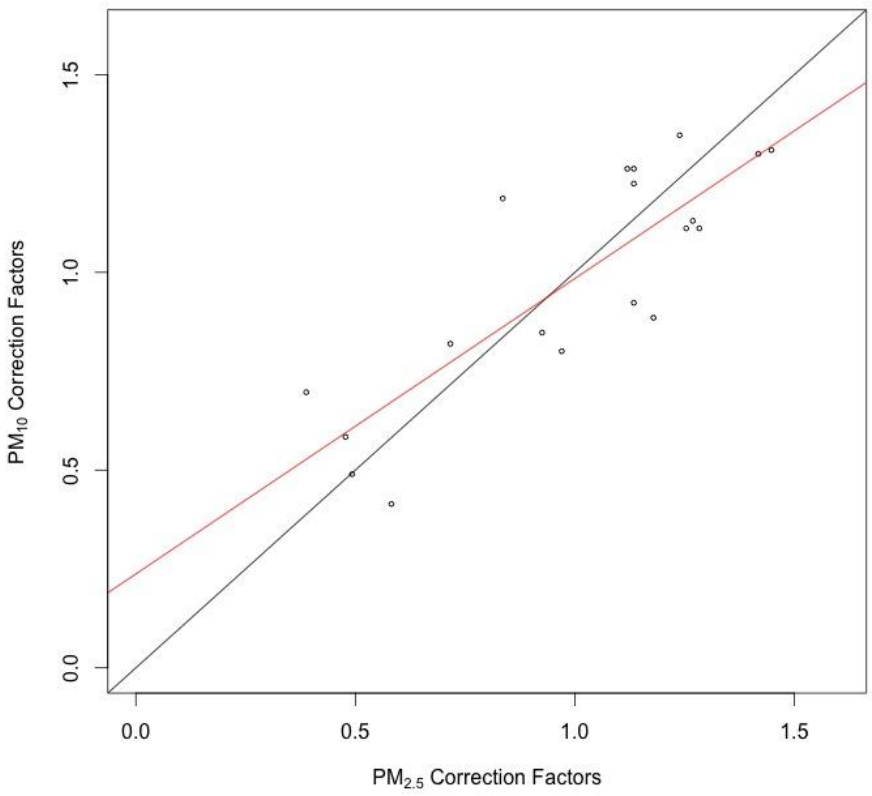

Figure 3.8 Between-day correction factor (CF3) for PM_{10} and $PM_{2.5}$. The black line shows a 1:1 relationship and the red line is the line of best fit.

Of the 44 mobile runs, 23 were performed during rush hours while 21 were performed during non-rush hours as defined earlier. Rush hour and non-rush hour stratified runs produced the following per-minute traffic counts corresponding with each of the 4 road segment classifications (Figure 3.9). Rush hours were found to have 0.8 ± 1.8 (NC LT), 3.6 ± 1.5 (C LT), 36.5 ± 8.9 (NC HT) and 8.3 ± 3.2 (C HT) vehicles/min. Non-rush hours were found to have 0.8 ± 0.4 (NC LT), 3.7 ± 1.3 (C LT), 32.6 ± 5.6 (NC HT) and 6.0 ± 1.9 (C HT) vehicles/min. As reported here, the variability in traffic counts was always lower in non-rush hours. Moreover, the

traffic counts were consistently greater in “high traffic” areas compared to “low traffic” areas. This analysis affirms the initial differentiation of high and low traffic.

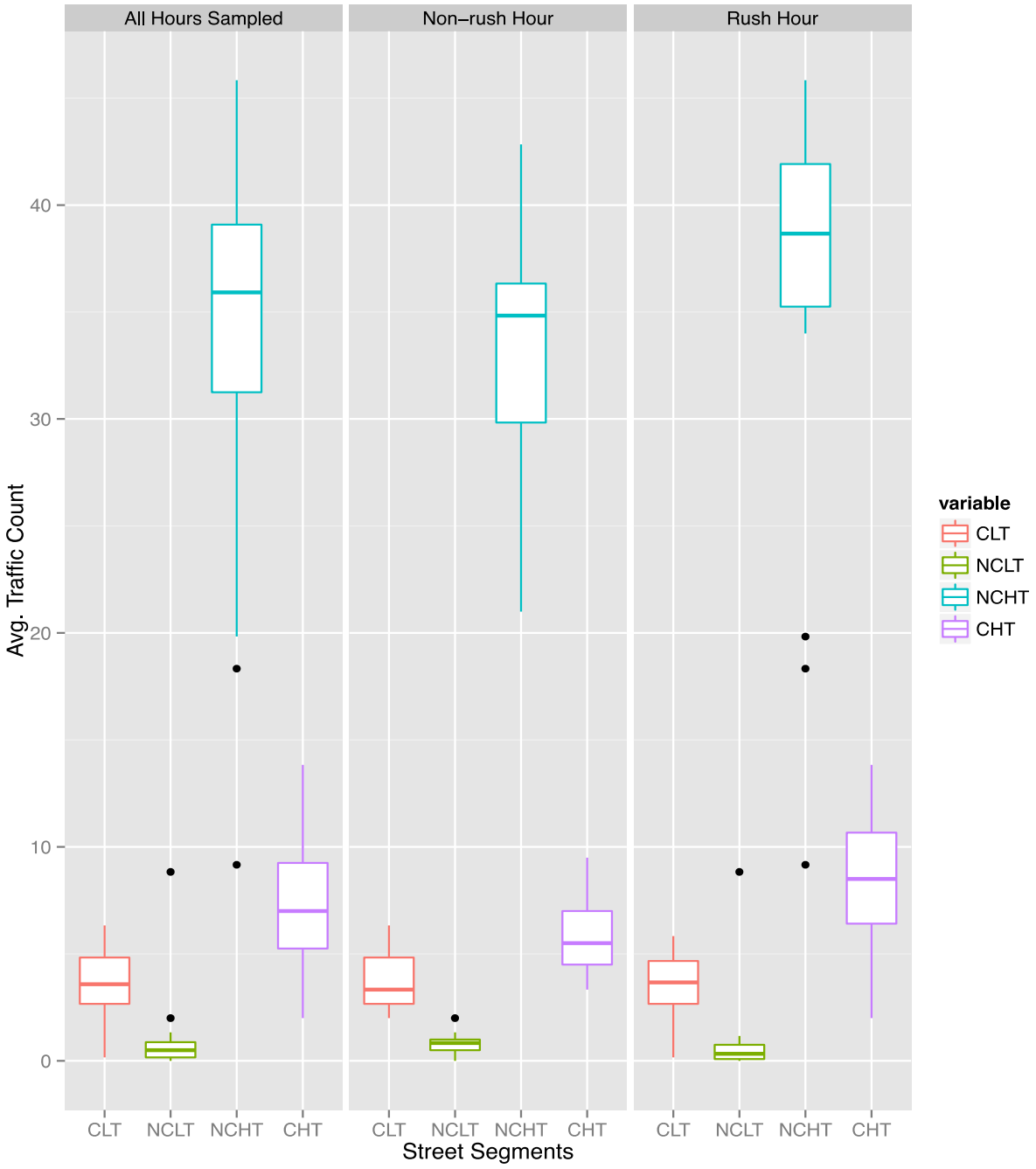

Figure 3.9 Boxplots for the average traffic counts during all hours sampled, non-rush hours, and rush hours. The horizontal lines within the box visualize the 25th percentile, the median and the 75th percentile. The upper and lower whiskers from the boxplot represent values of 1.5 times the interquartile range; outliers are plotted as points.

As one would expect, the descriptive statistics in Table 3.4 conveyed the likenesses between $PM_{2.5}$ and PM_{10} as both size fractions were measured simultaneously using one instrument (handheld DustTrak). And so, the remainder of the results focus on $PM_{2.5}$, as it is a better indicator of adverse health effects. Table 3.5 and Table 3.6 enable the stratified assessment of particulate pollution under forecasted rush hour and non-rush hour intervals. In non-rush hours, the roads experience an elevated variability in pollutant levels.

Table 3.5 Descriptive statistics for rush hour (RH)/ non-rush hour (NRH) stratified $PM_{2.5}$ in the 4 road segments. The total number of measurements is represented by n. Mean, standard deviation (SD), minimum (Min), maximum (Max) and geometric mean (Geo. Mean) are measured in µg/m^3. Geometric standard deviation (Geo. SD) is a dimensionless parameter. The averaging time was 10 seconds.

Time of Day	Parameter	n	Min	Max	Mean	SD	Geo. Mean	Geo. SD
RH	C LT	5983	0.43	874.98	18.12	20.49	13.55	2.19
	NC LT	3099	0.52	728.71	18.31	26.98	13.65	2.16
	NC HT	3582	0.48	4208.29	20.51	74.78	14.59	2.10
	C HT	4303	0.68	306.04	19.67	16.39	14.96	2.14
NRH	C LT	5500	0.22	722.76	21.03	23.71	15.90	2.21
	NC LT	2721	0.52	7805.20	22.50	151.48	13.70	2.53
	NC HT	3239	0.52	3257.67	29.33	90.94	16.63	2.74
	C HT	3692	0.36	2500.21	22.60	54.86	16.01	2.25

Table 3.6 Descriptive statistics for rush hour (RH)/ non-rush hour (NRH) stratified PNC in the 4 road segments. The total number of measurements is represented by n. Mean, standard deviation (SD), minimum (Min), maximum (Max) and geometric mean (Geo. Mean) are measured in particles/cm^3. Geometric standard deviation (Geo. SD) is a dimensionless parameter. The averaging time was 10 seconds.

Time of Day	Parameter	n	Min	Max	Mean	SD	Geo. Mean	Geo. SD
RH	C LT	5524	1072	247648	15089	12838	11138	2.24
	NC LT	2957	0	189813	13217	10828	9864	2.21
	NC HT	3408	0	175225	18284	14937	13917	2.24
	C HT	4119	1091	266661	23479	26079	15744	2.43
NRH	C LT	5240	0	188062	17803	12905	13931	2.09
	NC LT	2721	1494	112195	15177	12069	11913	2.01
	NC HT	3239	1557	184184	19051	15483	14474	2.14
	C HT	3692	2146	404351	19559	30406	13321	2.20

3.1.1 Linear mixed effects model

Two categorical variables were included in the final linear mixed effects model for $PM_{2.5}$ (AIC = 46761) and PNC (AIC = 50014) as outlined in Table 3.7 and Table 3.8, respectively. The street segment category was treated as a categorical variable with four levels (C HT, C LT, NC HT and NC LT) while rush hour was treated as a categorical variable with two levels (NRH = 0, RH = 1). Random effects for repeated measurements within runs were accounted for in the error term.

Table 3.7 Effect estimates for geometric mean concentrations of $PM_{2.5}$ (µg/m^3) and the corresponding 95% confidence intervals when compared to the reference category (NC LT).

	Effect Estimate	95% CI	p-value
Intercept (NC LT)	-	-	$< 2 \times 10^{-16}$ *
C HT	1.11	[1.09, 1.13]	$< 2 \times 10^{-16}$ *
C LT	1.08	[1.06, 1.09]	$< 2 \times 10^{-16}$ *
NC HT	1.16	[1.14, 1.18]	$< 2 \times 10^{-16}$ *
Rush Hour	0.92	[0.62, 1.36]	0.67

Table 3.8 Effect estimates for geometric mean of PNC and the corresponding 95% confidence intervals when compared to the reference category (NC LT).

	Effect Estimate	95% CI	p-value
Intercept (NC LT)	-	-	$< 2 \times 10^{-16}$ *
C HT	1.36	[1.34, 1.39]	$< 2 \times 10^{-16}$ *
C LT	1.17	[1.15, 1.19]	$< 2 \times 10^{-16}$ *
NC HT	1.34	[1.31, 1.36]	$< 2 \times 10^{-16}$ *
Rush Hour	0.94	[0.66, 1.34]	0.72

Table 3.7 indicates the $PM_{2.5}$ concentrations in the C HT, C LT and NC HT road segments were 1.11 fold, 1.08 fold and 1.34 fold greater than concentrations recorded in the NC LT road segment, respectively. Table 3.8 indicates the PNC concentrations in the C HT, C LT and NC HT road segments were 1.36 fold, 1.17 fold and 1.34 fold greater than concentrations recorded in the NC LT road segment, respectively.

3.2 Discussion

The downtown Vancouver multi-criteria evaluation model was established from the previous year's predominant wind direction and the aspect ratios of each road segment. Although these variables were given equal weighting when entering the analysis, the outcome of the multi-criteria evaluation (MCE values of 1.9, 1.0, 0.2 and 0.3 for C HT, C LT, NC HT and NC LT, respectively) remained largely driven by the aspect ratio variable (1.88, 1.04, 0.20 and 0.33 for the corresponding segments). Ideally, the MCE values for the street canyons in the mobile evaluation (C HT and C LT) would be more comparable so as to reduce uncertainty in downstream data interpretation.

A straightforward explanation for this phenomenon is that the Easterly wind direction evenly impacts pollutant removal in the downtown core's diagonally oriented road network.

With southwest-northeast and southeast-northwest roads alike, an Easterly wind will not be perfectly perpendicular to any roadway, thereby reducing the impact of wind in the model.

The street segment classifications of C HT, C LT, NC HT and NC LT were based in part on the ability to characterize traffic density as high or low. The appeal of the approach taken—that is, to combine traffic levels with the canyon characterization allowed an assessment of the impact of rush hour conditions on high and low traffic canyon and non-canyon road segments.

Traffic rates in vehicles/minute during rush hour were 8.3 ± 3.2 for C HT, 3.6 ± 1.5 for C LT, 36.5 ± 8.9 for NC HT and 0.8 ± 1.8 for NC LT. Traffic rates in vehicles/minute during non-rush hour were 6.0 ± 1.9 for C HT, 3.7 ± 1.3 C LT, 32.6 ± 5.6 NC HT and 0.8 ± 0.4 NC LT. These measurements act as affirmation that roads classified as "high traffic" did indeed experience greater traffic levels on average than those roads classified as "low traffic" throughout both rush hour and non-rush hour conditions (Table 3.5 for $PM_{2.5}$ and Table 3.6 for PNC). Notably, large differences in traffic were experienced between the NC HT and C HT road segments. This makes it less likely that any canyon effects can be observed. Another trend that was observed was the lower variability (as expressed by standard deviation) in non-rush hour conditions compared to rush-hour conditions. This reduced variability is likely a function of fewer vehicles traveling on the same road segments during non-rush hour conditions.

When comparing the final linear mixed effect models with the null models which excluded the rush hour fixed effect, rush hour effects were not statistically significant ($\alpha = 0.05$) in the final $PM_{2.5}$ ($p = 0.66$) and PNC ($p = 0.72$) models despite a slight improvement in model fit. Rush hour conditions resulted in an 8% reduction (95% CI: -38% to 36%) in the geometric mean of $PM_{2.5}$ concentrations and a 6% reduction (95% CI: -34% to 34%) in the geometric mean of PNC when compared with non-rush hour conditions. The effect of rush hour on particulate

matter concentrations is counterintuitive as the expected outcome should indicate higher concentrations during rush hours; however, the large confidence intervals around the effects estimates make these results difficult to interpret.

The street segment category levels were statistically significant predictors of $PM_{2.5}$ mass concentration and PNC in both final models. In the final model for $PM_{2.5}$, the estimates for the effects of C HT, C LT, and NC HT were an increase of 11%, 8%, and 16%, respectively, on the geometric mean of $PM_{2.5}$ concentrations compared with NC LT. Similarly, the final model for PNC showed C HT, C LT, and NC HT were associated with a 36%, 17% and 34% increase, respectively, on the geometric mean for PNC compared with NC LT. These outcomes clearly depict the street segment effect sizes were greater in the PNC model over the $PM_{2.5}$ model. This may demonstrate that PNC is a more sensitive metric of road traffic pollution than $PM_{2.5}$.

The finding that C LT had greater concentrations of $PM_{2.5}$ and PNC than NC LT in the linear fixed effects model is consistent with the study by Chau et al. (249) which found that 70% of the variability in PM_{10} concentration along a canyon is attributed to the aspect ratio of the road. This reinforces the underlying principle of using aspect ratios to define potential canyons.

Spadaro and Rabl (111) contend that the canyon effect is more pertinent for primary pollutants as secondary species have shorter residence times in canyons compared to the chemical reaction times. Given this, the effect estimates in the PNC model may more accurately represent the changes in local TRAP concentrations (when compared with the $PM_{2.5}$ model) as PNC is emitted as a primary pollutant whereas $PM_{2.5}$ can be emitted in a primary and secondary form. This is consistent with what other researchers have found. (150,250) The street canyon evaluation did not have the capabilities to distinguish the relative contribution of primary versus

secondary particulate matter pollution. Perhaps further investigations of primary TRAP pollutants in a street canyon (e.g. NO) will illustrate more apparent canyon effects.

For the street segment variable, the reference category was defined as NC LT as this segment was anticipated to experience the lowest concentrations among the four levels. Indeed, the results corroborate this reference category selection. Contrary to the expectation that the C HT level would show the largest fold-difference in particles concentration, this result was only evident in the more responsive PNC model. From the road segment effect estimates, the findings reveal C LT resulted in the smallest effect on concentration in both models (8% greater than NC LT for $PM_{2.5}$ and 17% greater than NC LT for PNC). Comparatively, the fixed effects of NC HT as compared with NC LT (i.e. the effect of traffic) showed an effect estimate increase of 16% and 34% for $PM_{2.5}$ and PNC, respectively. This noteworthy observation suggests it is not the classification as canyon/non-canyon that primarily influences the hypothesized increase in particulate matter concentrations, but more so the impact of traffic density as there is a doubling of the effect estimates. The larger effect estimate of traffic density is likely in part a result of elevated traffic causing turbulent conditions and road dust resuspension.

Collectively, the interaction analysis uncovers potential insufficiencies in the initial categorization of the street segment variable, as the effect estimate directionality is not consistent between the $PM_{2.5}$ and PNC models. The primary classification was motivated by field constraints and the best way to sort road types. The constraints included the necessity to select four roughly equidistant segments to capture predominantly canyon or non-canyon areas while accounting for low and high traffic patterns given limited traffic count data and instrument battery life. Future studies may benefit from a design that maintains canyon/ non-canyon, low

traffic/ high traffic, rush hour/ non-rush hour as three separate explanatory variables to further examine the underlying relationships.

This study was mainly constrained by the raw data limitations. Some inaccuracies in the public street data found in the City of Vancouver catalogue may have hindered precise aspect ratio calculations. In view of the fact that buildings are often setback from property lines, where possible, the street width was estimated using the addition of the shortest distance between the street segment centroid and the two nearest perpendicular neighbors. For street segments that only had one building nearby (within 35 m), the right-of-way street width was utilized as a substitute. A degree of uncertainty is inserted into the model due to these restrictions.

Another deficiency is the lack of finer-scale (e.g. downtown Vancouver) historical wind data as this model was limited to the regional scale (i.e. Vancouver). Unsuccessful attempts were made to secure more relevant wind data. Wind data collected during sampling was not inputted into the linear mixed effects model since the wind roses illustrated the tendency for the local wind direction to align with the traffic flow at the sampling positions.

As a whole, this street canyon study possesses a number of strengths. This work is among the first to characterize street canyons in a geographical area using a simple GIS-based model for aspect ratio and prevailing wind direction. This research stands out as it aims to assess a measure of urban morphology for an entire city center whereas the bulk of current canyon investigations explore the pollution differentials within a short stretch of road deemed a canyon as compared against a non-canyon.

In the mobile evaluations of the model (n = 44), measures were taken to ensure randomized sampling; the mobile monitoring direction and the side of the street were randomized using two successive coin tosses at the onset of each sampling run to minimize

systematic and predictable data influences. To obtain a representative sample of temporal variability, the sampling scheme was arranged to acquire equal runs of rush hour (7:00 – 9:00 and 16:00 – 18:00) and non-rush hour conditions. Furthermore, all hours between 7:00 and 23:00 were sampled to describe the temporal variation in concentrations that may develop during daytime traffic hours. Lastly, dataset normalization was accomplished by incorporating pre- and post-sampling co-locations of the DustTraks to correct for both inter-instrument correction (CF1) and within-run adjustment (CF2). A third correction factor smoothed the day-to-day variability (CF3).

Taken together, this model can be easily adapted to another geographical region. The model withstood the mobile monitoring evaluation indicating some achievement in correctly identifying canyons and non-canyons. Additional strategies worthy of consideration include generating more definitive explanatory variables to re-appraise this model.

Chapter 4: Conclusion

The thesis objectives of 1) evaluating AQMesh performance via co-location and 2) creation and appraisal of a street canyon model were accomplished throughout this body of work.

Our project outcomes suggest that AQMesh, as assayed in the side-by-side London and Vancouver comparison requires further improvement to data quality before its incorporation into robust monitoring applications. Nonetheless, promising co-location comparisons since this project indicate that post-processing adjustments may have improved data output for these instruments. In order to move the state of air quality technologies (e.g. AQMesh) forward, the research community should continue to develop standardized assessments for data quality, data validation, calibration and field evaluations to support the successful integration of novel instrumentation into the industry. This is consistent with the recommendation of the 1st EuNetAir Air Quality Joint Intercomparison Exercise. (217,241)

A basic street canyon model was built using GIS-sourced building footprints, building heights, street width and predominant wind direction. This basic model has laid some of the framework for future iterations of canyon prediction modeling and may support efforts to better define personal exposures in intra-urban LUR models. In addition, a simplistic model with fewer inputs can help select potential canyons for more detailed analyses. (74) TRAP in the form of $PM_{2.5}$ and PNC concentrations were shown to increase in C HT, C LT and NC HT street segments when compared to the reference level, NC LT. More specifically, the effect estimates suggest that traffic density plays a greater role in the determination of TRAP exposures than street canyons. Although the results of this study indicate that traffic level characterization

requires more attention than street canyon identification, further investigations are needed to confirm which of the two variables is indeed more important in personal exposure classification.

Bibliography

1. Bell ML, Samet JM. Air Pollution. In: Howard Frumkin, editor. Environmental Health: From Global to Local. 2nd ed. San Francisco (CA): Jossey-Bass; 2010.

2. GBD 2015 Risk Factors Collaborators. Global, regional, and national comparative risk assessment of 79 behavioural, environmental and occupational, and metabolic risks or clusters of risks, 1990-2015: a systematic analysis for the Global Burden of Disease Study 2015. Lancet Lond Engl. 2016 Oct 8;388(10053):1659–724.

3. Harrison RM. Sources of Air Pollution. In: Air Quality Guidelines: Global Update 2005 Particulate matter, ozone, nitrogen dioxide and sulfur dioxide. World Health Organization; 2006.

4. Brunekreef B, Holgate S. Air pollution and health. The Lancet. 2002 Oct 19;360(9341):1233–42.

5. Dashdendev B, Fukushima LK, Woo MS, Ganbaatar E, Warburton D. Carbon monoxide pollution and lung function in urban compared with rural Mongolian children. Respirology. 2011;16(4):653–658.

6. Environment Canada. Volatile Organic Compounds (VOCs) [Internet]. Environment Canada. 2004 [cited 2013 Jul 4]. Available from: http://www.ec.gc.ca/air/default.asp?lang=En&n=15B9B65A-1

7. Environment Canada. Particulate Matter [Internet]. Environment Canada. 2004 [cited 2013 Jul 4]. Available from: http://www.ec.gc.ca/air/default.asp?lang=En&n=2C68B45C-1

8. Environment Canada. Particulate Matter Main Emission Sources [Internet]. Environment Canada. 2004 [cited 2013 Jul 4]. Available from: http://www.ec.gc.ca/air/default.asp?lang=En&n=9A24D6D1-1

9. Lawrence S, Sokhi R, Ravindra K, Mao H, Prain HD, Bull ID. Source apportionment of traffic emissions of particulate matter using tunnel measurements. Atmos Environ. 2013 Oct;77:548–57.

10. Charron A, Harrison RM. Fine (PM2.5) and coarse (PM2.5-10) particulate matter on a heavily trafficked London highway: sources and processes. Environ Sci Technol. 2005 Oct 15;39(20):7768–76.

11. Wahlina P, Palmgren F, Van Dingenen R. Experimental studies of ultrafine particles in streets and the relationship to traffic. Atmos Environ. 2001 Jan 1;35:S63–9.

12. World Health Organization. WHO Air quality guidelines for particulate matter, ozone, nitrogen dioxide and sulfur dioxide: Global update 2005 Summary of risk assessment [Internet]. World Health Organization. 2006 [cited 2013 May 10]. Available from: http://whqlibdoc.who.int/hq/2006/WHO_SDE_PHE_OEH_06.02_eng.pdf

13. Zhou Y, Levy JI. Factors influencing the spatial extent of mobile source air pollution impacts: a meta-analysis. BMC Public Health. 2007;7:89.

14. Kroll JH, Seinfeld JH. Chemistry of secondary organic aerosol: Formation and evolution of low-volatility organics in the atmosphere. Atmos Environ. 2008 May;42(16):3593–624.

15. Health Effects Institute. Traffic-Related Air Pollution: A Critical Review of the Literature on Emissions, Exposure, and Health Effects. Special Report No. 17 [Internet]. Health Effects Institute. 2010 [cited 2013 May 12]. Available from: http://pubs.healtheffects.org/getfile.php?u=553

16. Brauer M, Reynolds C, Hystad P. Traffic-related air pollution and health : a Canadian perspective on scientific evidence and potential exposure-mitigation strategies [Internet]. 2012 [cited 2013 May 22]. Available from: https://circle.ubc.ca/bitstream/handle/2429/41542/2012-03-01%20Traffic%20and%20Health%20FINAL.pdf?sequence=1

17. Johnson JY, Rowe BH, Allen RW, Peters PA, Villeneuve PJ. A case-control study of medium-term exposure to ambient nitrogen dioxide pollution and hospitalization for stroke. BMC Public Health. 2013;13:368.

18. Wellenius GA, Schwartz J, Mittleman MA. Air pollution and hospital admissions for ischemic and hemorrhagic stroke among medicare beneficiaries. Stroke J Cereb Circ. 2005 Dec;36(12):2549–53.

19. Yorifuji T, Kashima S, Tsuda T, Ishikawa-Takata K, Ohta T, Tsuruta K, et al. Long-term exposure to traffic-related air pollution and the risk of death from hemorrhagic stroke and lung cancer in Shizuoka, Japan. Sci Total Environ. 2013 Jan 15;443:397–402.

20. Rivera M, Basagaña X, Aguilera I, Foraster M, Agis D, de Groot E, et al. Association between long-term exposure to traffic-related air pollution and subclinical atherosclerosis: the REGICOR study. Environ Health Perspect. 2013 Feb;121(2):223–30.

21. Hoffmann B, Moebus S, Möhlenkamp S, Stang A, Lehmann N, Dragano N, et al. Residential exposure to traffic is associated with coronary atherosclerosis. Circulation. 2007 Jul 31;116(5):489–96.

22. Bauer M, Moebus S, Möhlenkamp S, Dragano N, Nonnemacher M, Fuchsluger M, et al. Urban Particulate Matter Air Pollution Is Associated With Subclinical Atherosclerosis: Results From the HNR (Heinz Nixdorf Recall) Study. J Am Coll Cardiol. 2010 Nov 23;56(22):1803–8.

23. Künzli N, Jerrett M, Garcia-Esteban R, Basagaña X, Beckermann B, Gilliland F, et al. Ambient Air Pollution and the Progression of Atherosclerosis in Adults. PLoS ONE. 2010 Feb 8;5(2):e9096.

24. Gan WQ, Koehoorn M, Davies HW, Demers PA, Tamburic L, Brauer M. Long-term exposure to traffic-related air pollution and the risk of coronary heart disease hospitalization and mortality. Environ Health Perspect. 2011 Apr;119(4):501–7.

25. Tsai D-H, Wang J-L, Chuang K-J, Chan C-C. Traffic-related air pollution and cardiovascular mortality in central Taiwan. Sci Total Environ. 2010 Mar 15;408(8):1818–23.

26. Lindgren A, Stroh E, Montnémery P, Nihlén U, Jakobsson K, Axmon A. Traffic-related air pollution associated with prevalence of asthma and COPD/chronic bronchitis. A cross-sectional study in Southern Sweden. Int J Health Geogr. 2009 Jan 20;8(1):2.

27. Pujades-Rodríguez M, Lewis S, McKeever T, Britton J, Venn A. Effect of living close to a main road on asthma, allergy, lung function and chronic obstructive pulmonary disease. Occup Environ Med. 2009 Oct;66(10):679–84.

28. Meng X, Wang C, Cao D, Wong C-M, Kan H. Short-Term Effect of Ambient Air Pollution on COPD Mortality in Four Chinese Cities. Atmos Environ [Internet]. [cited 2013 May 23]; Available from: http://www.sciencedirect.com/science/article/pii/S1352231013003440

29. Lewis SA, Antoniak M, Venn AJ, Davies L, Goodwin A, Salfield N, et al. Secondhand Smoke, Dietary Fruit Intake, Road Traffic Exposures, and the Prevalence of Asthma: A Cross-Sectional Study in Young Children. Am J Epidemiol. 2005 Mar 1;161(5):406–11.

30. Clark NA, Demers PA, Karr CJ, Koehoorn M, Lencar C, Tamburic L, et al. Effect of early life exposure to air pollution on development of childhood asthma. Environ Health Perspect. 2010 Feb;118(2):284–90.

31. Gehring U, Wijga AH, Brauer M, Fischer P, de Jongste JC, Kerkhof M, et al. Traffic-related air pollution and the development of asthma and allergies during the first 8 years of life. Am J Respir Crit Care Med. 2010 Mar 15;181(6):596–603.

32. Schildcrout JS, Sheppard L, Lumley T, Slaughter JC, Koenig JQ, Shapiro GG. Ambient air pollution and asthma exacerbations in children: an eight-city analysis. Am J Epidemiol. 2006 Sep 15;164(6):505–17.

33. Patel MM, Chillrud SN, Deepti KC, Ross JM, Kinney PL. Traffic-related air pollutants and exhaled markers of airway inflammation and oxidative stress in New York City adolescents. Environ Res. 2013 Feb;121:71–8.

34. Samoli E, Nastos PT, Paliatsos AG, Katsouyanni K, Priftis KN. Acute effects of air pollution on pediatric asthma exacerbation: Evidence of association and effect modification. Environ Res. 2011 Apr;111(3):418–24.

35. Carlsten C, Dybuncio A, Becker A, Chan-Yeung M, Brauer M. Traffic-related air pollution and incident asthma in a high-risk birth cohort. Occup Environ Med. 2011 Apr;68(4):291–5.

36. Anderson HR, Favarato G, Atkinson RW. Long-term exposure to air pollution and the incidence of asthma: meta-analysis of cohort studies. Air Qual Atmosphere Health. 2013 Mar 1;6(1):47–56.

37. Wang H-Y, Pizzichini MMM, Becker AB, Duncan JM, Ferguson AC, Greene JM, et al. Disparate geographic prevalences of asthma, allergic rhinoconjunctivitis and atopic eczema among adolescents in five Canadian cities. Pediatr Allergy Immunol Off Publ Eur Soc Pediatr Allergy Immunol. 2010 Aug;21(5):867–77.

38. Patel MM, Quinn JW, Jung KH, Hoepner L, Diaz D, Perzanowski M, et al. Traffic density and stationary sources of air pollution associated with wheeze, asthma, and immunoglobulin E from birth to age 5 years among New York City children. Environ Res. 2011 Nov;111(8):1222–9.

39. Ryan PH, LeMasters G, Biagini J, Bernstein D, Grinshpun SA, Shukla R, et al. Is it traffic type, volume, or distance? Wheezing in infants living near truck and bus traffic. J Allergy Clin Immunol. 2005 Aug;116(2):279–84.

40. Venn A, Yemaneberhan H, Lewis S, Parry E, Britton J. Proximity of the home to roads and the risk of wheeze in an Ethiopian population. Occup Environ Med. 2005 Jun;62(6):376–80.

41. Karr CJ, Demers PA, Koehoorn MW, Lencar CC, Tamburic L, Brauer M. Influence of ambient air pollutant sources on clinical encounters for infant bronchiolitis. Am J Respir Crit Care Med. 2009 Nov 15;180(10):995–1001.

42. Karr CJ, Rudra CB, Miller KA, Gould TR, Larson T, Sathyanarayana S, et al. Infant exposure to fine particulate matter and traffic and risk of hospitalization for RSV bronchiolitis in a region with lower ambient air pollution. Environ Res. 2009 Apr;109(3):321–7.

43. Ségala C, Poizeau D, Mesbah M, Willems S, Maidenberg M. Winter air pollution and infant bronchiolitis in Paris. Environ Res. 2008 Jan;106(1):96–100.

44. MacIntyre EA, Karr CJ, Koehoorn M, Demers PA, Tamburic L, Lencar C, et al. Residential air pollution and otitis media during the first two years of life. Epidemiol Camb Mass. 2011 Jan;22(1):81–9.

45. Yorifuji T, Naruse H, Kashima S, Ohki S, Murakoshi T, Takao S, et al. Residential proximity to major roads and preterm births. Epidemiol Camb Mass. 2011 Jan;22(1):74–80.

46. Brauer M, Lencar C, Tamburic L, Koehoorn M, Demers P, Karr C. A cohort study of traffic-related air pollution impacts on birth outcomes. Environ Health Perspect. 2008 May;116(5):680–6.

47. Lee P-C, Talbott EO, Roberts JM, Catov JM, Bilonick RA, Stone RA, et al. Ambient air pollution exposure and blood pressure changes during pregnancy. Environ Res. 2012 Aug;117:46–53.

48. Wu J, Wilhelm M, Chung J, Ritz B. Comparing exposure assessment methods for traffic-related air pollution in an adverse pregnancy outcome study. Environ Res. 2011 Jul;111(5):685–92.

49. Llop S, Ballester F, Estarlich M, Esplugues A, Rebagliato M, Iñiguez C. Preterm birth and exposure to air pollutants during pregnancy. Environ Res. 2010 Nov;110(8):778–85.

50. Chiu Y-H, Bellinger DC, Coull BA, Anderson S, Barber R, Wright RO, et al. Associations between Traffic-Related Black Carbon Exposure and Attention in a Prospective Birth Cohort of Urban Children. Environ Health Perspect. 2013 May 10;

51. Raaschou-Nielsen O, Andersen ZJ, Hvidberg M, Jensen SS, Ketzel M, Sørensen M, et al. Lung cancer incidence and long-term exposure to air pollution from traffic. Environ Health Perspect. 2011 Jun;119(6):860–5.

52. Beelen R, Hoek G, van den Brandt PA, Goldbohm RA, Fischer P, Schouten LJ, et al. Long-term exposure to traffic-related air pollution and lung cancer risk. Epidemiol Camb Mass. 2008 Sep;19(5):702–10.

53. Slezakova K, Castro D, Begonha A, Delerue-Matos C, Alvim-Ferraz M da C, Morais S, et al. Air pollution from traffic emissions in Oporto, Portugal: Health and environmental implications. Microchem J. 2011 Sep;99(1):51–9.

54. Parent M-É, Goldberg MS, Crouse DL, Ross NA, Chen H, Valois M-F, et al. Traffic-related air pollution and prostate cancer risk: a case-control study in Montreal, Canada. Occup Environ Med. 2013 Mar 26;

55. Crouse DL, Goldberg MS, Ross NA, Chen H, Labrèche F. Postmenopausal breast cancer is associated with exposure to traffic-related air pollution in Montreal, Canada: a case-control study. Environ Health Perspect. 2010 Nov;118(11):1578–83.

56. Finkelstein MM, Jerrett M, Sears MR. Traffic air pollution and mortality rate advancement periods. Am J Epidemiol. 2004 Jul 15;160(2):173–7.

57. Hoek G, Brunekreef B, Goldbohm S, Fischer P, van den Brandt PA. Association between mortality and indicators of traffic-related air pollution in the Netherlands: a cohort study. The Lancet. 2002 Oct 19;360(9341):1203–9.

58. Finkelstein MM, Jerrett M. A study of the relationships between Parkinson's disease and markers of traffic-derived and environmental manganese air pollution in two Canadian cities. Environ Res. 2007 Jul;104(3):420–32.

59. Power MC, Weisskopf MG, Alexeeff SE, Coull BA, Spiro A 3rd, Schwartz J. Traffic-related air pollution and cognitive function in a cohort of older men. Environ Health Perspect. 2011 May;119(5):682–7.

60. Ranft U, Schikowski T, Sugiri D, Krutmann J, Krämer U. Long-term exposure to traffic-related particulate matter impairs cognitive function in the elderly. Environ Res. 2009 Nov;109(8):1004–11.

61. Thiering E, Cyrys J, Kratzsch J, Meisinger C, Hoffmann B, Berdel D, et al. Long-term exposure to traffic-related air pollution and insulin resistance in children: results from the GINIplus and LISAplus birth cohorts. Diabetologia. 2013 May 11;

62. Dales RE, Cakmak S, Vidal CB, Rubio MA. Air pollution and hospitalization for acute complications of diabetes in Chile. Environ Int. 2012 Oct 1;46:1–5.

63. Brook RD, Jerrett M, Brook JR, Bard RL, Finkelstein MM. The relationship between diabetes mellitus and traffic-related air pollution. J Occup Environ Med Am Coll Occup Environ Med. 2008 Jan;50(1):32–8.

64. Brimblecombe P. Urban Air Pollution. In: Brimblecombe P, Maynard RL, editors. The Urban Atmosphere and Its Effects. London: Imperial College Press; 2001.

65. United Nations Environment Programme. Urban Air Pollution [Internet]. United Nations Environment Programme: Urban Environment Unit. [cited 2013 Jun 10]. Available from: http://www.unep.org/urban_environment/Issues/urban_air.asp

66. United Nations. World Urbanization Prospects: The 2011 Revision [Internet]. United Nations. 2012 [cited 2013 May 17]. Available from: http://esa.un.org/unup/pdf/FINAL-FINAL_REPORT%20WUP2011_Annextables_01Aug2012_Final.pdf

67. Clougherty JE, Wright RJ, Baxter LK, Levy JI. Land use regression modeling of intra-urban residential variability in multiple traffic-related air pollutants. Environ Health Glob Access Sci Source. 2008;7:17.

68. Seaman NL. Meteorological modeling for air-quality assessments. Atmos Environ. 2000;34(12–14):2231–59.

69. Arain MA, Blair R, Finkelstein N, Brook JR, Sahsuvaroglu T, Beckerman B, et al. The use of wind fields in a land use regression model to predict air pollution concentrations for health exposure studies. Atmos Environ. 2007 May;41(16):3453–64.

70. Gryparis A, Coull BA, Schwartz J, Suh HH. Semiparametric latent variable regression models for spatiotemporal modelling of mobile source particles in the greater Boston area. J R Stat Soc Ser C Appl Stat. 2007;56(2):183–209.

71. Zou B, Wilson JG, Zhan FB, Zeng Y. Spatially differentiated and source-specific population exposure to ambient urban air pollution. Atmos Environ. 2009 Aug;43(26):3981–8.

72. Murena F, Favale G, Vardoulakis S, Solazzo E. Modelling dispersion of traffic pollution in a deep street canyon: Application of CFD and operational models. Atmos Environ. 2009 May;43(14):2303–11.

73. Xie S, Zhang Y, Qi L, Tang X. Spatial distribution of traffic-related pollutant concentrations in street canyons. Atmos Environ. 2003 Jul;37(23):3213–24.

74. Vardoulakis S, Fisher BE., Pericleous K, Gonzalez-Flesca N. Modelling air quality in street canyons: a review. Atmos Environ. 2003 Jan;37(2):155–82.

75. Taseiko OV, Mikhailuta SV, Pitt A, Lezhenin AA, Zakharov YV. Air pollution dispersion within urban street canyons. Atmos Environ. 2009 Jan;43(2):245–52.

76. Jensen SS, Larson T, Deepti KC, Kaufman JD. Modeling traffic air pollution in street canyons in New York City for intra-urban exposure assessment in the US Multi-Ethnic Study of atherosclerosis and air pollution. Atmos Environ. 2009 Sep;43(30):4544–56.

77. Zhu Y, Hinds WC, Kim S, Shen S, Sioutas C. Study of ultrafine particles near a major highway with heavy-duty diesel traffic. Atmos Environ. 2002 Sep;36(27):4323–35.

78. Ntziachristos L, Ning Z, Geller MD, Sheesley RJ, Schauer JJ, Sioutas C. Fine, ultrafine and nanoparticle trace element compositions near a major freeway with a high heavy-duty diesel fraction. Atmos Environ. 2007 Sep;41(27):5684–96.

79. Padró-Martínez LT, Patton AP, Trull JB, Zamore W, Brugge D, Durant JL. Mobile monitoring of particle number concentration and other traffic-related air pollutants in a near-highway neighborhood over the course of a year. Atmos Environ. 2012 Dec;61:253–64.

80. Gómez-Perales J., Colvile R., Nieuwenhuijsen M., Fernández-Bremauntz A, Gutiérrez-Avedoy V., Páramo-Figueroa V., et al. Commuters' exposure to PM2.5, CO, and benzene in public transport in the metropolitan area of Mexico City. Atmos Environ. 2004 Mar;38(8):1219–29.

81. Bloomer BJ, Vinnikov KY, Dickerson RR. Changes in seasonal and diurnal cycles of ozone and temperature in the eastern U.S. Atmos Environ. 2010 Jul;44(21–22):2543–51.

82. Pryor SC, Steyn DG. Hebdomadal and diurnal cycles in ozone time series from the Lower Fraser Valley, B.C. Atmos Environ. 1995 May;29(9):1007–19.

83. Wallace J, Corr D, Kanaroglou P. Topographic and spatial impacts of temperature inversions on air quality using mobile air pollution surveys. Sci Total Environ. 2010 Oct 1;408(21):5086–96.

84. Mooibroek D, Schaap M, Weijers EP, Hoogerbrugge R. Source apportionment and spatial variability of PM2.5 using measurements at five sites in the Netherlands. Atmos Environ. 2011 Aug;45(25):4180–91.

85. Van Atten C, Brauer M, Funk T, Gilbert NL, Graham L, Kaden D, et al. Assessing population exposures to motor vehicle exhaust. Rev Environ Health. 2005 Sep;20(3):195–214.

86. Hertel O, Hvidberg M, Ketzel M, Storm L, Stausgaard L. A proper choice of route significantly reduces air pollution exposure — A study on bicycle and bus trips in urban streets. Sci Total Environ. 2008 Jan 15;389(1):58–70.

87. Mayer H. Air pollution in cities. Atmos Environ. 1999 Oct;33(24–25):4029–37.

88. Marr LC, Harley RA. Spectral analysis of weekday–weekend differences in ambient ozone, nitrogen oxide, and non-methane hydrocarbon time series in California. Atmos Environ. 2002 May;36(14):2327–35.

89. Chinkin LR, Main HH, Roberts PT. Weekday/Weekend Ozone Observations in the South Coast Air Basin Volume III: Analysis of Summer 2000 Field Measurements and Supporting Data [Internet]. 2002. Available from: https://www.arb.ca.gov/research/weekendeffect/final_wknd_7_1/dafr_06-06-02_report.pdf

90. Tang W, Zhao C, Geng F, Peng L, Zhou G, Gao W, et al. Study of ozone "weekend effect" in Shanghai. Sci China Ser Earth Sci. 2008 Sep 1;51(9):1354–60.

91. Vingarzan R, Taylor B. Trend analysis of ground level ozone in the greater Vancouver/Fraser Valley area of British Columbia. Atmos Environ. 2003 May;37(16):2159–71.

92. Fleming SW. An information theoretic perspective on mesoscale seasonal variations in ground-level ozone. Atmos Environ. 2007 Sep;41(27):5746–55.

93. Larson T, Su J, Baribeau A-M, Buzzelli M, Setton E, Brauer M. A spatial model of urban winter woodsmoke concentrations. Environ Sci Technol. 2007 Apr 1;41(7):2429–36.

94. Fine PM, Cass GR, Simoneit BRT. Organic compounds in biomass smoke from residential wood combustion: Emissions characterization at a continental scale. J Geophys Res Atmospheres. 2002;107(D21):ICC 11-1–ICC 11-9.

95. McGowan JA, Hider RN, Chacko E, Town GI. Particulate air pollution and hospital admissions in Christchurch, New Zealand. Aust N Z J Public Health. 2002 Feb;26(1):23–9.

96. Karner AA, Eisinger DS, Niemeier DA. Near-roadway air quality: synthesizing the findings from real-world data. Environ Sci Technol. 2010 Jul 15;44(14):5334–44.

97. Mavroidis I, Ilia M. Trends of NOx, NO2 and O3 concentrations at three different types of air quality monitoring stations in Athens, Greece. Atmos Environ. 2012 Dec;63:135–47.

98. Barrefors G. Air pollutants in road tunnels. Sci Total Environ. 1996 Oct 28;189–190:431–5.

99. Knibbs LD, de Dear RJ, Morawska L, Mengersen KL. On-road ultrafine particle concentration in the M5 East road tunnel, Sydney, Australia. Atmos Environ. 2009 Jul;43(22–23):3510–9.

100. Frumkin H. Environmental Health: From Global to Local. 2nd ed. Jossey-Bass; 2010. 1280 p.

101. Gan WQ, McLean K, Brauer M, Chiarello SA, Davies HW. Modeling population exposure to community noise and air pollution in a large metropolitan area. Environ Res. 2012 Jul;116:11–6.

102. Patel MM, Chillrud SN, Correa JC, Feinberg M, Hazi Y, Deepti KC, et al. Spatial and temporal variations in traffic-related particulate matter at New York City high schools. Atmos Environ. 2009 Oct;43(32):4975–81.

103. Cole-Hunter T, Morawska L, Stewart I, Jayaratne R, Solomon C. Inhaled particle counts on bicycle commute routes of low and high proximity to motorised traffic. Atmos Environ. 2012 Dec;61:197–203.

104. Tong HY, Hung WT, Cheung CS. On-road motor vehicle emissions and fuel consumption in urban driving conditions. J Air Waste Manag Assoc 1995. 2000 Apr;50(4):543–54.

105. Su JG, Brauer M, Buzzelli M. Estimating urban morphometry at the neighborhood scale for improvement in modeling long-term average air pollution concentrations. Atmos Environ. 2008 Nov;42(34):7884–93.

106. Classification and Criteria for Setting Up Air-Quality Monitoring Stations [Internet]. ADEME Publications. 2002 [cited 2013 Aug 21]. Available from: http://www2.ademe.fr/servlet/KBaseShow?sort=-1&cid=96&m=3&catid=17618&p1=00&p2=00

107. Baker J, Walker HL, Cai X. A study of the dispersion and transport of reactive pollutants in and above street canyons—a large eddy simulation. Atmos Environ. 2004 Dec;38(39):6883–92.

108. Allard F, Ghiaus C. Natural Ventilation in the Urban Environment Assessment and Design. London, UK; 2005.

109. Georgakis C, Santamouris M. On the estimation of wind speed in urban canyons for ventilation purposes—Part 1: Coupling between the undisturbed wind speed and the canyon wind. Build Environ. 2008 Aug;43(8):1404–10.

110. Oke TR. Street design and urban canopy layer climate. Energy Build. 1988 Mar 22;11(1):103–13.

111. Spadaro J, Rabl A. Damage costs due to automotive air pollution and the influence of street canyons. Atmos Env 1994. 2001;4763–75.

112. Johansson C, Norman M, Gidhagen L. Spatial & temporal variations of PM10 and particle number concentrations in urban air. Environ Monit Assess. 2007 Apr 1;127(1–3):477–87.

113. Rose D, Wehner B, Ketzel M, Engler C, Voigtländer J, Tuch T, et al. Atmospheric number size distributions of soot particles and estimation of emission factors. Atmos Chem Phys. 2006 Mar 30;6(4):1021–31.

114. Tsai MY, Chen KS. Measurements and three-dimensional modeling of air pollutant dispersion in an Urban Street Canyon. Atmos Environ. 2004 Nov;38(35):5911–24.

115. Väkevä M, Hämeri K, Kulmala M, Lahdes R, Ruuskanen J, Laitinen T. Street level versus rooftop concentrations of submicron aerosol particles and gaseous pollutants in an urban street canyon. Atmos Environ. 1999 Apr 1;33(9):1385–97.

116. Eeftens M, Beekhuizen J, Beelen R, Wang M, Vermeulen R, Brunekreef B, et al. Quantifying urban street configuration for improvements in air pollution models. Atmos Environ. 2013 Jun;72:1–9.

117. Vardoulakis S, Valiantis M, Milner J, ApSimon H. Operational air pollution modelling in the UK—Street canyon applications and challenges. Atmos Environ. 2007 Jul;41(22):4622–37.

118. Brauer M, Hoek G, van Vliet P, Meliefste K, Fischer P, Gehring U, et al. Estimating Long-Term Average Particulate Air Pollution Concentrations: Application of Traffic Indicators and Geographic Information Systems. Epidemiology. 2003 Mar;14(2):228–39.

119. Government of Canada EC. National Air Pollution Surveillance Program (NAPS) [Internet]. Environment Canada. 2010 [cited 2014 Feb 23]. Available from: http://www.ec.gc.ca/rnspa-naps/

120. Health Canada and Environment Canada. Chapter 2—Air Quality Health Index (Status Report of the Commissioner of the Environment and Sustainable Development) [Internet]. 2009 [cited 2014 Feb 24]. Available from: http://www.oag-bvg.gc.ca/internet/docs/parl_cesd_200903_02_e.pdf

121. Metro Vancouver. 2014 Lower Fraser Valley Air Quality Monitoring Report [Internet]. 2015 [cited 2017 Apr 21]. Available from: http://www.metrovancouver.org/services/air-quality/AirQualityPublications/2014_LFV_AQ_Monitoring_Report.pdf

122. Hystad P, Setton E, Cervantes A, Poplawski K, Deschenes S, Brauer M, et al. Creating National Air Pollution Models for Population Exposure Assessment in Canada. Environ Health Perspect. 2011 Aug;119(8):1123–9.

123. Demerjian KL. A review of national monitoring networks in North America. Atmos Environ. 2000;34(12–14):1861–84.

124. Canadian Council of Ministers of the Environment. Ambient Air Monitoring Protocol for PM2.5 and Ozone [Internet]. Canadian Council of Ministers of the Environment; 2011 [cited 2014 Mar 9]. Available from: http://www.ccme.ca/assets/pdf/pm_oz_cws_monitoring_protocol_pn1456_e.pdf

125. Snyder EG, Watkins TH, Solomon PA, Thoma ED, Williams RW, Hagler GSW, et al. The Changing Paradigm of Air Pollution Monitoring. Environ Sci Technol. 2013 Oct 15;47(20):11369–77.

126. Marshall JD, Nethery E, Brauer M. Within-urban variability in ambient air pollution: Comparison of estimation methods. Atmos Environ. 2008 Feb;42(6):1359–69.

127. United States Environmental Protection Agency. Next Generation Air Monitoring [Internet]. United States Environmental Protection Agency. 2013 [cited 2013 May 19]. Available from: http://www.epa.gov/research/airscience/air-sensor-research.htm

128. Généreux M, Auger N, Goneau M, Daniel M. Neighbourhood socioeconomic status, maternal education and adverse birth outcomes among mothers living near highways. J Epidemiol Community Health. 2008 Aug;62(8):695–700.

129. Smargiassi A, Berrada K, Fortier I, Kosatsky T. Traffic intensity, dwelling value, and hospital admissions for respiratory disease among the elderly in Montreal (Canada): a case-control analysis. J Epidemiol Community Health. 2006 Jun;60(6):507–12.

130. Band PR, Jiang H, Zielinski JM. Analysis of lung cancer incidence relating to air pollution levels adjusting for cigarette smoking: a case-control study. In 2011 [cited 2014 Feb 13]. p. 445–53. Available from: http://library.witpress.com/pages/PaperInfo.asp?PaperID=22819

131. Cakmak S, Mahmud M, Grgicak-Mannion A, Dales RE. The influence of neighborhood traffic density on the respiratory health of elementary schoolchildren. Environ Int. 2012 Feb;39(1):128–32.

132. Değer L, Plante C, Goudreau S, Smargiassi A, Perron S, Thivierge RL, et al. Home environmental factors associated with poor asthma control in Montreal children: a population-based study. J Asthma Off J Assoc Care Asthma. 2010 Jun;47(5):513–20.

133. Jerrett M, Finkelstein MM, Brook JR, Arain MA, Kanaroglou P, Stieb DM, et al. A cohort study of traffic-related air pollution and mortality in Toronto, Ontario, Canada. Environ Health Perspect. 2009 May;117(5):772–7.

134. Crouse DL, Peters PA, van Donkelaar A, Goldberg MS, Villeneuve PJ, Brion O, et al. Risk of nonaccidental and cardiovascular mortality in relation to long-term exposure to low concentrations of fine particulate matter: a Canadian national-level cohort study. Environ Health Perspect. 2012 May;120(5):708–14.

135. Nawrot TS, Perez L, Künzli N, Munters E, Nemery B. Public health importance of triggers of myocardial infarction: a comparative risk assessment. The Lancet. 2011 Mar 4;377(9767):732–40.

136. Amram O, Abernethy R, Brauer M, Davies H, Allen RW. Proximity of public elementary schools to major roads in Canadian urban areas. Int J Health Geogr. 2011 Dec 21;10(1):68.

137. Yu CH, Morandi MT, Weisel CP. Passive dosimeters for nitrogen dioxide in personal/indoor air sampling: a review. J Expo Sci Environ Epidemiol. 2008 Sep;18(5):441–51.

138. Krupa SV, Legge AH. Passive sampling of ambient, gaseous air pollutants: an assessment from an ecological perspective. Environ Pollut Barking Essex 1987. 2000 Jan;107(1):31–45.

139. Klánová J, Kohoutek J, Hamplová L, Urbanová P, Holoubek I. Passive air sampler as a tool for long-term air pollution monitoring: Part 1. Performance assessment for seasonal and spatial variations. Environ Pollut Barking Essex 1987. 2006 Nov;144(2):393–405.

140. Wheeler AJ, Smith-Doiron M, Xu X, Gilbert NL, Brook JR. Intra-urban variability of air pollution in Windsor, Ontario—Measurement and modeling for human exposure assessment. Environ Res. 2008 Jan;106(1):7–16.

141. Guéguen F, Stille P, Dietze V, Gieré R. Chemical and isotopic properties and origin of coarse airborne particles collected by passive samplers in industrial, urban, and rural environments. Atmos Environ. 2012 Dec;62:631–45.

142. Wagner J, Naik-Patel K, Wall S, Harnly M. Measurement of ambient particulate matter concentrations and particle types near agricultural burns using electron microscopy and passive samplers. Atmos Environ. 2012 Jul;54:260–71.

143. Barn P, Jackson P, Suzuki N, Kosatsky T, Jennejohn D, Henderson S, et al. Air Quality Assessment Tools: A Guide for Public Health Practitioners [Internet]. 2011 [cited 2014 Feb 23]. Available from: http://ncceh.ca/sites/default/files/Air_Quality_Assessment_Tools_Dec_2011.pdf

144. Arnold SJ, ApSimon H, Barlow J, Belcher S, Bell M, Boddy JW, et al. Introduction to the DAPPLE Air Pollution Project. Sci Total Environ. 2004 Oct 1;332(1–3):139–53.

145. Van Poppel M, Peters J, Bleux N. Methodology for setup and data processing of mobile air quality measurements to assess the spatial variability of concentrations in urban environments. Environ Pollut [Internet]. [cited 2013 Jul 6]; Available from: http://www.sciencedirect.com/science/article/pii/S0269749113000961

146. DeLuca PF, Corr D, Wallace J, Kanaroglou P. Effective mitigation efforts to reduce road dust near industrial sites: Assessment by mobile pollution surveys. J Environ Manage. 2012 May 15;98:112–8.

147. Lightowlers C, Nelson T, Setton E, Peter Keller C. Determining the spatial scale for analysing mobile measurements of air pollution. Atmos Environ. 2008 Jul;42(23):5933–7.

148. Briggs DJ, de Hoogh K, Morris C, Gulliver J. Effects of travel mode on exposures to particulate air pollution. Environ Int. 2008 Jan;34(1):12–22.

149. Gulliver J, Briggs DJ. Journey-time exposure to particulate air pollution. Atmos Environ. 2007 Nov;41(34):7195–207.

150. Boogaard H, Borgman F, Kamminga J, Hoek G. Exposure to ultrafine and fine particles and noise during cycling and driving in 11 Dutch cities. Atmos Environ. 2009 Sep;43(27):4234–42.

151. Thai A, McKendry I, Brauer M. Particulate matter exposure along designated bicycle routes in Vancouver, British Columbia. Sci Total Environ. 2008 Nov 1;405(1–3):26–35.

152. McNabola A, Broderick BM, Gill L. Reduced exposure to air pollution on the boardwalk in Dublin, Ireland. Measurement and prediction. Environ Int. 2008 Jan;34(1):86–93.

153. Hankey S, Lindsey G, Wang X, Borah J, Hoff K, Utecht B, et al. Estimating use of non-motorized infrastructure: Models of bicycle and pedestrian traffic in Minneapolis, MN. Landsc Urban Plan. 2012 Sep 15;107(3):307–16.

154. Tang UW, Wang Z. Determining gaseous emission factors and driver's particle exposures during traffic congestion by vehicle-following measurement techniques. J Air Waste Manag Assoc 1995. 2006 Nov;56(11):1532–9.

155. Buonocore JJ, Lee HJ, Levy JI. The influence of traffic on air quality in an urban neighborhood: a community-university partnership. Am J Public Health. 2009 Nov;99 Suppl 3:S629-635.

156. Wang X, Westerdahl D, Chen LC, Wu Y, Hao J, Pan X, et al. Evaluating the air quality impacts of the 2008 Beijing Olympic Games: On-road emission factors and black carbon profiles. Atmos Environ. 2009 Sep;43(30):4535–43.

157. Westerdahl D, Wang X, Pan X, Zhang KM. Characterization of on-road vehicle emission factors and microenvironmental air quality in Beijing, China. Atmos Environ. 2009 Jan;43(3):697–705.

158. Poplawski K, Setton E. MAML- Mobile Air Monitoring Laboratory Data Collection Report- James Bay Air Quality Study June-August 2009 [Internet]. 2010 [cited 2014 Feb 23]. Available from: http://www.viha.ca/NR/rdonlyres/E9167F08-04E0-4A72-A303-F2B0BD1054B7/0/jbaq_maml_2010.pdf

159. Setton E. Mobile Air Quality Monitoring: Targeting Local Issues [Internet]. [cited 2014 Feb 23]. Available from: http://www.bc.lung.ca/association_and_services/documents/07Setton-MobileMonitoring.pdf

160. Wallace J, Corr D, Deluca P, Kanaroglou P, McCarry B. Mobile monitoring of air pollution in cities: the case of Hamilton, Ontario, Canada. J Environ Monit. 2009 May 1;11(5):998–1003.

161. Steed A, Milton R. Using tracked mobile sensors to make maps of environmental effects. Pers Ubiquitous Comput. 2008 Feb;12(4):331–342.

162. Isakov V, Touma JS, Khlystov A. A method of assessing air toxics concentrations in urban areas using mobile platform measurements. J Air Waste Manag Assoc 1995. 2007 Nov;57(11):1286–95.

163. Westerdahl D, Fruin S, Sax T, Fine PM, Sioutas C. Mobile platform measurements of ultrafine particles and associated pollutant concentrations on freeways and residential streets in Los Angeles. Atmos Environ. 2005 Jun;39(20):3597–610.

164. Bowker GE, Baldauf R, Isakov V, Khlystov A, Petersen W. The effects of roadside structures on the transport and dispersion of ultrafine particles from highways. Atmos Environ. 2007 Dec;41(37):8128–39.

165. Castell N, Viana M, Minguillón MC, Guerreiro C, Querol X. Real-world application of new sensor technologies for air quality monitoring (European Topic Centre on Air Pollution and Climate Change Mitigation Technical Paper 2013/16) [Internet]. 2013 [cited 2014 Feb 28]. Available from: http://acm.eionet.europa.eu/docs/ETCACM_TP_2013_16_new_AQ_SensorTechn.pdf

166. Briggs DJ, Collins S, Elliott P, Fischer P, Kingham S, Lebret E, et al. Mapping urban air pollution using GIS: a regression-based approach. Int J Geogr Inf Sci. 1997;11(7):699–718.

167. Ryan PH, LeMasters GK. A review of land-use regression models for characterizing intraurban air pollution exposure. Inhal Toxicol. 2007;19 Suppl 1:127–33.

168. Gilliland F, Avol E, Kinney P, Jerrett M, Dvonch T, Lurmann F, et al. Air pollution exposure assessment for epidemiologic studies of pregnant women and children: lessons learned from the Centers for Children's Environmental Health and Disease Prevention Research. Environ Health Perspect. 2005 Oct;113(10):1447–54.

169. Hoek G, Beelen R, de Hoogh K, Vienneau D, Gulliver J, Fischer P, et al. A review of land-use regression models to assess spatial variation of outdoor air pollution. Atmos Environ. 2008 Oct;42(33):7561–78.

170. Jerrett M, Arain A, Kanaroglou P, Beckerman B, Potoglou D, Sahsuvaroglu T, et al. A review and evaluation of intraurban air pollution exposure models. J Expo Anal Environ Epidemiol. 2005 Mar;15(2):185–204.

171. Kanaroglou PS, Jerrett M, Morrison J, Beckerman B, Arain MA, Gilbert NL, et al. Establishing an air pollution monitoring network for intra-urban population exposure assessment: A location-allocation approach. Atmos Environ. 2005 Apr;39(13):2399–409.

172. Henderson SB, Beckerman B, Jerrett M, Brauer M. Application of land use regression to estimate long-term concentrations of traffic-related nitrogen oxides and fine particulate matter. Environ Sci Technol. 2007 Apr 1;41(7):2422–8.

173. Wang R, Henderson SB, Sbihi H, Allen RW, Brauer M. Temporal stability of land use regression models for traffic-related air pollution. Atmos Environ. 2013 Jan;64:312–9.

174. Larson T, Henderson SB, Brauer M. Mobile monitoring of particle light absorption coefficient in an urban area as a basis for land use regression. Environ Sci Technol. 2009 Jul 1;43(13):4672–8.

175. Abernethy RC, Allen RW, McKendry IG, Brauer M. A Land Use Regression Model for Ultrafine Particles in Vancouver, Canada. Environ Sci Technol. 2013 May 21;47(10):5217–25.

176. Novotny EV, Bechle MJ, Millet DB, Marshall JD. National satellite-based land-use regression: NO2 in the United States. Environ Sci Technol. 2011 May 15;45(10):4407–14.

177. Poplawski K, Gould T, Setton E, Allen R, Su J, Larson T, et al. Intercity transferability of land use regression models for estimating ambient concentrations of nitrogen dioxide. J Expo Sci Environ Epidemiol. 2009 Jan;19(1):107–17.

178. Allen RW, Amram O, Wheeler AJ, Brauer M. The transferability of NO and NO2 land use regression models between cities and pollutants. Atmos Environ. 2011 Jan;45(2):369–78.

179. Brauer M. How much, how long, what, and where: air pollution exposure assessment for epidemiologic studies of respiratory disease. Proc Am Thorac Soc. 2010 May;7(2):111–5.

180. Beelen R, Hoek G, Pebesma E, Vienneau D, de Hoogh K, Briggs DJ. Mapping of background air pollution at a fine spatial scale across the European Union. Sci Total Environ. 2009 Mar 1;407(6):1852–67.

181. Cyrys J, Hochadel M, Gehring U, Hoek G, Diegmann V, Brunekreef B, et al. GIS-Based Estimation of Exposure to Particulate Matter and NO2 in an Urban Area: Stochastic versus Dispersion Modeling. Environ Health Perspect. 2005 Aug;113(8):987–92.

182. Mölter A, Lindley S, de Vocht F, Simpson A, Agius R. Modelling air pollution for epidemiologic research — Part I: A novel approach combining land use regression and air dispersion. Sci Total Environ. 2010 Nov 1;408(23):5862–9.

183. Mölter A, Lindley S, de Vocht F, Simpson A, Agius R. Modelling air pollution for epidemiologic research – Part II: Predicting temporal variation through land use regression. Sci Total Environ. 2010 Dec 1;409(1):211–7.

184. Wilton D, Szpiro A, Gould T, Larson T. Improving spatial concentration estimates for nitrogen oxides using a hybrid meteorological dispersion/land use regression model in Los Angeles, CA and Seattle, WA. Sci Total Environ. 2010 Feb 1;408(5):1120–30.

185. Finkelstein MM, Jerrett M, DeLuca P, Finkelstein N, Verma DK, Chapman K, et al. Relation between income, air pollution and mortality: a cohort study. Can Med Assoc J. 2003 Sep 2;169(5):397–402.

186. Mercer LD, Szpiro AA, Sheppard L, Lindström J, Adar SD, Allen RW, et al. Comparing universal kriging and land-use regression for predicting concentrations of gaseous oxides of nitrogen (NOx) for the Multi-Ethnic Study of Atherosclerosis and Air Pollution (MESA Air). Atmos Environ. 2011 Aug;45(26):4412–20.

187. United States Environmental Protection Agency. DRAFT Roadmap for Next Generation Air Monitoring [Internet]. 2013 [cited 2013 Nov 4]. Available from: http://www.epa.gov/research/airscience/docs/roadmap-20130308.pdf

188. Norwegian Institute for Air Research. Project [Internet]. CITI-SENSE. 2012 [cited 2014 Feb 18]. Available from: http://www.citi-sense.eu/Project.aspx

189. Williams R, Kilaru V, Snyder E, Kaufman A, Dye T, Rutter A, et al. Air Sensor Guidebook [Internet]. United States Environmental Protection Agency; 2014 [cited 2017 Jun 11]. Available from: https://www.epa.gov/air-sensor-toolbox/how-use-air-sensors-air-sensor-guidebook

190. Bart M, Williams DE, Ainslie B, McKendry I, Salmond J, Grange SK, et al. High Density Ozone Monitoring Using Gas Sensitive Semi-Conductor Sensors in the Lower Fraser Valley, British Columbia. Environ Sci Technol. 2014 Feb 28;48(7):3970–7.

191. Miskell G, Salmond J, Alavi-Shoshtari M, Bart M, Ainslie B, Grange S, et al. Data Verification Tools for Minimizing Management Costs of Dense Air-Quality Monitoring Networks. Environ Sci Technol. 2015 Dec 10;50(2):835–46.

192. Pijolat C, Pupier C, Sauvan M, Tournier G, Lalauze R. Gas detection for automotive pollution control. Sens Actuators B Chem. 1999 Oct 19;59(2–3):195–202.

193. Fujita EM, Campbell DE. Review of Current Air Monitoring Capabilities near Refineries in the San Francisco Bay Area [Internet]. 2013 [cited 2014 Feb 26]. Available from: http://councilofindustries.org/wp-content/uploads/2013/06/BAAQMD-Comm-Monitoring-DRI-Report_2013.pdf

194. Wan J, Yu Y, Wu Y, Feng R, Yu N. Hierarchical Leak Detection and Localization Method in Natural Gas Pipeline Monitoring Sensor Networks. Sensors. 2011 Dec 27;12(1):189–214.

195. Bennett M, Christie SM, Graham A, Garry KP, Velikov S, Poll DI, et al. Abatement of an Aircraft Exhaust Plume Using Aerodynamic Baffles. Environ Sci Technol. 2013 Mar 5;47(5):2346–52.

196. Alfoldy B, Balzani J, Lagler F. Final Report on: Remote Sensing of Ships' Emissions of Sulphur Dioxide [Internet]. 2011 [cited 2014 Feb 26]. Available from: http://ec.europa.eu/environment/air/transport/pdf/ships/Final-report.pdf

197. Gerboles M. Developments and Applications of Sensor Technologies for Ambient Air Monitoring. Workshop "Current and Future Air Quality Monitoring" [Internet]. 2012 Apr 25 [cited 2014 Feb 26]; Barcelona, Spain. Available from: http://www.airmontech.eu/fileadmin/airmontech/user/2012-presentations/Day_2_09h10_MGerboles_26_April_2012.pdf

198. Mun M, Reddy S, Shilton K, Yau N, Burke J, Estrin D, et al. PEIR, the personal environmental impact report, as a platform for participatory sensing systems research. In: Proceedings of the 7th international conference on Mobile systems, applications, and services [Internet]. New York, NY, USA: ACM; 2009 [cited 2013 Feb 19]. p. 55–68. (MobiSys '09). Available from: http://doi.acm.org/10.1145/1555816.1555823

199. Ferrero L, Mocnik G, Ferrini BS, Perrone MG, Sangiorgi G, Bolzacchini E. Vertical profiles of aerosol absorption coefficient from micro-Aethalometer data and Mie calculation over Milan. Sci Total Environ. 2011 Jun 15;409(14):2824–37.

200. Chou J. Chapter 1: Introduction. In: Hazardous Gas Monitors: A Practical Guide to Selection, Operation and Applications. New York: McGraw-Hill; 2000. p. 27–35.

201. Mead MI, Popoola OAM, Stewart GB, Landshoff P, Calleja M, Hayes M, et al. The use of electrochemical sensors for monitoring urban air quality in low-cost, high-density networks. Atmos Environ. 2013 May;70:186–203.

202. Vaughn DL, Dye TS, Roberts PT, Ray AE, DeWinter JL. Characterization of Low-Cost NO2 Sensors (Draft Final Report Prepared for U.S. Environmental Protection Agency) [Internet]. 2010 [cited 2014 Feb 25]. Available from: http://airqualityegg.wikispaces.com/file/view/NO2%20Sensors%20Report.pdf/284357322/NO2%20Sensors%20Report.pdf

203. Liu X, Cheng S, Liu H, Hu S, Zhang D, Ning H. A Survey on Gas Sensing Technology. Sensors. 2012 Jul 16;12(7):9635–65.

204. Choi K-Y, Park J-S, Park K-B, Kim HJ, Park H-D, Kim S-D. Low power micro-gas sensors using mixed SnO2 nanoparticles and MWCNTs to detect NO2, NH3, and xylene gases for ubiquitous sensor network applications. Sens Actuators B Chem. 2010 Sep 21;150(1):65–72.

205. Moon SE, Lee HK, Choi NJ, Lee J, Yang WS, Kim J, et al. Low-power-Consumption metal oxide NO2 gas sensor based on micro-heater and screen printing technology. J Nanosci Nanotechnol. 2012 Jul;12(7):5543–6.

206. Chou J. Chapter 5: Infrared Gas Sensors. In: Hazardous Gas Monitors: A Practical Guide to Selection, Operation and Applications. New York: McGraw-Hill; 2000. p. 55–71.

207. Othman MF, Shazali K. Wireless Sensor Network Applications: A Study in Environment Monitoring System. Procedia Eng. 2012;41:1204–10.

208. Arora A, Dutta P, Bapat S, Kulathumani V, Zhang H, Naik V, et al. A line in the sand: A wireless sensor network for target detection, classification, and tracking. Comput Netw Elsevier. 2004;46:605–634.

209. Owojaiye G, Sun Y. Focal design issues affecting the deployment of wireless sensor networks for pipeline monitoring. Ad Hoc Netw. 2013 May;11(3):1237–53.

210. Zhu Y, Song J, Dong F. Applications of wireless sensor network in the agriculture environment monitoring. Procedia Eng. 2011;16:608–14.

211. Erol-Kantarci M, Mouftah HT. Wireless multimedia sensor and actor networks for the next generation power grid. Ad Hoc Netw. 2011 Jun;9(4):542–51.

212. Grgić K, Zagar D, Križanović V. Medical applications of wireless sensor networks - current status and future directions. Med Glas Off Publ Med Assoc Zenica-Doboj Cant Bosnia Herzeg. 2012 Feb;9(1):23–31.

213. Akyildiz IF, Su W, Sankarasubramaniam Y, Cayirci E. Wireless sensor networks: a survey. Comput Netw. 2002 Mar 15;38(4):393–422.

214. Metro Vancouver. Metro Vancouver Integrated Air Quality and Greenhouse Gas Management Plan: October 2011 [Internet]. 2011 [cited 2013 May 14]. Available from: http://public.metrovancouver.org/about/publications/Publications/IntegratedAirQualityGreenhouseGasManagementPlan-October2011.pdf

215. Hart JK, Martinez K. Environmental Sensor Networks: A revolution in the earth system science? Earth-Sci Rev. 2006 Oct;78(3–4):177–91.

216. Fu H-L, Chen H-C, Lin P. APS: Distributed air pollution sensing system on Wireless Sensor and Robot Networks. Comput Commun. 2012 May 15;35(9):1141–50.

217. Borrego C, Costa AM, Ginja J, Amorim M, Coutinho M, Karatzas K, et al. Assessment of air quality microsensors versus reference methods: The EuNetAir joint exercise. 246-263 [Internet]. 2016 [cited 2017 May 14]; Available from: https://brage.bibsys.no/xmlui/handle/11250/2435490

218. Wang A, Brauer M. Review of Next Generation Air Monitors for Air Pollution [Internet]. 2014 [cited 2017 Apr 28]. Available from: https://open.library.ubc.ca/cIRcle/collections/facultyresearchandpublications/52383/items/1.0132725

219. South Coast Air Quality Management District. AQ-SPEC Air Quality Sensor Performance Evaluation Center [Internet]. South Coast Air Quality Management District. [cited 2017 Jun 11]. Available from: http://www.aqmd.gov/aq-spec/evaluations/summary

220. Williams R, Long R, Beaver M, Kaufman A, Zeiger F, Heimbinder M, et al. Sensor Evaluation Report [Internet]. United States Environmental Protection Agency; 2014 [cited 2017 Jun 11]. Available from: http://www.aqmd.gov/docs/default-source/aq-spec/resources-page/us-epa---sensor-evaluation-report.pdf?sfvrsn=0

221. Williams R, Kaufman A, Garvey S. Next Generation Air Monitoring (NGAM) VOC Sensor Evaluation Report [Internet]. United States Environmental Protection Agency; 2015 [cited 2017 Jun 11]. Available from: https://cfpub.epa.gov/si/si_public_record_report.cfm?dirEntryId=308114&simpleSearch=1&searchAll=Next+generation+air+monitoring

222. Holstius DM, Pillarisetti A, Smith KR, Seto E. Field calibrations of a low-cost aerosol sensor at a regulatory monitoring site in California. Atmos Meas Tech Discuss. 2014 Jan 27;7(1):605–32.

223. Mykhaylova N, Sabaliauskas K, Wang JM, Jaroudi E, Jeong C-H, Brook J, et al. A Novel Method for Reliable Long-term Assessment of Exposure to Traffic-related Air Pollution Mixtures. 2013 Oct 29.

224. Aberer K, Sathe S, Chakraborty D, Martinoli A, Barrenetxea G, Faltings B, et al. OpenSense: Open Community Driven Sensing of Environment [Internet]. 2010. Available from: http://saketsathe.net/papers/iwgs10_vision.pdf

225. Williams R, Kaufman A, Hanley T, Rice J, Garvey S. Evaluation of Field-deployed Low Cost PM Sensors [Internet]. United States Environmental Protection Agency; 2014 [cited 2017 Jun 11]. Available from: https://cfpub.epa.gov/si/si_public_record_report.cfm?dirEntryId=297517&simpleSearch=1&searchAll=EPA%2F600%2FR-14%2F464

226. Williams R, Kaufman A, Hanley T, Rice J, Garvey S. Evaluation of Elm and Speck Sensors [Internet]. United States Environmental Protection Agency; 2016 [cited 2017 Jun 11]. Available from: https://cfpub.epa.gov/si/si_public_record_report.cfm?dirEntryId=310285

227. Hasenfratz D, Saukh O, Thiele L. On-the-Fly Calibration of Low-Cost Gas Sensors. In: Picco GP, Heinzelman W, editors. Wireless Sensor Networks [Internet]. Springer Berlin Heidelberg; 2012 [cited 2014 Feb 27]. p. 228–44. (Lecture Notes in Computer Science). Available from: http://link.springer.com.ezproxy.library.ubc.ca/chapter/10.1007/978-3-642-28169-3_15

228. Pinto AR, Montez C, Araújo G, Vasques F, Portugal P. An approach to implement data fusion techniques in wireless sensor networks using genetic machine learning algorithms. Inf Fusion. 2014 Jan;15:90–101.

229. Tan R, Xing G, Yuan Z, Liu X, Yao J. System-Level Calibration for Fusion-Based Wireless Sensor Networks. In: Real-Time Systems Symposium (RTSS), 2010 IEEE 31st. 2010. p. 215–24.

230. AQMesh – realising a new approach to air quality monitoring [Internet]. Geotech. 2013 [cited 2014 Feb 1]. Available from: http://www.geotechuk.com/latest-news/latest-news/aqmesh-%E2%80%93-realising-a-new-approach-to-air-quality-monitoring.aspx

231. AQMesh Inc. AQMesh Technical specification V4 [Internet]. [cited 2017 May 13]. Available from: http://www.aqmesh.com/product/technical-details/

232. Geotech. Geotech AQMesh Technical Specification (Iss.01).

233. Outdoor air quality [Internet]. Geotech. 2011 [cited 2014 Jan 30]. Available from: http://www.geotechuk.com/products/outdoor-air-quality.aspx

234. Geotech. AQMesh air quality monitor (AQMesh Version: 33) [Internet]. [cited 2014 Feb 1]. Available from: http://www.geotechuk.com/products/outdoor-air-quality/aqmesh/public-pdf.aspx

235. Barratt B. 2013-11-26 15.05.50. 2013.

236. Metro Vancouver. Station Information: Lower Fraser Valley Air Quality Monitoring Network [Internet]. Metro Vancouver. 2012 [cited 2013 May 19]. Available from: http://www.metrovancouver.org/about/publications/Publications/LowerFraserValleyAirQualityMonitoringNetwork2012StationInformation.pdf

237. Site Information for London Marylebone Road (UKA00315) [Internet]. Department for Environment Food & Rural Affairs. [cited 2015 Jun 12]. Available from: http://uk-air.defra.gov.uk/networks/site-info?site_id=MY1

238. Department of Environment Food & Rural Affairs. Conversion Factors Between ppb and µgm-3 and ppm and mgm-3 [Internet]. UK-AIR: Air Information Resource. 2014 [cited 2015 Jul 11]. Available from: http://uk-air.defra.gov.uk/assets/documents/reports/cat06/0502160851_Conversion_Factors_Between_ppb_and.pdf

239. European Commission. Guidance on the Commission Implementing Decision laying down rules for Directives 2004/107/EC and 2008/50/EC of the European Parliament and of the Council as regards the reciprocal exchange of information and reporting on ambient air [Internet]. European Commission. 2013 [cited 2015 Jul 11]. Available from: http://ec.europa.eu/environment/air/quality/legislation/pdf/IPR_guidance1.pdf

240. AQMesh Inc. Co-location comparison trials [Internet]. AQMesh. [cited 2016 Sep 17]. Available from: http://www.aqmesh.com/performance/co-location-comparison-trials/

241. Jones RL. Using a commercial low cost sensor network (AQMesh) to quantify urban air quality: comparing measured and modelled (ADMS-urban) pollutant concentrations [Internet]. 2016 Dec 13 [cited 2017 May 13]; Air Quality Monitoring: Evolving Issues and New Technologies. Available from: http://www.ch.cam.ac.uk/files/aw534/RLJ%20AAMG%202016%20c.pdf

242. City of Vancouver. Open Data catalogue [Internet]. City of Vancouver. 2014 [cited 2015 Jul 17]. Available from: http://vancouver.ca/your-government/open-data-catalogue.aspx

243. Environment Canada. Wind Direction over the Last Year (monthly data) for Vancouver [Internet]. [cited 2014 Jan 24]. Available from: http://vancouver.weatherstats.ca/charts/wind_direction-1year.html

244. Tchoukanski I. EasyCalculate10 [Internet]. [cited 2015 Jul 17]. Available from: http://www.ian-ko.com/free/EC10/EC10_main.htm

245. City of Vancouver. Why we collect traffic count data [Internet]. 2014. Available from: http://vancouver.ca/streets-transportation/traffic-count-data.aspx

246. Wallace LA, Wheeler AJ, Kearney J, Van Ryswyk K, You H, Kulka RH, et al. Validation of continuous particle monitors for personal, indoor, and outdoor exposures. J Expo Sci Environ Epidemiol. 2011 Feb;21(1):49–64.

247. TSI Incorporated. DustTra™ DRX Aerosol Monitors Models 8533, 8533EP and 8534 (P/N 6001981 Rev G) [Internet]. TSI Incorporated. 2014 [cited 2015 Jul 28]. Available from: http://www.tsi.com/uploadedFiles/_Site_Root/Products/Literature/Spec_Sheets/DustTrak-DRX-6001981_USA-web.pdf

248. Hornung RW, Reed LD. Estimation of Average Concentration in the Presence of Nondetectable Values. Appl Occup Environ Hyg. 1990;5(1):46–51.

249. Chau CK, Pun-Cheng LSC, Ng WY, Hui WK. Study of the PM10 concentration variations along two intra-urban roads within a compact city. Environ Monit Assess. 2012 Jun 1;184(6):3943–58.

250. Lianou M, Chalbot M-C, Kotronarou A, Kavouras IG, Karakatsani A, Katsouyanni K, et al. Dependence of home outdoor particulate mass and number concentrations on residential and traffic features in urban areas. J Air Waste Manag Assoc 1995. 2007 Dec;57(12):1507–17.

251. Fraunhofer Institute for Physical Measurement Techniques IPM. Semiconducting Gas Sensors Using Thin and Thick Film Technology [Internet]. [cited 2014 Feb 17]. Available from: http://www.ipm.fraunhofer.de/content/dam/ipm/en/PDFs/Product%20sheet/GP/ISS/Metalloxid-Sensor_en_V3.pdf

252. AppliedSensor. Metal Oxide Semiconductor (MOS) Sensors [Internet]. 2008 [cited 2014 Feb 17]. Available from: https://www.appliedsensor.com/pdfs/Metal_Oxide_Semiconductor_%28MOS%29.pdf

Appendices

Appendix A Principles of operation for gas sensors

A.1 Electrochemical sensors

Electrochemical gas sensors determine the concentration of a target gas by measuring the electrical signal in an electrochemical cell. Electrochemical cells house two electrodes (the anode and cathode) each contacting an electrolyte. Reduction-oxidation (redox) reactions guide electron transfer between electrodes via the wire connection. Oxidation and reduction reactions occur at the anode and cathode, respectively. Electrons are lost at the anode and transferred to the cathode so the latter gains electrons. Electric potential energy drives the directionality of the redox half-reactions. The reaction with the higher potential will proceed in the forward direction (i.e. reduction) while the reaction with the lower potential proceeds in reverse (i.e. oxidation). (200)

In practice, a gas must first pass a small capillary-like opening before diffusing across a gas permeable membrane (or hydrophobic barrier) with a specific pore size to reaching a sensing electrode. The barrier has a twofold function: to allow a suitable amount of gas to pass through and to counteract electrolyte leaks. At the contact surface, the analyte reacts by oxidation or reduction with the sensing electrode (designed for the gas of interest). The resister joining this electrode with the counter electrode has a measurable current proportional to the gas concentration flow between the electrodes. As current generation follows, this sensor is called amperometric. The reference electrode is maintained at a constant potential to fix the voltage of the nearby sensing electrode. Figure A.1 provides a visual for that described above. (200)

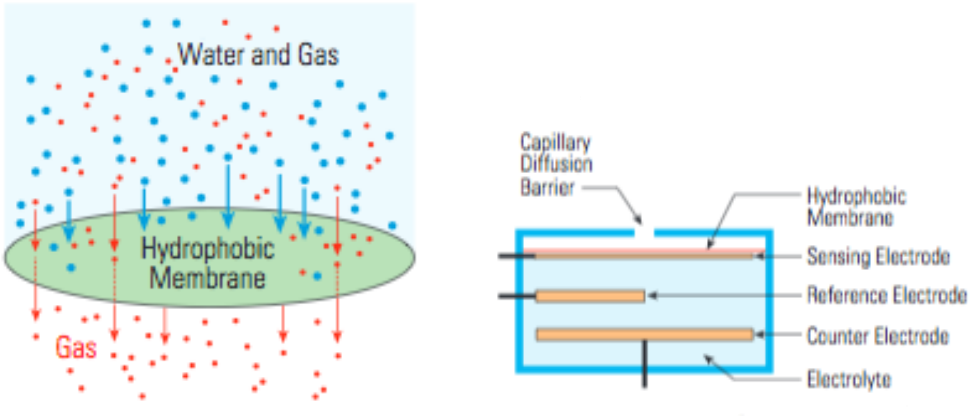

Figure A.1 Hydrophobic membrane and electrochemical sensor schematic. Reprinted from Chou (200) with permission from McGraw-Hill Global Education Holdings, LLC.

A.2 Infrared sensors

IR sensors use the IR region of the electromagnetic spectrum to detect gases, as energy absorption in this range is both selective and unique. Gas molecules have unique fingerprints or absorption peaks in the 2-15 µm range such that molecules with more atoms have more absorption bands. Interatomic bond vibrations, specific for a molecule and structure, occur at the gas' natural frequency. Smaller gas molecules have fewer natural frequency modes. (206)

Components of an IR system include: an IR source; an optical filter; a gas cell and a detector (Figure A.2). The IR source is typically a heated wire filament or an electronically produced source. Positioning of optical filters, either before the light source of in front of the detector, is detector dependent. Filters may be made dispersive with prisms or grating or nondispersive with bandpass filter. In nondispersive infrared (NDIR) sensors, the bandpass filter is responsible for target gas selectivity. The gas cell has an inlet and an outlet for light passage; the light path length is directly related to the radiation absorbed. Finally, the detector converts received electromagnetic energy or temperature displacements into electrical signals. (206)

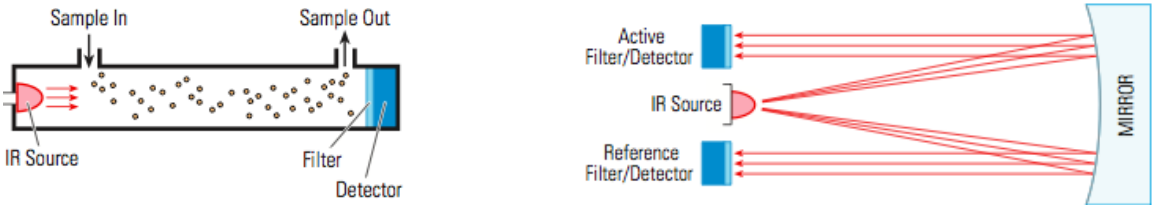

Figure A.2 A basic infrared gas detector and a two-detector layout. Reprinted from Chou (206) with permission from McGraw-Hill Global Education Holdings, LLC.

Two detection methods are possible stemming from the same premise: energy from the radiation matching the gas' natural frequency is absorbed whereas the rest is transmitted. When gases absorb radiation, the molecules vibrate more vigorously causing proportional temperature increases that are detectable. Conversely, the wavelength at which the gases absorbed radiation will show diminishing radiation energy that is measurable. (206)

A.3 Metal oxide semiconductor sensors

MOS sensors detect gases by redox reactions taking place between the gas and the oxide surface. (203) Metal oxides are the sensing layers in semiconductor sensors and are deposited by thick- or thin-film methods. (251) Tin oxide is frequently selected as the metal oxide because it is reactive with various gases and has large deflections in resistance. (165) As gases adsorb and desorb, the resistance of the metal oxides are altered. (194) Ideally, these reactions are reversible. (251) Environmental oxygen and water vapor-related species could be adsorbed at the surface of the sensing layer at ambient conditions. (252) Reducing gases (e.g. CO, H_2) react with these species to decrease the resistance. (252) In contrast, oxidizing gases (e.g. NO_2 and O_3) react with

these species to increase resistance. (252) At large, the relationship between a sensor's resistance and target gas concentration obeys a power law. (252)

Appendix B Meteorological correlation matrices

B.1 Temperature

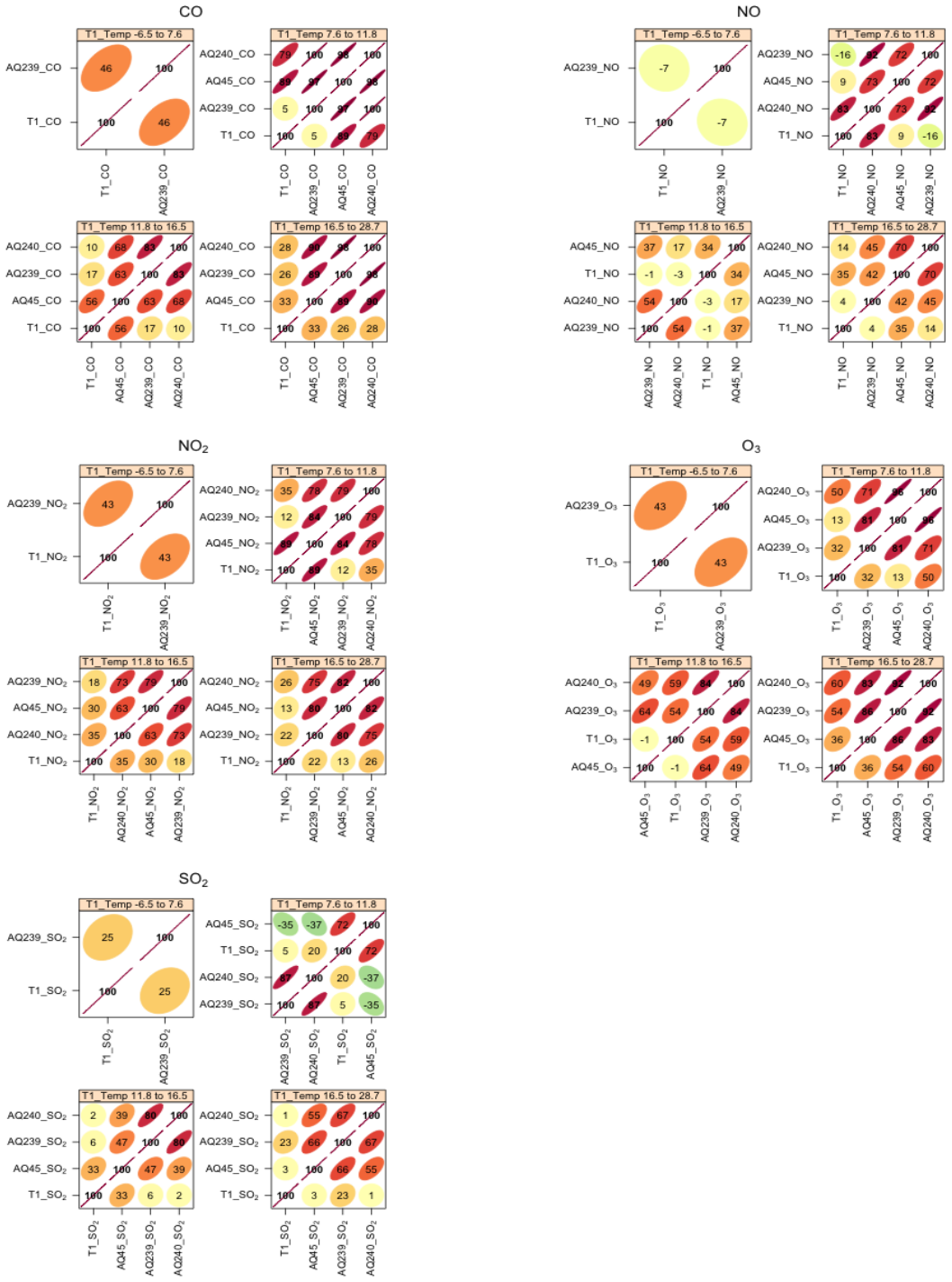

Figure B.1 Correlation matrices for co-located Vancouver sensors stratified by temperature (°C).

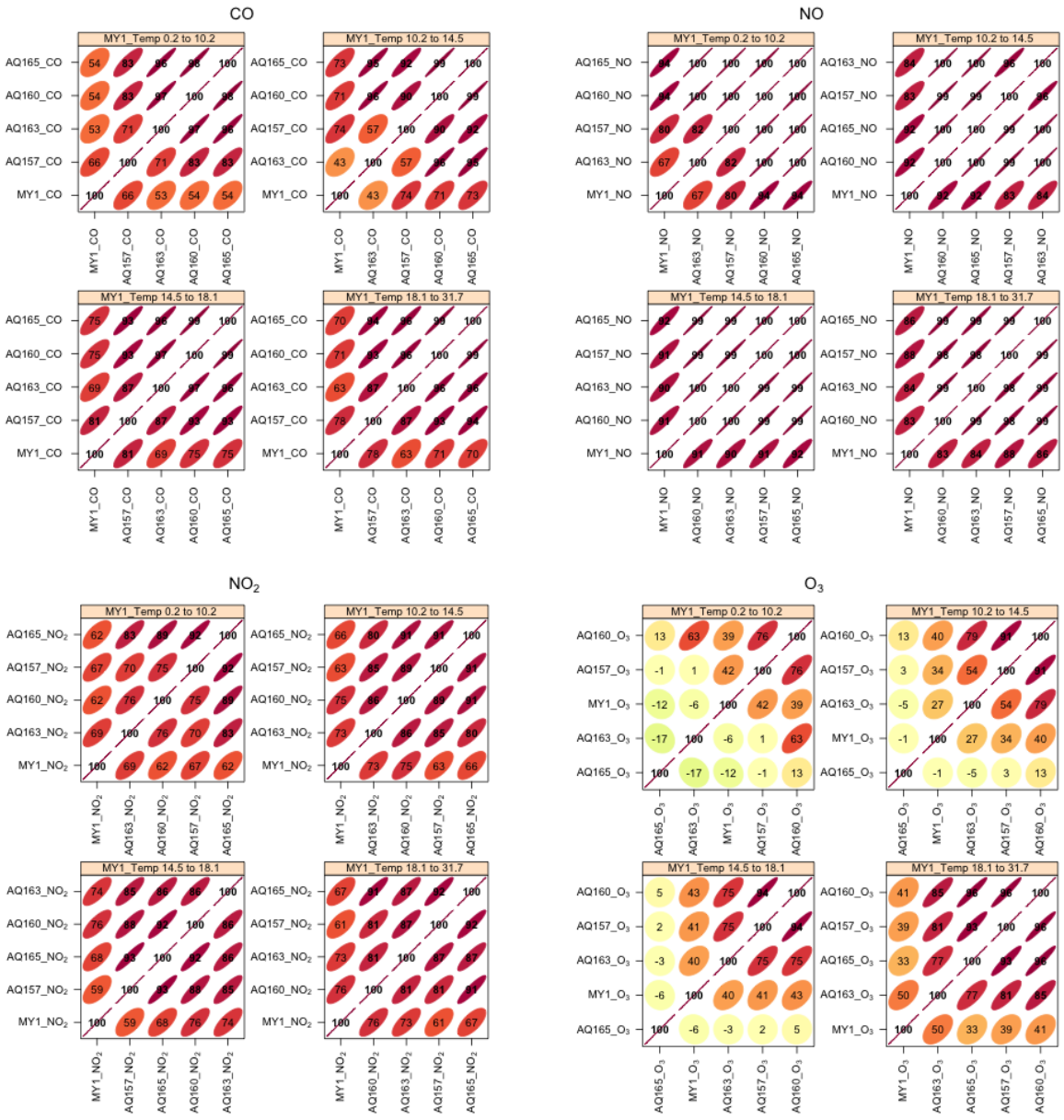

Figure B.2 Correlation matrices for co-located London sensors stratified by temperature (°C).

B.2 Humidity

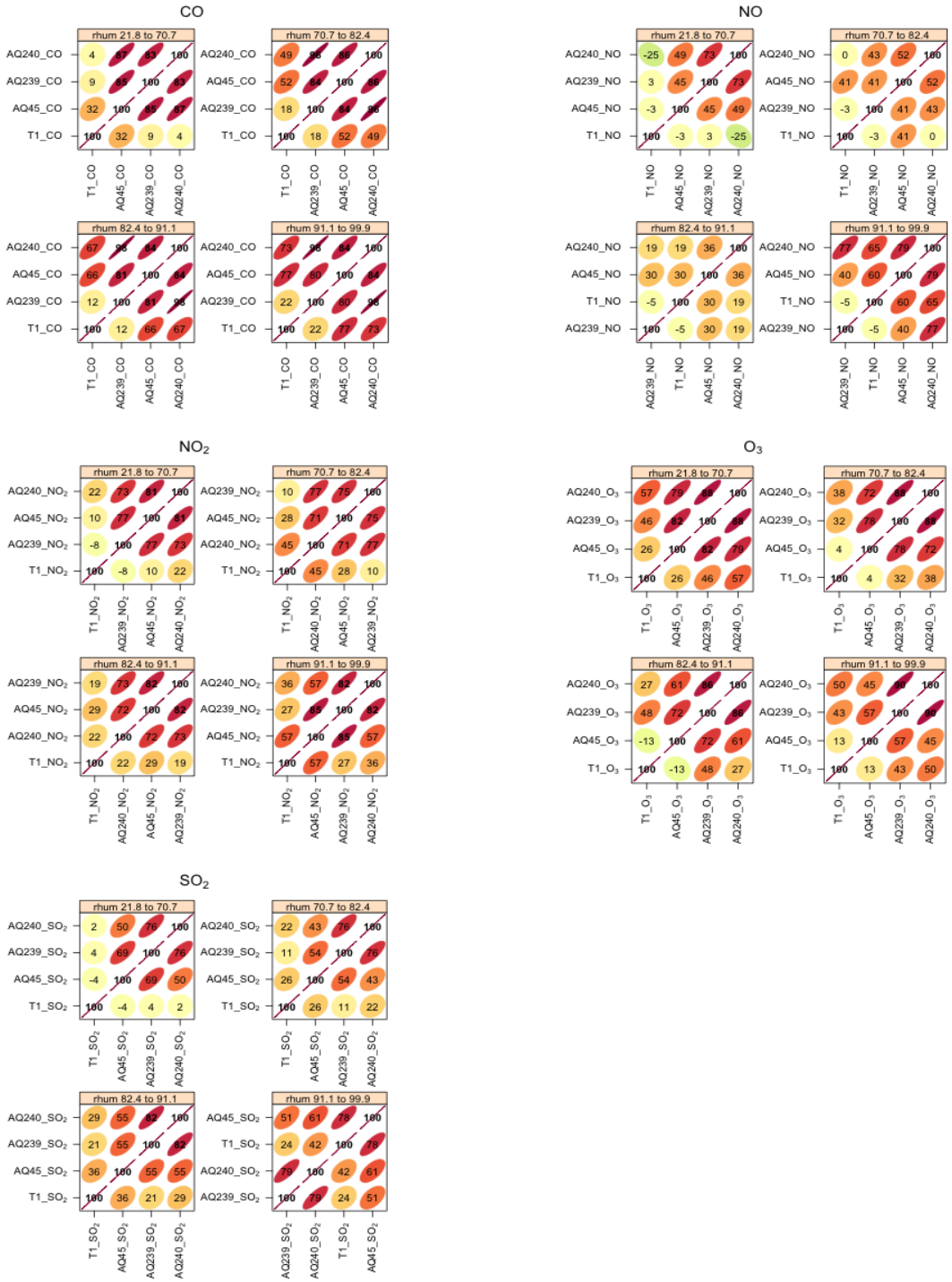

Figure B.3 Correlation matrices for co-located Vancouver sensors stratified by relative humidity (%RH).

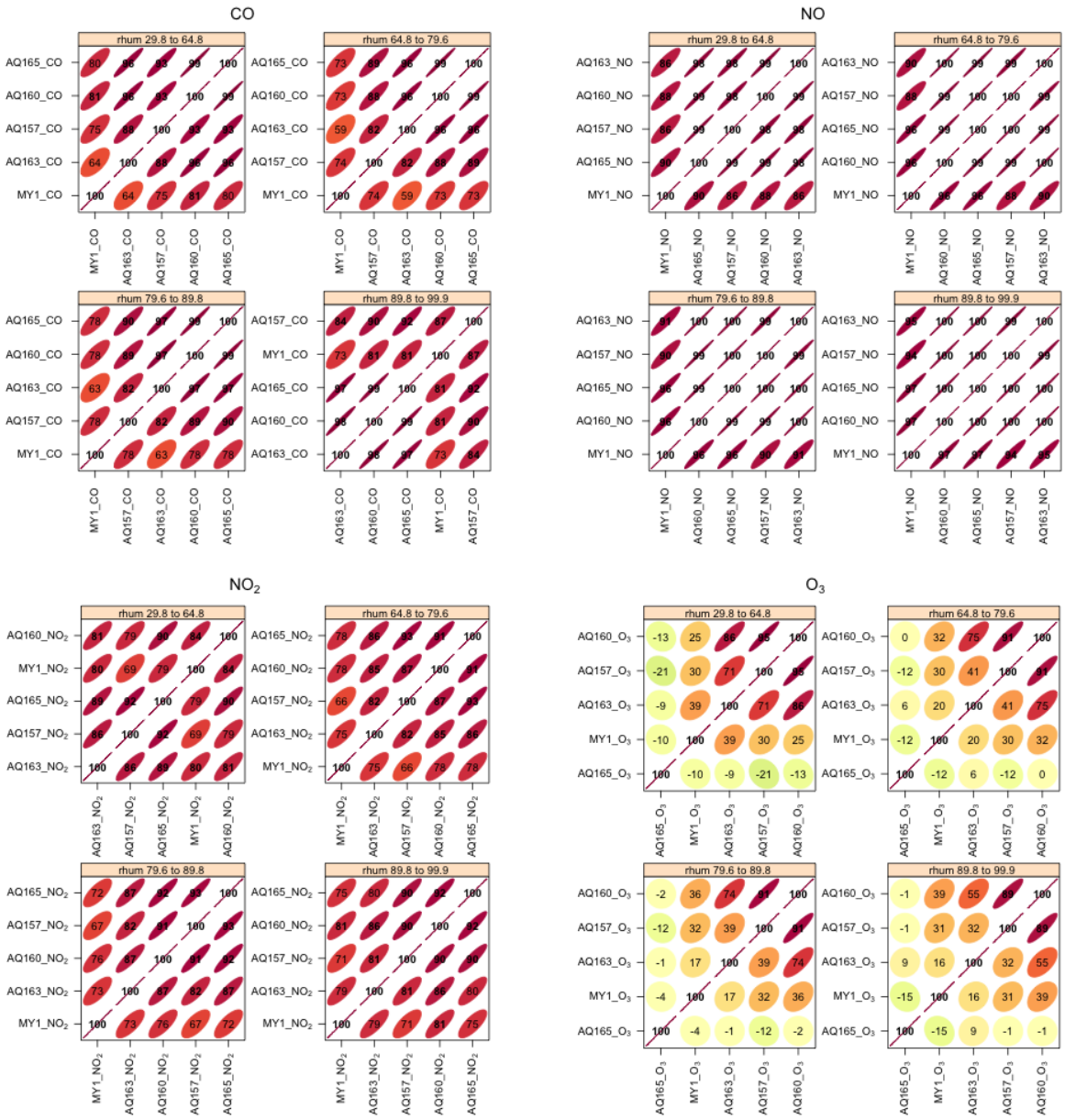

Figure B.4 Correlation matrices for co-located London sensors stratified by relative humidity (%RH).

B.3 Wind speed

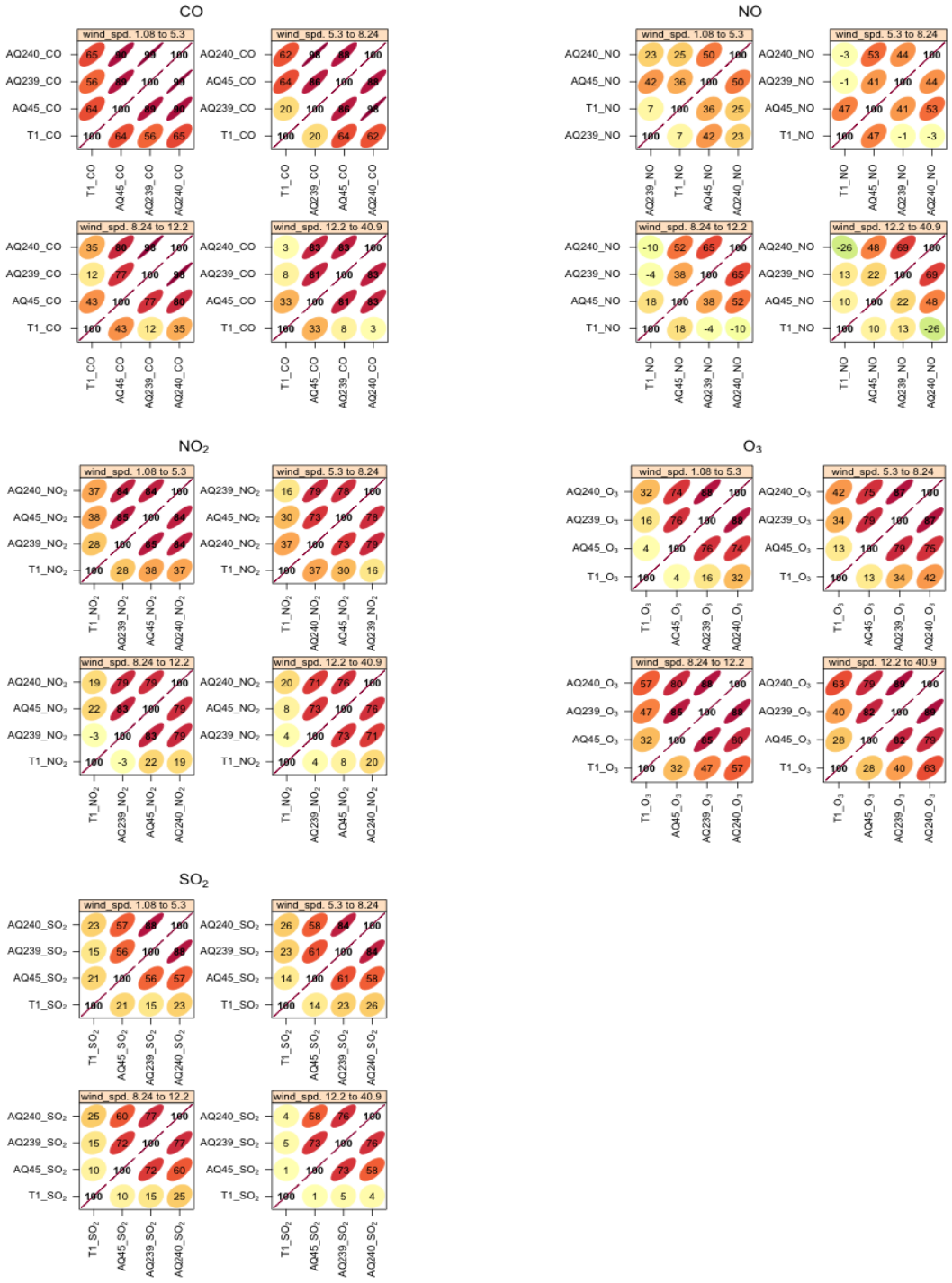

Figure B.5 Correlation matrices for co-located Vancouver sensors stratified by wind speed (km/h).

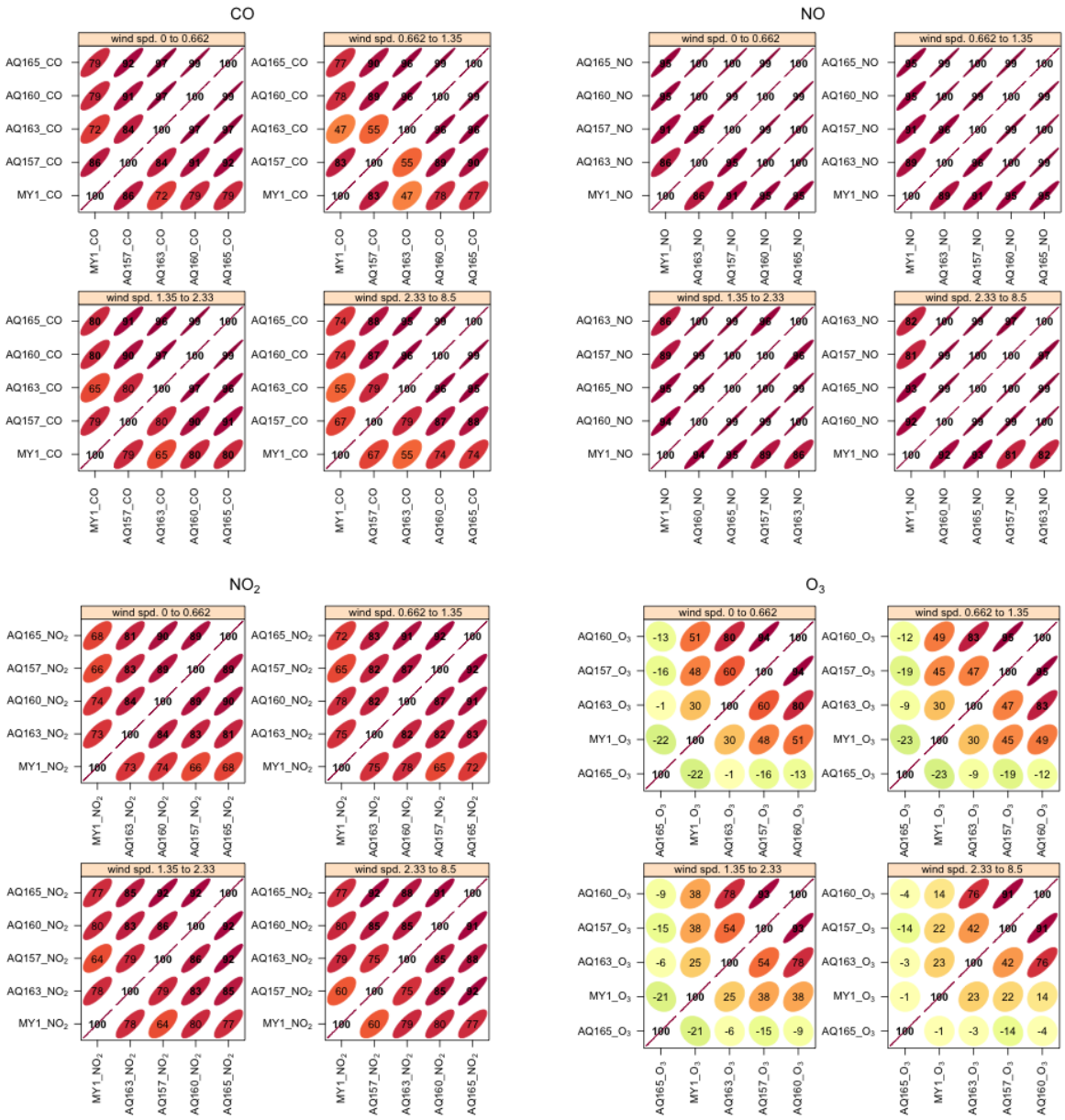

Figure B.6 Correlation matrices for co-located London sensors stratified by wind speed (m/s).

B.4 Season

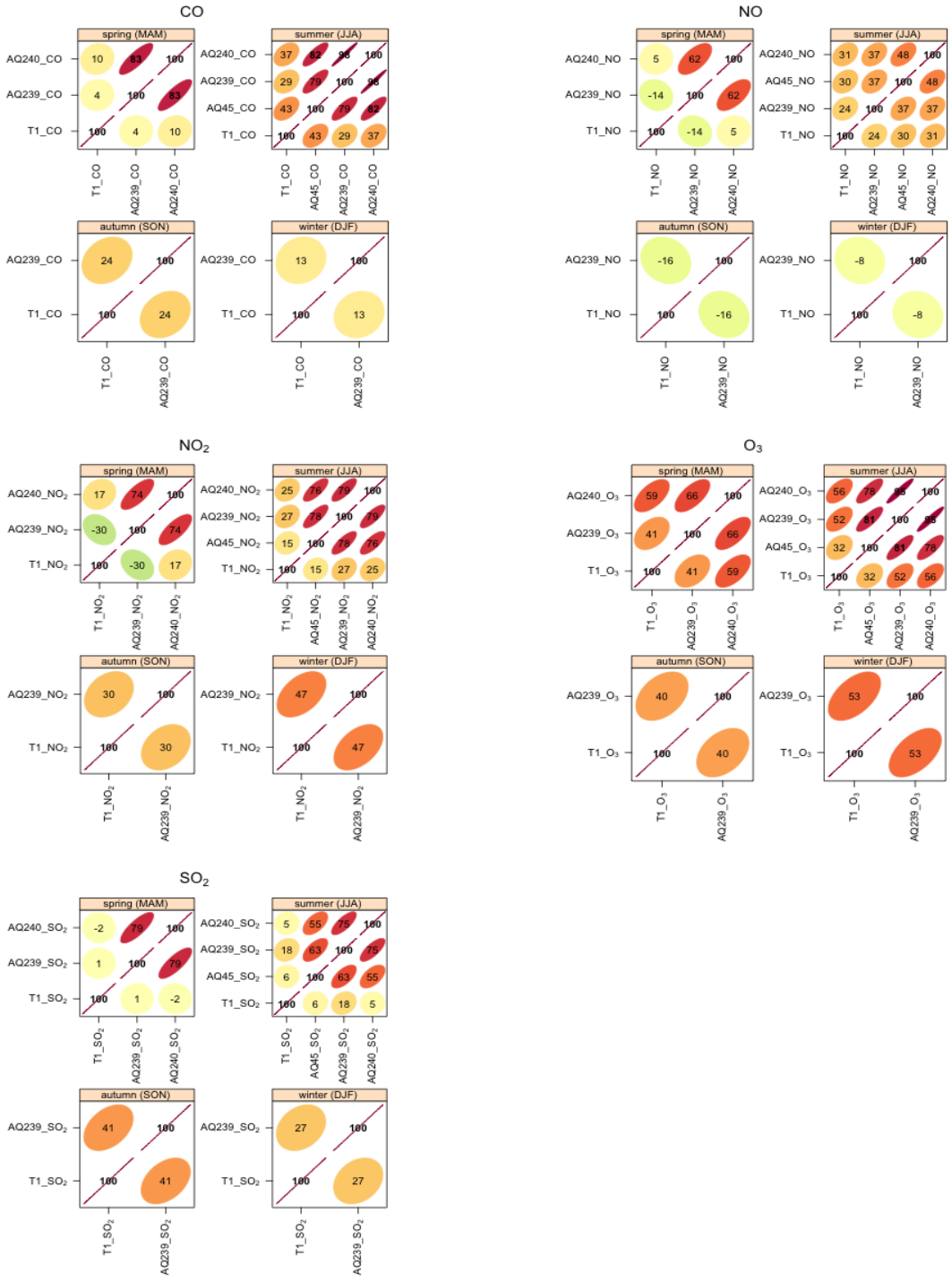

Figure B.7 Correlation matrices for co-located Vancouver sensors stratified by season.

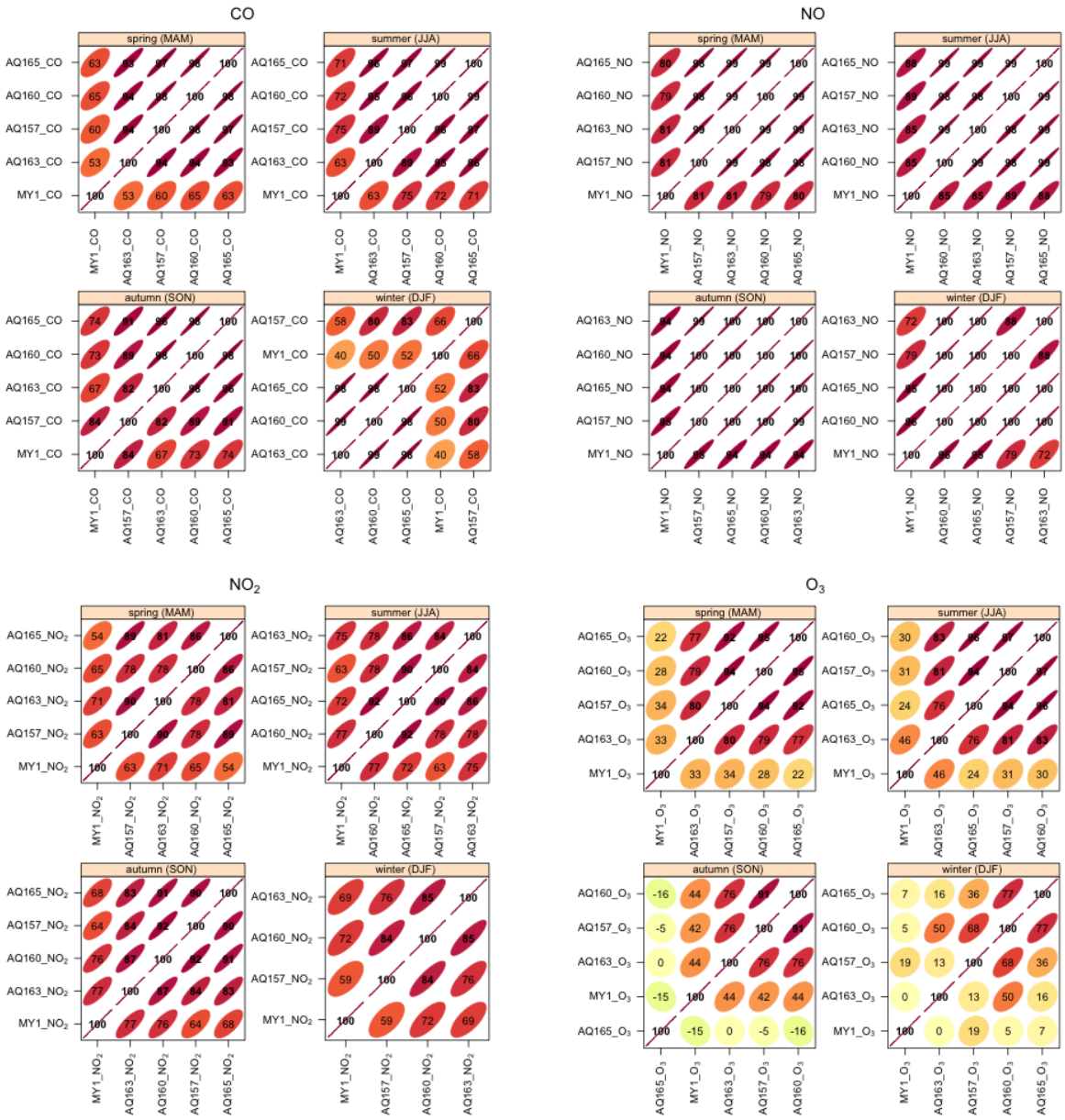

Figure B.8 Correlation matrices for co-located London sensors stratified by season.

Appendix C Mobile campaign supplementary information

C.1 Sampling schedule

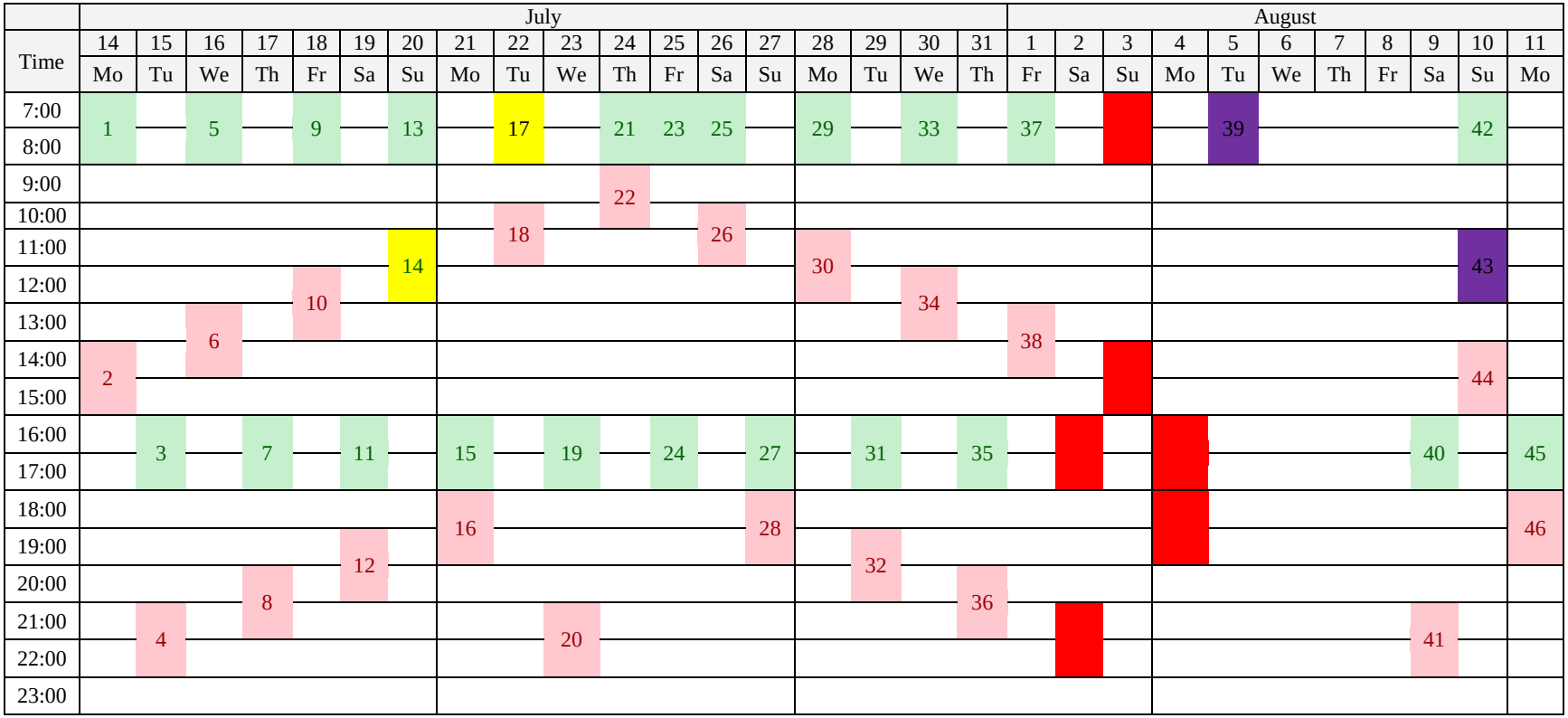

Figure C.1 Mobile monitoring sampling schedule. Rush hour periods (between 7:00 - 9:00 and 16:00 – 18:00) were coded in green while non-rush hour periods were coded in pink. Routes in yellow had flow errors so similar day of week and time of day re-runs were conducted in purple. Cancellations (in red) on August 2nd, 2014 through August 4th, 2014 as a result of the Celebration of Lights, Vancouver Pride Parade and British Columbia Day.

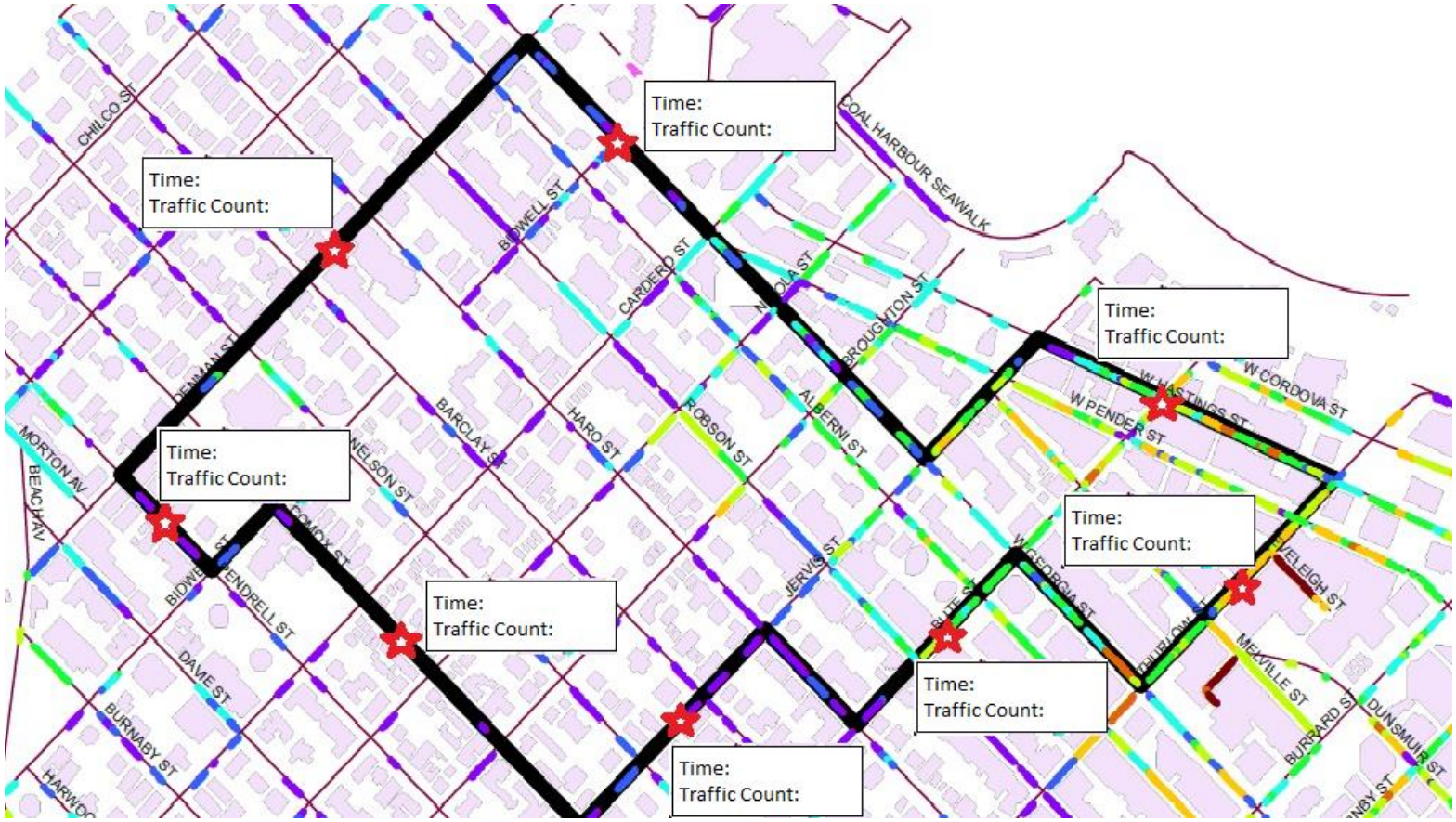

Direction: Clockwise or Counter Clockwise
Side of Street: Right or Left
Date:
Run Number:
Weather Conditions:

Figure C.2 Mobile monitoring data collection form

C.2 Between-day correlation factors (CF3)

Table C.1 Between-day correction factors based on $PM_{2.5}$ (and PM_{10} proxies) from the Burnaby South Station.

Date	CF3
Monday, 14 July, 2014	1.24
Tuesday, 15 July, 2014	1.13
Wednesday, 16 July, 2014	1.13
Thursday, 17 July, 2014	0.84
Friday, 18 July, 2014	1.12
Saturday, 19 July, 2014	0.58
Sunday, 20 July, 2014	0.49
Monday, 21 July, 2014	0.39
Tuesday, 22 July, 2014	1.13
Wednesday, 23 July, 2014	0.97
Thursday, 24 July, 2014	0.48
Friday, 25 July, 2014	0.72
Saturday, 26 July, 2014	0.93
Sunday, 27 July, 2014	1.18
Monday, 28 July, 2014	1.28
Tuesday, 29 July, 2014	1.42
Wednesday, 30 July, 2014	1.27
Thursday, 31 July, 2014	1.45
Friday, 1 August, 2014	1.25
Tuesday, 5 August, 2014	0.80
Saturday, 9 August, 2014	0.89
Sunday, 10 August, 2014	0.96
Monday, 11 August, 2014	1.64